AD-A163 013 AFRRI (ARMED FORCES RADIOBIOLOGY RESEARCH INSTITUTE) 1/1
REPORTS JULY-SEPTEMBER 1985(U) ARMED FORCES
RADIOBIOLOGY RESEARCH INST BETHESDA MD 1985

UNCLASSIFIED F/G 6/18 NL

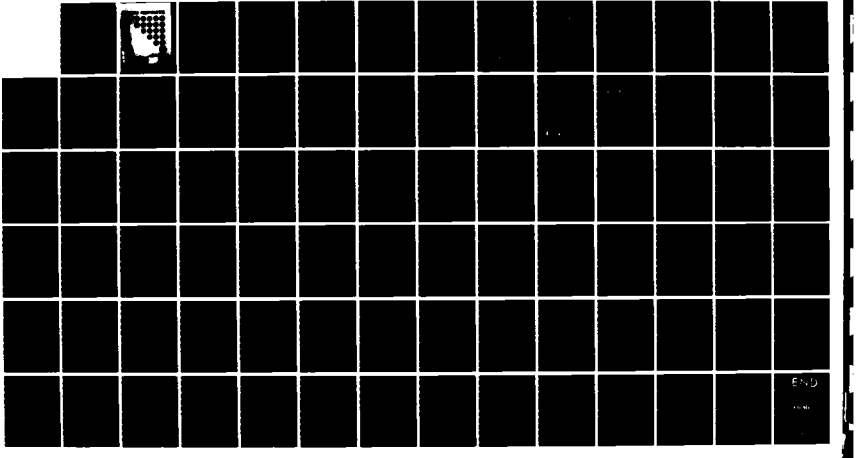

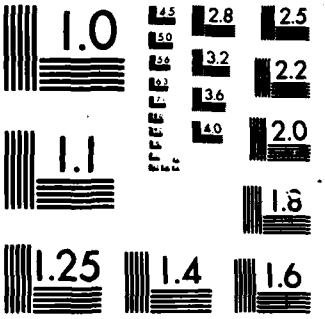

MICROCOPY RESOLUTION TEST CHART
NATIONAL BUREAU OF STANDARDS-1963-A

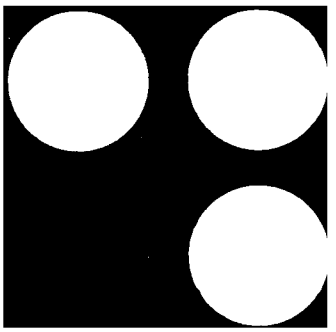

UNCLASSIFIED
SECURITY CLASSIFICATION OF THIS PAGE

AD-A163 813

REPORT DOCUMENTATION PAGE

1a. REPORT SECURITY CLASSIFICATION UNCLASSIFIED	1b. RESTRICTIVE MARKINGS
2a. SECURITY CLASSIFICATION AUTHORITY	3. DISTRIBUTION/AVAILABILITY OF REPORT Approved for public release; distribution unlimited.
2b. DECLASSIFICATION/DOWNGRADING SCHEDULE	
4. PERFORMING ORGANIZATION REPORT NUMBER(S) AFRRI SR85-26 through 85-32	5. MONITORING ORGANIZATION REPORT NUMBER(S)
6a. NAME OF PERFORMING ORGANIZATION Armed Forces Radiobiology Research Institute 6b. OFFICE SYMBOL (If applicable) AFRRI	7a. NAME OF MONITORING ORGANIZATION
6c. ADDRESS (City, State and ZIP Code) Defense Nuclear Agency Bethesda, Maryland 20814-5145	7b. ADDRESS (City, State and ZIP Code)
8a. NAME OF FUNDING/SPONSORING ORGANIZATION Defense Nuclear Agency 8b. OFFICE SYMBOL (If applicable) DNA	9. PROCUREMENT INSTRUMENT IDENTIFICATION NUMBER
8c. ADDRESS (City, State and ZIP Code) Washington, DC 20305	10. SOURCE OF FUNDING NOS PROGRAM ELEMENT NO: NWED QAXM; PROJECT NO; TASK NO; WORK UNIT NO
11. TITLE (Include Security Classification) AFRRI Reports, Jul-Sep 1985	
12. PERSONAL AUTHOR(S)	
13a. TYPE OF REPORT Reprints/Technical 13b. TIME COVERED FROM _____ TO _____	14. DATE OF REPORT (Yr., Mo., Day) 15. PAGE COUNT 82
16. SUPPLEMENTARY NOTATION	
17. COSATI CODES FIELD / GROUP / SUB GR	18. SUBJECT TERMS (Continue on reverse if necessary and identify by block number) N/A

19. ABSTRACT (Continue on reverse if necessary and identify by block number)

This volume contains AFRRI Scientific Reports SR85-26 through 85-32 for Jul-Sep 1985.

20. DISTRIBUTION/AVAILABILITY OF ABSTRACT UNCLASSIFIED/UNLIMITED ☒ SAME AS RPT ☐ DTIC USERS ☐	21. ABSTRACT SECURITY CLASSIFICATION UNCLASSIFIED
22a. NAME OF RESPONSIBLE INDIVIDUAL Junith A. Van Deusen	22b. TELEPHONE NUMBER (Include Area Code) (202)295-3536 22c. OFFICE SYMBOL ADMG

DD FORM 1473, 83 APR EDITION OF 1 JAN 73 IS OBSOLETE

UNCLASSIFIED
SECURITY CLASSIFICATION OF THIS PAGE

CONTENTS

Scientific Reports

SR85-26: Burghardt, W. F., Jr., and Hunt, W. A. Characterization of radiation-induced performance decrement using a two-lever shock-avoidance task;

SR85-27: Dagen, A. J., Alfano, R. R., Zilinskas, B. A., and Swenberg, C. E. Fluorescence kinetics of emission from a small finite volume of a biological system;

SR85-28: Dorval, E. D., Mueller, G. P., Eng, R. R., Durakovic, A., Conklin, J. J., and Dubois, A. Effect of ionizing radiation on gastric secretion and gastric motility in monkeys.

SR85-29: Ely, M. J., Speicher, J. M, Catravas, G. N., and Snyder, S. L. Radiation effects on diamine oxidase activities in intestine and plasma of the rat;

SR85-30: Ledney, G. D., Exum, E. D., and Jackson, W. E., III. Wound-induced alterations in survival of ^{60}Co irradiated mice: importance of wound timing;

SR85-31: Mickley, G. A., Stevens, K. E., and Galbraith, J. A. Quaternary naltrexone reverses morphine-induced behaviors.

SR85-32: Pope, M., and Swenberg, C. E. Electronic processes in organic solids.

RADIATION RESEARCH 103, 149–157 (1985)

Characterization of Radiation-Induced Performance Decrement Using a Two-Lever Shock-Avoidance Task

WALTER F. BURGHARDT, JR., AND WALTER A. HUNT

Behavioral Sciences Department, Armed Forces Radiobiology Research Institute, Bethesda, Maryland 20814-5145

BURGHARDT, W. F., AND HUNT, W. A. Characterization of Radiation-Induced Performance Decrement Using a Two-Lever Shock Avoidance Task. *Radiat. Res.* **103**, 149–157 (1985).

Rats were trained to perform a task involving responses on two levers. Responding on an avoidance lever delayed the onset of electrical footshock for 20 sec and responding on a warning lever turned on a light for 60 sec. When the light was on, the task on the avoidance lever was changed from unsignaled shock avoidance to signaled shock avoidance by preceding the shocks with 5-sec warning tones. The animals preferred the signaled avoidance condition. After 100 Gy of ^{60}Co irradiation, the animals were less able to avoid shock, an effect from which the animals recovered somewhat over 90 min. The response rate on the avoidance lever remained at or above control rates, while the response rate on the warning lever showed an initial increase, followed by a decrease below baseline. The increase in responding on the avoidance lever occurred in bursts just after presentation of the shocks. The data suggest that under these experimental conditions a subject will not respond appropriately to avoid shock or acquire cues that can facilitate the avoidance of shock. The effects, however, do not reflect an inability to perform the required movements but instead appear to reflect some characteristic of the task associated with a particular lever.

INTRODUCTION

Exposure to high doses of ionizing radiation can result in depression of the nervous system. In some cases, this is expressed as an early transient incapacitation (ETI), characterized as the inability to complete a task, and has been observed in a number of species (*1–4*). This phenomenon occurs shortly after exposure to moderate and high doses of radiation, with recovery to near normal performance on some tasks occurring within approximately 30 min after exposure. A performance decrement of some sort is often seen, even in the absence of an ETI (*1*). Frequently, some aspects of behavior remain unchanged or even enhanced, while others are disrupted. For example, a decrease in general activity and food intake in monkeys has been demonstrated, while learned task performance is maintained (*5*). In rats, maze performance is improved, while motor activity is decreased (*6*).

Ionizing radiation has been shown to disrupt active avoidance behavior (*7, 8*). In these studies, rats were trained to avoid successive electrical footshocks by jumping onto a retractable platform in response to an auditory cue. When the animals were exposed to high-energy electrons or γ photons, their ability to avoid shock was significantly reduced in a dose-dependent manner within the dose range of 25–200

0033-7587/85 $3.00

Gy. This decrement was transient lasting less than 30 min. Although the animals did not avoid shock, they would jump onto the platform in response to shock (*8*).

In the present experiments, we attempted to further characterize the effect of ionizing radiation on active avoidance behavior by using a modification of a paradigm designed to measure an animal's preference for signaled versus unsignaled avoidance (*9*). We wanted to find out whether the irradiated animals would request and use cues to avoid shock at a dose that would be expected to produce reliable and profound behavioral decrement, while not totally disrupting behavior (*8*). This paradigm is a two-lever, bar-press task in which animals may obtain auditory cues as a warning for impending footshock. Pressing one bar (avoidance lever) results in postponement of the shock. Pressing the other bar turns on a light. While the light is on, a 5-sec tone precedes the shock. Using this auditory cue, rats will learn very effectively when to press the avoidance bar to maintain a low shock frequency (signaled avoidance). In addition, this paradigm simultaneously measures behavior on two different tasks and assesses the ability of the animals to maintain more than one measured behavior after irradiation.

METHODS

Twelve Long Evans (Blue Spruce) rats (300 g) were housed separately and kept on a reversed 12-hr light cycle. The animals were watered and fed *ad libitum* throughout the course of the study.

Operant-conditioning chambers approximately 11 cm high, 25 cm deep, and 24 cm wide, each housed in separate sound-attenuating boxes, were used in these experiments. The floor consisted of aluminum rods through which scrambled electrical footshock (1.0 mA) could be applied using constant current ac shockers and electromechanical scramblers. On one wall were two response levers. A SONALERT speaker was centered on the wall to the left of the levers to provide, when required, a 1900-Hz tone at approximately 68 dB/SPL. A clear jeweled 1-W light was located in the middle of the ceiling. The units were maintained in a darkened climate-controlled room with white noise provided through a 16 cm speaker to mask outside sounds.

Prior to the first training session, animals were placed in the operant chambers for at least 2 hr to familiarize them with the apparatus. Thereafter, each experimental session lasted 4 hr.

The animals were trained to avoid a 0.5-sec electrical footshock by responding on an avoidance lever (*10*). A response on the avoidance lever postponed the onset of shock by 20 sec (RS 20). In the absence of responding on the avoidance lever, shock occurred at 5-sec intervals (SS 5). A single response on a separate lever (warning lever) turned on the overhead light for 1 min, during which shocks following a response on the avoidance lever were preceded by a warning tone during the last 5 sec of the response-to-shock interval (signaled avoidance) (*11*). If the animal responded on the avoidance lever during the tone, the tone was terminated and footshock was delayed 20 sec. Responses on the warning lever when the light was on were counted but had no scheduled effect. After 1 min of signaled avoidance, the overhead light was turned off. A single response on the warning lever could then turn the light back on and reinstate signaled avoidance. Training was complete when the animals could successfully avoid more than 90% of the shocks that could be presented (12/min) and when performance was maintained within 10% a constant amount of time in signaled avoidance.

For programming of the experimental paradigms and data collection, a PDP-8E computer operating under SCAT software was used. Data were recorded graphically by cumulative recorders and numerically by the computer. The following parameters were continuously measured: the number of shocks received, the number of responses made on each lever, the distribution of responses in time, the number of warning tones used, and the latency of responses after cues.

After training, subjects were habituated to the effects of schedule interruption and transport that occurred for irradiations. After 2 hr of performance, the session was suspended with all stimuli and responses disabled. The animal was placed in a Plexiglas restraining tube, transported to the ^{60}Co facility, and returned without being irradiated. The session was then resumed until there was less than a 10%

difference in the number of shocks received and in the number of responses made on each lever during the next hour, compared with those during the hour before removing the animals from the conditioning chambers.

After habituation, the animals were randomly assigned to two groups of six animals each. One group was irradiated once, while the other group served as controls (sham irradiated). For irradiations or sham irradiations, the animals were handled as they were for habituation, except that each irradiated animal was placed in the ^{60}Co exposure room and received a single bilateral dose of 100 Gy of γ radiation at a rate of approximately 66 Gy per minute. Control animals were handled identically, with the exception that they were not irradiated. The transport time from the radiation facility to the conditioning chambers was less than 5 min. At the end of the study, all animals were sacrificed via barbiturate overdose.

For radiation dosimetry, paired 50-ml ion chambers were used. Delivered dose was expressed as a ratio of the dose measured in a tissue-equivalent plastic phantom enclosed in a restraining tube to the dose measured free in air.

For analysis, only the measurements made 60 min prior and 90 min after irradiation were used, periods when the performance of the animals was most consistent. The data collected were divided into six 10-min blocks before removal from the apparatus for irradiations, and nine 10-min blocks after resumption of the session for analysis. For each lever, responses during each 10-min postirradiation period were totaled and expressed as the percentage of the mean number of responses for the six 10-min periods immediately preceding irradiation. Responses from the sham-irradiated rats were similarly recorded. All other measures were presented as totals for each 10-min period. The data were statistically analyzed using multiple factor analyses of variance with repeated measures on one factor (*12*). Radiation dose (0 or 100 Gy) was one factor, and time after treatment was the repeated factor. The level for statistical significance was 0.05.

RESULTS

While performing on the two-lever paradigm, the unirradiated rats avoided shock very well, receiving less than five shocks over a 10-min period. They also spent most of their time in signaled avoidance. In the hour before irradiation, the experimental subjects spent an average of 83.7% of their time in signaled avoidance (range 78.3–95.5%). During a comparable period, control subjects spent an average of 84.8% of their time in signaled avoidance (range 74.8–91.8%). Exposure to ionizing radiation degraded the ability of animals to avoid shock. Figure 1 is a representative sample of the performance of one of the animals on the avoidance lever subsequent to irradiation. Note the low shock density, high number of intervals of signaled avoidance, and overall rate and pattern of responding seen in the preirradiation performance found in the upper two tracings. In contrast, the postirradiation performance clearly shows an increase in shock density, a progressive decrease in the number and regularity of periods of signaled avoidance, and a small increase in overall response rates on the avoidance lever.

The numbers of shocks and warning tones received by the animals are illustrated in Fig. 2. The control values presented are the pooled averages for the unirradiated control group during the 90 min after sham exposure. During the first 10 min after irradiation, the animals received approximately eight times more shocks than the nonirradiated subjects. The number of shocks received decreased somewhat during the course of the session but remained at least three times control levels (effect due to radiation, $P < 0.05$; effect due to time after irradiation, $P < 0.01$; interaction, $P < 0.01$). The number of warning tones progressively decreased after irradiation and remained below the number of shocks received during the same interval. This

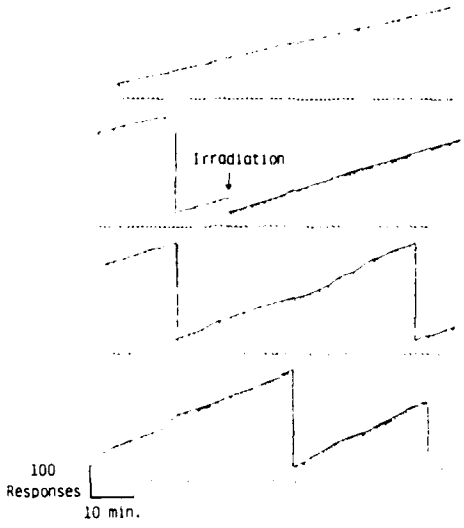

FIG. 1. Continuous cumulative record beginning in upper left corner from a representative subject on the day of irradiation. Downward vertical excursions on the lower tracing indicated periods when the overhead light was on and signaled avoidance was in effect. Upward vertical excursions on the upper tracing represent responses on the avoidance lever; the pen is reset downward every 300 responses. Diagonal hatches on the upper tracing indicate shocks presented. Time proceeds from left to right. Time and response scaling are provided on the lower left portion of the illustration. Time of irradiation is marked on the figure with an arrow and a reset of the upper pen.

suggested that the animals were not responding for the tones and therefore could not use them as aids in avoiding shock.

Response on each lever after irradiation, expressed as the percentage of preexposure rates of responding for each animal, is presented in Fig. 3. When compared to the nonirradiated group, the irradiated animals responded approximately 30–40% more

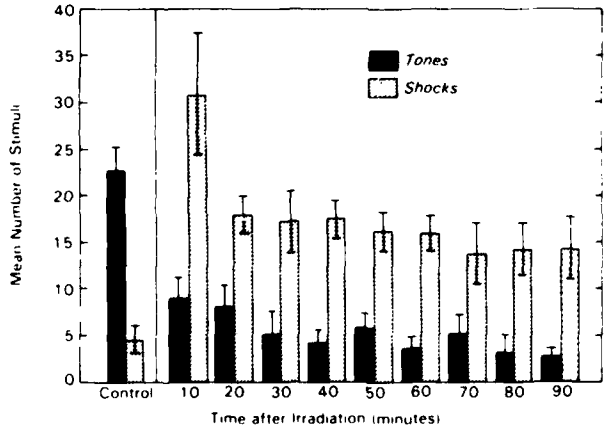

FIG. 2. Mean number of warning tones and shocks received by the experimental group after irradiation, plus or minus standard error of the mean. The control warning tone and shock rates consist of pooled rates of presentation for all subjects in the control group for the 90 min after sham treatment.

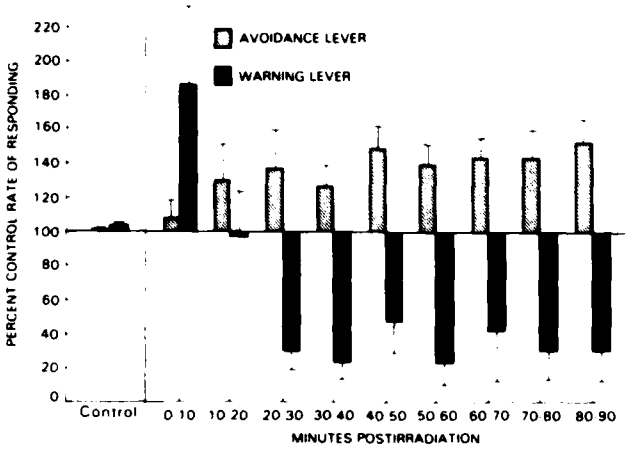

FIG. 3. Mean responding rates on the avoidance and warning levers expressed as percentage of the average rate of responding for each subject during the six intervals before treatment. The control values are pooled from the control group's performance during the same periods before and after sham irradiation. All values are expressed plus or minus standard error of the mean.

on the avoidance lever. This effect was consistent throughout the session (effect due to irradiation, $P < 0.05$; effects due to time after irradiation, interaction, n.s. at 0.05). In contrast, the irradiated animals initially responded more frequently on the warning lever, but within 20 min after irradiation, their performance dropped significantly below baseline levels and remained there during the remainder of the session (effects due to irradiation, time after irradiation, and interaction all significant at $P < 0.01$).

One way in which to determine the distribution of responses during a session is with interresponse time (IRT) histograms. Based on the requirements of the task, it was expected that animals would respond on the avoidance lever most often just after the onset of the warning tone (that began 15 sec after the last response on the avoidance lever), as can be found in the histogram of Fig. 4A. However, the irradiated animals responded more frequently after shock onset (that occurred 20 sec after the last response on the avoidance lever in either signaled or unsignaled avoidance and 5 sec after the onset of the warning tone in signaled avoidance) and tended to continue responding once initiated (Fig. 4B). In addition, rates of responding were comparatively low around the time a warning tone could be presented (beginning 15 sec after the last response on the avoidance lever), presumably because of the reduction in responding on the warning lever (Fig. 3). This would result in a lower number of warning tones available to assist performance (Fig. 2).

IRTs on the warning lever are presented in Fig. 5. Control animals responded mostly during the 20 sec after the overhead light was turned off (indicating a change from signaled to unsignaled avoidance) (Fig. 5A). The animals presumably do this to reinstate the signaled avoidance condition (Fig. 5A). These subjects also tend to respond in bursts (that is, interresponse time under 5 sec). Irradiated subjects make fewer overall responses with a much greater variation in IRTs and the appearance

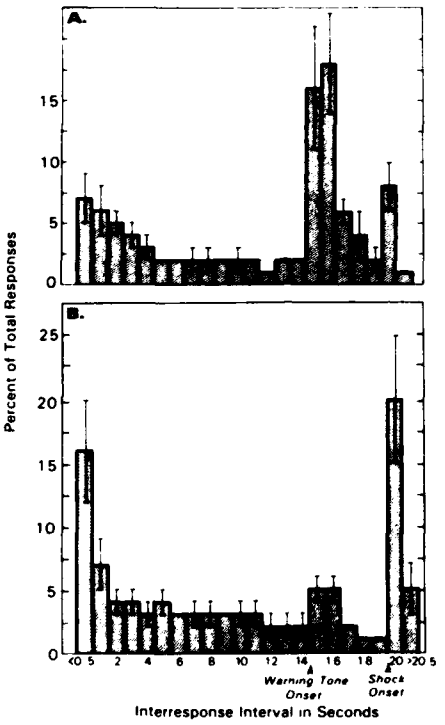

FIG. 4. (A) Interresponse time distribution on the avoidance lever for the control group after sham irradiation, plus or minus standard error of the mean. Arrows indicate the times of onset of warning tone and shock, when present (warning tones were presented on during signaled avoidance). (B) Interresponse time distribution on the avoidance lever for the experimental group after irradiation, plus or minus the standard error of the mean. Scales for both graphs are identical.

of very long IRTs (Fig. 5B). In general, these animals responded more randomly rather than immediately after the light went off.

If an animal is using the warning tone appropriately as a cue, the latency between the onset of the tone and a response on the avoidance lever should be short. In Fig. 6A, the control group shows a characteristic patterning of responses with short latencies, indicating detection and appropriate use of the warning signal. Similar latencies of the responses on the avoidance lever were found in the irradiated animals (Fig. 6B). However, the total number of responses to the warning tones was reduced, consistent with the decreased number of tones presented (Fig. 2).

It should be noted that following irradiation with the dose used in this study (100 Gy), the animals did not exhibit any gross abnormalities in spontaneous behavior and were able to move about freely during the course of the study.

DISCUSSION

Consistent with previous reports, the results of this study clearly demonstrate that exposure to ionizing radiation degrades performance of an active avoidance task at a dose of radiation that, based on previous studies using rats (*7, 8*), would be expected to induce profound and reliable behavioral decrement. After irradiation,

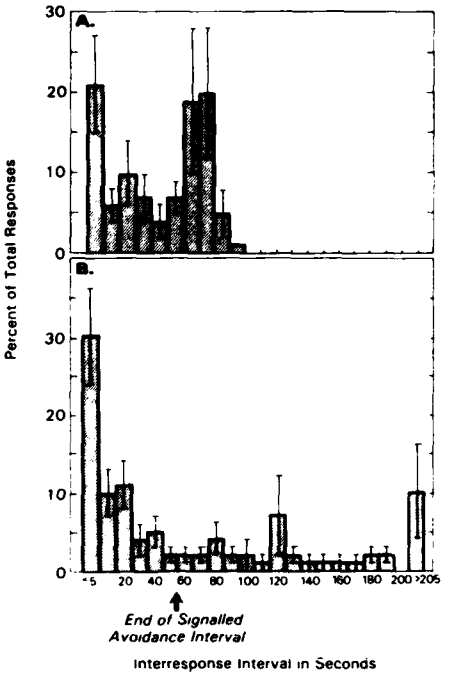

FIG. 5. (A) Interresponse time distribution on the warning lever in the control group after sham irradiation, plus or minus the standard error of the mean. The arrow indicates the end of the 1-min periods of signaled avoidance, after which the chambers were dark. (B) Interresponse time distribution for the experimental group after irradiation on the warning lever, plus or minus the standard error of the mean.

animals received a significantly greater number of shocks. However, it does not appear that they were incapable of responding to avoid shock. To the contrary, the animals responded at a significantly higher rate on the avoidance lever. Although some recovery in the ability to avoid shock was noted, an increased shock density remained throughout the measurement period. This is in contrast to other reports where animals recovered completely from behavioral decrements such as ETI within 30 min, implying that the degree of recovery observed after irradiation may depend on the nature of the task.

The IRT distribution for the avoidance lever (Fig. 4) shows that irradiated animals responded less at times appropriate to avoid shock, that is, just subsequent to the presentation of the warning tone. This is due to the reduced number of tones presented (Fig. 2). When tones were presented, the animals apparently used them by responding shortly thereafter (Fig. 6). In addition, the animals tended to respond in bursts to the shocks. Such bursts of responses would contribute very little to the success of subsequent shock avoidance. Maintenance of escape behavior with depressed shock avoidance after irradiation has previously been demonstrated using rats in a platform avoidance task (*8*).

In contrast to the sustained increase in the rate of responding on the avoidance lever, responding on the warning lever was substantially reduced. The IRT distribution on the warning lever (Fig. 5) became less regular and much more erratic in the

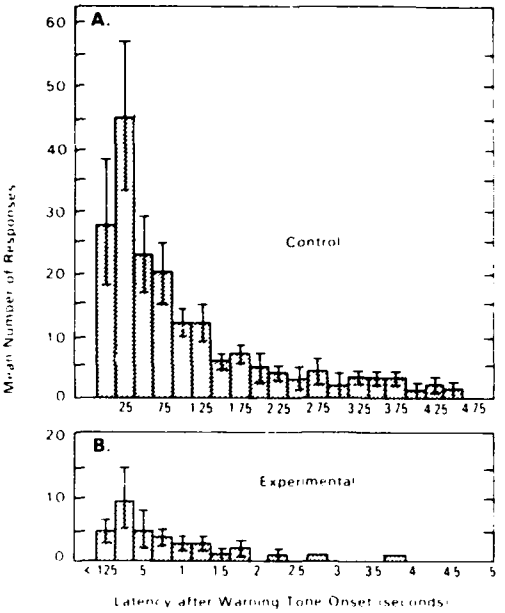

FIG. 6. (A) Distribution of latencies of responses on the avoidance lever to the onset of the warning tone in the control group for the 90 min after sham irradiation, plus or minus the standard error of the mean. (B) Distribution of latencies of responses on the avoidance lever to the onset of the warning tone in the experimental group in the 90 min after irradiation, plus or minus the standard error of the mean. These graphs include only responses made during the presence of the warning tone and before the onset of shock.

irradiated animals. This implies that the subjects did not respond to the appropriate visual cue (lights off). Rather, they responded at a greatly reduced rate overall and without regard to any of the cues present.

The factors that underlie the radiation-induced decrement in two-lever active avoidance behavior, such as sensory, motor, or cognitive factors, are uncertain. One possibility involving sensory perception would be a reduced sensitivity for detecting the electrical shock. This seems unlikely since the increased number and the IRT distribution of the responses on the avoidance lever (Fig. 4) suggest that the animals are responding *to* the shocks. In addition, the pain threshold after exposure to 100 Gy of γ radiation appears to be unaltered (*13*). The ability of irradiated animals to detect visual and auditory stimuli has not been examined.

The inability to perform the required movements to successfully complete the task also appears unlikely, since a general overall increase in responses on the avoidance lever was noted. A reduction in responses on both levers would have been expected if the animals were experiencing a gross motor deficit.

Perhaps the findings in the present paper are not the result of a gross sensory or motor decrement, but are dependent on the nature and number of tasks required and of the cues associated with these tasks, i.e., cognitive factors. The irradiated animals used the auditory cues (tones), but not the visual cues (lights out). However, the cues are not independent from each other in this paradigm. The visual cue is used to obtain the auditory cue. Also, the consequences of not having these cues

are different. If the avoidance lever is not pressed at the appropriate time, the animal is shocked. If the warning lever is not pressed, nothing happens to the rat other than the loss of the auditory cue. Therefore, each cue has a different level of immediacy. The animals first response is to attempt to avoid the shock. Secondarily, they respond for peripheral cues, such as the auditory cue which aids in avoiding the shock. Irradiated animals may be focusing more of their attention and actions on the shock and the immediate need to avoid it, rather than to initiate the movements required to obtain additional cues. Such a possibility was suggested in a previous study in which irradiated rats performed better in a maze, even though their general activity was reduced (*6*).

RECEIVED: December 6, 1984; REVISED: March 29, 1985

REFERENCES

1. A. BRUNER, V. BOGO, and R. K. JONES, Delayed match-to-sample performance decrement in monkeys after ^{60}Co irradiation. *Radiat. Res.* **63,** 83–96 (1975).
2. A. P. CASARETT, Swim-tank measurement of radiation-induced behavioral incapacitation. *Psychol. Rep.* **33,** 731–736 (1973).
3. R. L. CHAPUT and R. T. KOVACIC, Miniature pig performance after fractionated supralethal doses of ionizing radiation. *Radiat. Res.* **44,** 807–820 (1970).
4. A. L. CASEY and W. L. BROWN, *Incapacitation of the Goat following Massive Doses of Mixed Neutron and Gamma Radiation.* RTD TDR-63-3077, Air Force Weapons Laboratory, Kirtland A.F.B., NM, 1963.
5. W. L. BROWN, J. E. OVERALL, L. C. LOGIE, and J. E. WICKER, Lever-pressing behavior of albino rats during prolonged exposures to X-radiation. *Radiat. Res.* **13,** 617–631 (1960).
6. W. C. BLAIR, The effects of cranial X-radiation on maze acquisition in rats. *J. Comp. Physiol. Psychol.* **51,** 175–177 (1958).
7. G. A. MICKLEY and H. TEITELBAUM, Persistence of lateral hypothalamic-mediated behaviors after a supralethal dose of ionizing radiation. *Aviat. Space Environ. Med.* **49,** 868–873 (1978).
8. W. A. HUNT, Comparative effects of exposure to high-energy electrons and gamma radiation on active avoidance behavior. *Int. J. Radiat. Biol.* **44,** 257–260 (1983).
9. P. BADIA, S. CULBERTSON, and B. ABBOTT, The relative aversiveness of signalled vs. unsignalled avoidance. *J. Exp. Anal. Behav.* **16,** 113–131 (1971).
10. M. SIDMAN, Two temporal parameters in the maintenance of avoidance behavior by the white rat. *J. Comp. Physiol. Psychol.* **46,** 253–261 (1953).
11. M. SIDMAN, Some properties of the warning stimulus in avoidance behavior. *J. Comp. Physiol. Psychol.* **48,** 444–450 (1955).
12. B. J. WINER, *Statistical Principles in Experimental Design,* pp. 514–539. McGraw-Hill, New York, 1971.
13. W. F. BURGHARDT and W. A. HUNT, The interactive effects of morphine and ionizing radiation on the latency of tail withdrawal from warm water in the rat. In *Proceedings of the Ninth Symposium on Psychology in the Department of Defense,* pp. 73–76. United States Air Force Academy, 1984.

Chemical Physics 96 (1985) 483–488
North-Holland, Amsterdam

FLUORESCENCE KINETICS OF EMISSION FROM A SMALL FINITE VOLUME OF A BIOLOGICAL SYSTEM

A.J. DAGEN, R.R. ALFANO

Institute for Ultrafast Spectroscopy and Lasers, Department of Physics, The City College, New York 10031, USA

B.A. ZILINSKAS

Department of Biochemistry and Microbiology, Cook College, Rutgers University, New Brunswick, New Jersey 08903, USA

and

C.E. SWENBERG

Radiation Sciences Department, Armed Forces Radiobiology Research Institute, Bethesda, Maryland 20814, USA

Received 29 August 1984; in final form 19 November 1984

The fluorescence decay, apparent quantum yield and transmission from chromophores constrained to a microscopic volume using a single picosecond laser excitation were measured as a function of incident intensity. The β subunit of phycoerythrin aggregate isolated from the photosynthetic antenna system of *Nostoc* sp. was selected since it contains only four chromophores in a volume of less than 5.6×10^4 Å^3. The non-exponential fluorescence decay profiles were intensity independent for the intensity range studied (5×10^{13}–2×10^{15} photon cm^{-2} per pulse). The apparent decrease in the relative fluorescence quantum yield and increase of the relative transmission with increasing excitation intensity is attributed to the combined effects of ground state depletion and upper excited state absorption. Evidence suggests that exciton annihilation is absent within isolated β subunits.

1. Introduction

Over the past 30 years energy transfer dynamics of excited electronic states has been extensively studied and applied to a wide range of processes in biological and chemical systems [1–8]. Most of the theoretical and experimental studies have been concerned with systems composed of chromophores randomly distributed in either solutions or solids of *infinite spatial extent*. There are however, many important molecular systems where the distributions of chromophores are limited to a *small finite volume*, e.g., the chlorophyll light harvesting pigments of the photosynthetic unit of green plants, chromophores incorporated into small micellar units, as well as polymers which are constrained to volumes of microscopic dimensions. Recently, Ediger and Fayer [9] have constructed a theoretical formalism for calculating observables when electronic energy is transported among molecules confined to small volumes. Their results demonstrate that time-dependent observables can be significantly altered in small systems relative to their behavior for infinite systems. In particular the fluorescence kinetics, in the absence of bimolecular annihilation, are fluence independent and non-exponential. An ideal biological system to study the properties of electronic energy transfer in small domains is the β subunit of phycoerythrin isolated from the photosynthetic antenna system of the blue-green alga *Nostoc* sp. The phycoerythrin pigment is one component of the phycobilisomes, the well defined organelles, on the exterior surface of the thylakoid membranes of these organisms. In trimer form phycoerythrin of blue-green algae occupies a volume approximated

0301-0104/85/$03.30

by a right circular disk of radius 60 Å and height 30 Å [10]. The basic monomer of the pigment consists of two dissimilar polypeptide chains to which chromophores are covalently bonded; these chains, called the α and β subunits, contain two and four chromophores and have molecular weights of 16600 and 19500 dalton respectively [11,12]. In this paper we report the first picosecond fluorescence kinetic measurements of the phycoerythrobolin chromophores in the β subunit of phycoerythrin. We present evidence that the observed decrease in the fluorescence quantum yield with increasing laser intensity arises from enhanced transmission (with possible contributions from upper excited state absorption) and not bimolecular exciton annihilation [13]. The non-exponential fluorescence kinetic profiles were found to be intensity independent and could be fitted to either a double exponential or the Green function theory of Ediger and Fayer for energy transfer in small volumes.

2. Materials and methods

Nostoc sp. (Strain Mac) was grown in a 14 ℓ fermentor with pink or cool white fluorescent light as described previously [14]. Phycobilisomes were isolated from these cells according to the protocol of Troxler et al. [15]. Phycoerythrin was obtained from dissociated phycobilisomes by use of calcium phosphate chromatography and sedimentation on linear gradients of sucrose as detailed by Zilinskas and Howell [14]. The smallest phycoerythrin aggregate so obtained (trimers $(\alpha\beta)_3$) were removed from the gradient, dialyzed exhaustively against 1 mM potassium phosphate, *pH* 5.0, containing 0.02% sodium azide, and were then lyophilized. This sample was dissolved at 10 mg/mℓ in 8.0 M urea, 0.01 M potassium phosphate *pH* 8.0, and 0.01 M β-mercaptoethanol and incubated at 37°C for 2 h. The denatured phycoerythrin was then applied to a DEAE-Sephacel column preequilibrated with the denaturation solution. The α and β subunits were eluted (in that order) with a linear gradient of increasing NaCl in equilibrating solution. The peak fractions were pooled separately, dialyzed against 0.1 M potassium phosphate, *pH* 5.0 to effect renaturation, and their identities assessed by absorption, sedimentation on linear gradients, and electrophoresis on SDS-polyacrylamide gels. Details of these procedures are as described earlier [15].

Experiments were performed on the β subunit component suspended in 0.1 M potassium phosphate at *pH* 5. The sample OD at the excitation frequency was 0.38. The effects of self-absorption are minimized because the sample is frontally excited and most of the observed fluorescence is beyond 580 nm, where the absorption of the sample is small. A frequency doubled (530 nm) 8 ps single pulse from a mode locked Nd:glass laser was used to excite the sample at room temperature. The intensity of the incident fluence was varied by placing appropriate neutral density filters in the excitation pathway. An RCA 7265 PMT was employed for relative quantum yield measurements, whereas the transmitted light was monitored with a diode located behind the sample. A streak camera and OMA system with a 12 ps resolution was utilized to record the fluorescence kinetic decays which were digitized and stored in a computer for later analysis.

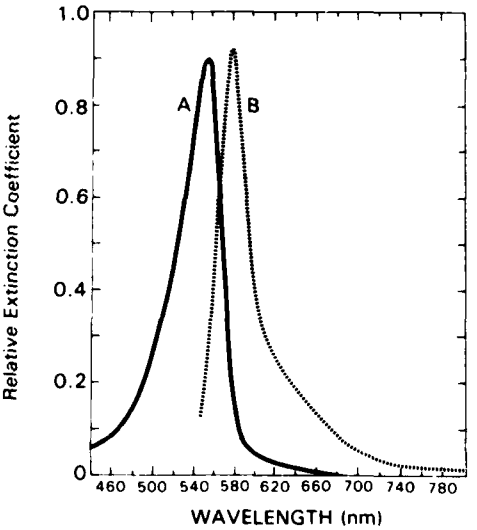

Fig. 1. (A) Relative extinction coefficient for β subunit, (max) at 550 nm = 310000 M^{-1} cm^{-1}. (B) Relative fluorescence intensity versus wavelength; excitation wavelength 530 nm, T = 300 K.

3. Results

Fig. 1 shows the relative extinction coefficient and fluorescence emission spectra of the β subunit. These spectra are nearly mirror images of each other and are similar to those reported by Zickendraht-Wendelstadt et al. [12] for the β subunit isolated from Pseudanabaena W1173. The fluorescence kinetic profiles (experimental points indicated by dotted curve) for low and high photon fluence (5.4×10^{13}–1.7×10^{15} photon cm^{-2}) are shown in fig. 2. The decays are highly non-exponential as can be seen on comparisons with exponential fits shown in fig. 2A (curves 1 and 2). The decays are unchanged in shape over the intensity range investigated. Emission rise times are within experimental resolution of the system, i.e. less than or equal to 12 ps. The decays reach one-third of their peak value in about 400 ps. Illustrated in fig. 3 is the relative fluorescence quantum yield (defined as the integrated fluorescence emission divided by the incident number of photons, normalized to unity at low laser intensity) as a function of pulse intensity. Its form is quite similar to quenching curves reported by other workers for complexes of photosynthetic bacteria [16] and green plant photosynthetic components [17]. Also shown in fig. 3 are the relative transmission data which are approximately a mirror image of the quantum yield curve and offset the quantum yield's apparent decrease at high intensity. The two curves break from unity at $\approx 1.75 \times 10^{14}$ photons cm^{-2}.

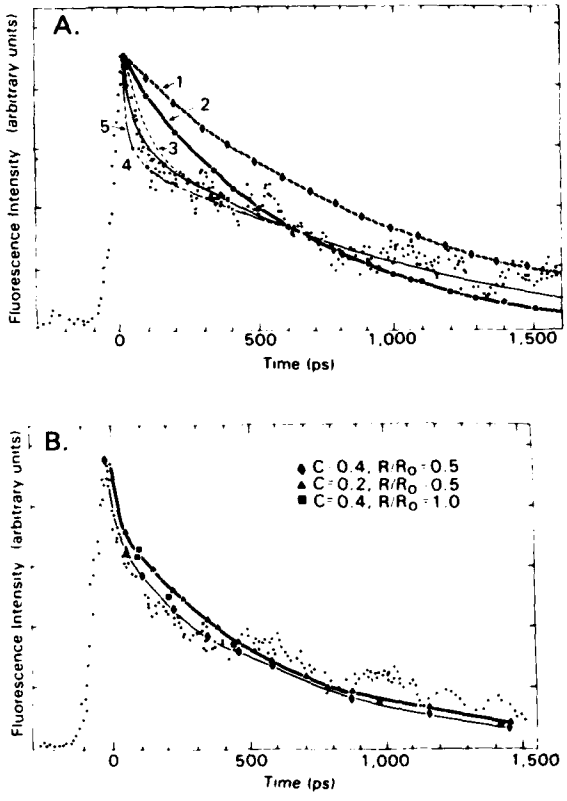

Fig. 2. Fluorescence intensity decays for single pulse excitation. Dotted curves experimental data. (A) Incident fluence 5.46×10^{13} photons cm^{-2} per pulse. Theoretical fits: (1) exponential, $k = 1.0 \times 10^9$ s^{-1}, (2) exponential, $k = 1.6 \times 10^9$ s^{-1}, (3) double exponential $0.65 \exp(-kt) + 0.33 \exp(-11kt)$, $k = 1.0 \times 10^9$ s^{-1}, (4) Paillotin et al. [13], exciton annihilation theory with $r = 0.1$, $Z = 1$ and $k = 1.0 \times 10^9$ s^{-1}, [corresponds to $0.65 \exp(-kt) + 0.32 \exp(-22kt)$], (5) double exponential $0.65 \exp(-kt) + 0.33 \exp(-44kt)$, $k = 1.0 \times 10^9$ s^{-1}. (B) Incident fluence 1.75×10^{15} photons cm^{-2} per pulse. Fits to the expression $[1 + CG_1(N, V, t)] \exp(-kt)$, $k = 1.72 \times 10^9$ s^{-1}, $N = 4$ with ■ $C = 0.4$, $R/R_0 = 1.0$; ▲ $C = 0.2$, $R/R_0 = 0.5$ and ◆ $C = 0.4$, $R/R_0 = 0.5$.

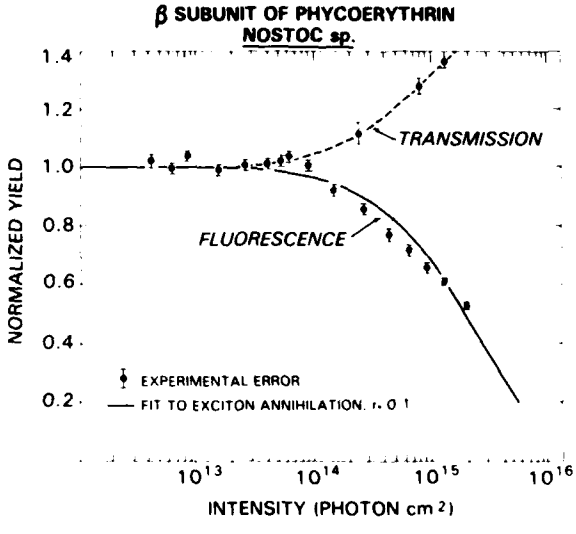

Fig. 3. Relative apparent quantum yield and transmission versus incident single-pulse fluence (photon cm^{-2}). Solid line denotes theoretical fit to exciton fusion model with $r = 0.1$ [13].

4. Discussion

The kinetic curve profiles are intensity independent with an overall e $^{-1}$ time of ≈ 400 ps (see fig. 2). They can be made to fit the exciton annihilation theory of Paillotin et al. [13] with values of $r = 0.1$, $k = 1.0 \times 10^9$ s $^{-1}$, and $Z = 1.0$, where r is the ratio of twice the monomolecular decay rate to the exciton annihilation rate and $Z = y(1 + X)$, where the constant $X \leqslant 1$ and y is the average number of excitons per domain at $t = 0$. The theory predicts multiexponential expressions for the fluorescence decay curves. For these values of r and Z, the decay is approximately a double exponential of the form

$$0.65 \exp(-kt) + 0.32 \exp(-22kt).$$

The observation that the decay profiles are independent of excitation intensity however invalidates interpreting the non-exponential decay in terms of exciton fusion since a five-fold increase or decrease in Z should produce observable shape differences in the fluorescence curves. For the β subunit, $\epsilon_{550} = 310000$ M^{-1} cm^{-1} [12] implies $\sigma I = y = 1$ at an incident fluence of 1.3×10^{15} photon cm^{-2} and therefore variations in Z are within the experimentally probed intensity range. The extreme sensitivity of the shape of the fluorescence decays to changes in Z over the excitation intensity range investigated ensures that we would have noticed such changes if bimolecular exciton annihilation processes were responsible for the non-exponential decays. Furthermore, the experimental data in fig. 3 demonstrate that corresponding to the decrease in the apparent fluorescence quantum yield with increasing pulse intensity there is an increase in transmission. The theory of exciton annihilation as given by Paillotin et al. [13] is known to be applicable only if the transmission is intensity independent. We cannot offer a quantitative explanation for the single pulse data reported in fig. 3. However, the observation that the relative transmission (T_R) and apparent fluorescence yield (ϕ_R) are approximately mirror reflection of each other about the unit axis is strongly suggestive of ground-state depletion since under steady-state excitation a three-level system gives $\phi_R = T_R^{-1}$ provided the incident intensity is less than the saturation intensity; the saturation intensity being defined as that intensity required to obtain a fluorescence yield decrease of 50% relative to its low intensity yield. Without a quantitative theory, contributions of upper excited-state absorption to the observed decrease in fluorescence quantum yield cannot be ruled out.

It is possible to fit the fluorescence profiles to an expression of the form $\exp(-at^{1/3} - kt)$ with $k = 4.4 \times 10^8$ s^{-1}, $a = 1.27 \times 10^3$ s$^{-1/3}$; however, such a fit must be considered fortuitous since this functional behavior is predicted under assumptions that are not applicable to the β-subunit, namely energy transfer limited to two-dimensions in a system of infinite extent [2]. Our data can best be explained by ascribing the fluence independent, non-exponentiality of the fluorescence kinetics to emission arising from more than a single chromophore. A good fit to the decays can be obtained assuming a minimum two-component model (see fig. 2A, curve 3). The zero of time in figs. 2A and 2B was set at the peak of the fluorescence intensity. All theoretical curves were set equal to the maximum intensity.

It is interesting to note that Fayer's approximation for the solution to the rate equations governing excitation on a finite number of chromophore, randomly dispersed in a finite volume, also provides a reasonable quantitative fit to the kinetic profiles. Several theoretical curves are shown in fig. 2B. The key quantity in Ediger–Fayer theory [9] for electronic excited-state transport among a finite number N molecules distributed randomly in a finite volume V is the probability, $G_s(N, V, t)$, that an excitation is on the originally excited chromophore at time t in the absence of decay due to its finite lifetime. $G_s(N, V, t)$ is a function of both N, the number of chromophores in the domain and R/R_0, where R_0 is the Forster critical radius [3,4] and R is the radius of the sphere which approximates the volume of the domain (for the β subunit R is ≈ 22 Å).

In terms of the response function, $G_s(t)$, the fluorescence decay $F(t)$ we observe is given by

$$F(t) = F_{\parallel}(t) + F_{\perp}(t) \propto \exp(-kt)\left[1 + CG_s(N, V, t)\right], \quad (1)$$

where C is a constant which depends on the initial excitation distribution and the chromophores' intrinsic anisotropy and $F_\perp$ and $F_\parallel$ denote the fluorescence emission viewed perpendicular and parallel to the incident polarization direction. As indicated in fig. 2B a value of R/R_0 on the order of 0.5 with $k = 1.72 \times 10^9$ s^{-1} gives good fits with $N = 4$. The neglect of the rotational diffusion in eq. (1) is justified since $\tau_{rot} = \eta V/KT \approx 10^{-6}$ s at room temperature assuming η is unity. The four chromophores of the β-subunit have definite orientations relative to each other and therefore in a strict sense violate the assumptions employed in deriving eq. (1). Either the fits to eq. (1) are fortuitous or for small R/R_0 and N, eq. (1) has a much broader range of applicability than the randomization of chromophore distances (averaging) implies. This could be rationalized by assuming that few configurations contribute for $R/R \leq 1$ with N small. There is also the possibility that the solvent produces slight positional shifts of the β-subunit chromophores thereby providing some degree of spatial randomness. For N fixed, eq. (1) constitutes a three-parameter k, R/R_0, and C. For example, with $R = 22$ Å (the radius of a sphere approximating the β-subunit volume), $R/R_0 \approx 0.5$ as determined from the fluorescence decay curves implies a Forster transfer distance (R) on the order of 40 Å. This is comparable to $R_0 = 21$ Å determined for the α-subunit [18].

In summary, the simplest model consistent with the experimental data reported in figs. 2 and 3 is that the domain size is too small to accommodate more than a single excitation, a view consistent with the onset of bleaching at a fluence of $\approx 2 \times 10^{14}$ photon cm^{-2} ($y \approx 0.2$). Our model suggests that after the absorption of one photon by a single chromophore the excitation energy is quickly dispersed among the other three chromophores comprising the β subunit. The time for randomization of the initial excitation is on the order of hundreds of picoseconds, the time it takes $G_2(N, V, t)$ to approach 0.25. The fast rise-time (< 10 ps) is indicative of the time for the initial emitting chromophore to begin fluorescing. The bleaching indicated by fig. 3 is interpreted in terms of the inability of 530 nm photons to connect the doubly excited state of the β aggregate to its first excited state. Hence in contrast to the non-linear process of singlet-exciton annihilation observed in larger size aggregates of the α and β subunits, for example the c-phycoerythrin [19], it appears that exciton fusion is absent in very small domains. The critical size of a domain for the inoperativeness of exciton annihilation in the general case presumably depends not only on the number of chromophores but also on the rate (proportional to R_{ij}^{-n}, $n = 6$) at which energy is transferred among them. A general theory of when exciton annihilation is inoperative for a small aggregate of chromophores constitutes an intriguing theoretical problem still lacking a solution.

Acknowledgement

A. Dagen and R. Alfano thank NSF, AFOSR, NIH and PSC-BHE of C.U.N.Y. for support and B. Zilinskas acknowledges support of USDA and NJAES state and U.S. Hatch Funds. We thank Mr. P. Sekuler for technical help and Drs. M.D. Ediger and M.D. Faver for their computer programs. A. Dagen thanks Ms. I. Bluman of Bendix Corp. for technical assistance.

References

[1] D.L. Huber, Phys. Rev. 20 (1979) 2307, 20 (1979) 5333.
[2] A. Blumen and J. Manz, J. Chem. Phys. 68 (1978) 1879.
[3] Th. Forster, Z. Naturforsch. 4a (1949) 321.
[4] R.S. Knox, in: Bioenergetics of photosynthesis, ed. Govindjee (Academic Press, New York, 1975) pp. 183–221.
[5] S.W. Hahn and R. Zwanzig, J. Chem. Phys. 68 (1978) 1879.
[6] R.F. Loring, H.C. Anderson and M.D. Faver, J. Chem. Phys. 76 (1982) 2015.
[7] P.Y. Lu, Z.X. Yu, R.R. Alfano and J.I. Gersten, Phys. Rev. A26 (1982) 3610.
[8] G. Porter, C.J. Tredwell, C.F.W. Seale and J. Barber, Biochem. Biophys. Acta 501 (1978) 232.
[9] M.D. Ediger and M.D. Faver, J. Chem. Phys. 78 (1983) 2518.
[10] D.A. Bryant, G. Guglielmi, N.T. deMarsac, A.M. Castets and G. Cohen-Bazire, Arch. Microbiol. 123 (1979) 113.
[11] A.N. Glazer, Mol. Cellular Biochem. 18 (1977) 125.
[12] B. Zickendraht-Wendelstadt, J. Friedrich and W. Rudiger, Photochem. Photobiol. 31 (1980) 367.
[13] G. Paillotin, C.E. Swenberg, J. Breton and N.E. Geacintov, Biophys. J. 25 (1979) 513.

[14] B.A. Zilinskas and D.A. Howell, Plant Physiol. 71 (1983) 379.
[15] R.R. Troxler, L.S. Greenwald and B.A. Zilinskas, J. Biol. Chem. 255 (1980) 9380.
[16] R. van Grondelle, C.N. Hunter, J.G.C. Bakker and H.J.M. Kramer, Biochem. Biophys. Acta 723 (1983) 30.
[17] N.E. Geacintov and J. Breton, in: Biological events probed by ultrafast laser spectroscopy, ed. R.R. Alfano (Academic Press, New York, 1982) pp. 158–189.
[18] A.J. Dagen, R.R. Alfano, B.A. Zilinskas and C.E. Swenberg, submitted for publication.
[19] D.F. Wong, F. Pellegrino, R.R. Alfano and B.A. Zilinskas, Photochem. Photobiol. 33 (1981) 651.

GASTROENTEROLOG

Effect of Ionizing Radiation on Gastric Secretion and Gastric Motility in Monkeys

ETIENNE DANQUECHIN DORVAL, GREGORY P. MUELLER, ROBERT R. ENG, ASAF DURAKOVIC, JAMES J. CONKLIN, and ANDRE DUBOIS

Digestive Diseases Division, Department of Medicine, Uniformed Services University of the Health Sciences; Department of Physiology, Uniformed Services University of the Health Sciences; and Nuclear Sciences Division, Armed Forces Radiobiology Research Institute, Bethesda, Maryland

The prodromal syndrome of radiation sickness is characterized by nausea and vomiting but the pathophysiology and the treatment of this entity is largely unknown. We investigated this problem by determining the effects of ionizing radiation on gastric function with and without administration of the dopamine antagonist domperidone. We measured gastric electrical control activity (waves per minute), fractional emptying rate (percent per minute), acid output (microequivalents per minute), and plasma levels of immunoreactive β-endorphin. Twelve conscious, chair-adapted rhesus monkeys were studied twice before, once immediately after, and once 2 days after a single 800-cGy (800 rads) ^{60}Co total body irradiation. In addition to causing vomiting, total body irradiation transiently suppressed gastric electrical control activity, gastric emptying and gastric secretion, while increasing plasma levels of immunoreactive β-endorphin. Domperidone had no effect on vomiting or gastric function either before or after irradiation, but it significantly increased plasma immunoreactive β-endorphin.

Emesis occurs immediately after whole body irradiation and is the most obvious and the best documented prodromal symptom of radiation sickness (1, 2). Time of onset, duration, and intensity of this vomiting depend on the species (3) as well as on the type, dose rate, and total dose of irradiation (2). These symptoms are clearly different from those observed during the intestinal syndrome, which occurs 7–15 days after irradiation and is characterized by diarrhea, often accompanied by intestinal bleeding (4).

We recently studied emesis produced in dogs by total body γ-irradiation and evaluated the concurrent effect of irradiation on gastric emptying. We also determined the efficacy of an antiemetic agent, the dopamine antagonist domperidone, on vomiting as well as its effect on gastric emptying. In this dog model, gastric emptying was suppressed during the prodromal syndrome of radiation sickness. Prevention of radiation-induced vomiting with domperidone did not improve the suppression of gastric emptying (5).

The present studies were undertaken to further examine the relation between radiation-induced vomiting and stomach function in an animal model that appears to be closer to humans in terms of brain

Received May 25, 1984. Accepted February 5, 1985.

Address requests for reprints to: Andre Dubois, M.D., Ph.D., Department of Medicine, Uniformed Services University, 4301 Jones Bridge Road, Bethesda, Maryland 20814-4799.

The present address for E. Danquechin Dorval is CHR Tours, Hopital Trousseau, 37044 Tours Cedex, France.

This research was supported in part by the Uniformed Services University of the Health Sciences Protocol No. RO-8342.

The opinions and assertions contained herein are the private ones of the authors and are not to be construed as official or reflecting the views of the Department of Defense or the Uniformed Services University of the Health Sciences.

The experiments reported herein were conducted according to the principles set forth in the "Guide for the Care and Use of Laboratory Animals," Institute of Animal Resources, National Research Council, DHEW Publ. No. (NIH) 78-23.

The authors thank Dr. J. Long and M. Morton, Janssen R and D Inc., N.J., for their generous supply of domperidone and placebo. The authors also thank M. Flynn, J. Stewart, J. Warrenfeltz, and N. L. Fleming for their valuable support in animal handling and radiopharmaceutical preparation, and J. Barchers for her expert editorial assistance.

Abbreviations used in this paper: DTPA, diethylene triamine pentaacetic acid; ECA, electrical control activity; FER, fractional emptying rate; iβ-END, immunoreactive β-endorphin.

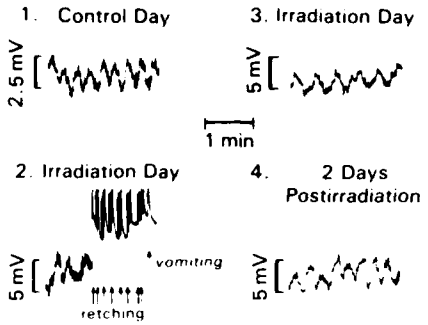

Figure 1. Examples of recording of electrical control activity obtained from abdominal bipolar electrode in 1 monkey. 1, Control day; 2, slow activity preceding six retching episodes characterized by bursts of spastic movements of the chest and abdomen (arrows) followed by a vomitus; 3, irradiation day, no vomiting but slowing of electrical activity; 4, 2 days after irradiation; no change compared with 1.

organization and gastric function. We produced vomiting in rhesus monkeys with a single dose of total body irradiation and we measured gastric acid secretion, gastric emptying of liquids, and gastric electrical control activity (ECA) before, during, and after the acute prodromal syndrome of radiation sickness. In addition, we determined plasma levels of immunoreactive β-endorphin (iβ-END) and evaluated the effect of domperidone on each of these parameters.

Materials and Methods

Twelve conscious, chair-adapted rhesus monkeys were studied on 4 separate days after an overnight fast: (a) control day after i.v. administration of placebo, (b) control day after i.v. administration of domperidone (1.0 mg/kg body wt), (c) irradiation day after administration of either placebo or domperidone, and (d) 2 days after irradiation (no drug given). This dose of domperidone was selected based on previous experiments in the dog showing that similar doses did not produce any side effect. Placebo and domperidone were given blindly and in random order on control days. Studies were performed in the morning and started 30 min after drug administration and 20 min after either sham irradiation on control days or after irradiation on irradiation day. On control days, the animals were brought to the exposure room and the doors were closed for 3 min. On irradiation day, each monkey was exposed to 800 cGy (800 rads) total body irradiation delivered at 500 cGy/min by two large, 10^5 Ci ^{60}Co irradiators placed anteriorly and posteriorly. Phantom studies demonstrated that the midline abdomen received 800 cGy and that the head received 600 cGy.

Each monkey was visually monitored for 3 h on control days and 6 h on irradiation days. Bipolar electrical potentials were recorded from two abdominal disposable skin electrodes on a multichannel recorder (Beckman R612, Beckman Instruments, Schiller Park, Ill.). Abdominal bipolar recordings displayed periodic waves in the 3-min range that have been shown to correlate with gastric ECA when gastric serosal electrodes were used in conjunction with skin electrodes (6,7). Each fasting and postload tracing was examined blindly by one of us (E. D. D.). First, the total duration during which gastric waves could be counted was determined by visual inspection (e.g., Figure 1, panels 1, 3, and 4). Of the 96 tracings obtained (12 monkeys studied on 4 separate days during fasting and after the load), 77 (80%) could be completely analyzed. Within each tracing, artifacts due to intragastric mixing or movements of the animals (e.g., retching and vomiting; Figure 1, panel 2) made the recording inadequate during ~10% of the time. Mean fasting and postload frequencies obtained in each animal on each study day were used to compute the grand mean (±SE) for each type of study in each group of animals.

Vomiting was defined as a succession of strong and brief contractions of thoracic and abdominal muscles leading to the expulsion of gastric contents through the mouth; retching was defined as a nonproductive vomiting (8). During both events, recordings displayed a succession of brief bursts of high potential spikes (Figure 1) that were clearly different from the movement artifacts that were sometimes superimposed.

A previously described and validated marker dilution technique (9,10) was used concurrently to determine gastric secretion and gastric emptying during a 40-min fasting period and for 60 min after the injection of an 80-ml water load (postload period). In the present studies, this technique was slightly modified in that ^{99m}Tc-DTPA (diethylene triamine pentaacetic acid) was used instead of phenol red as the marker. This intubation method requires only the sequential sampling of the gastric contents and permits concurrent measurement of intragastric volume, gastric emptying, and gastric secretion. A 12F double-lumen nasogastric tube was placed in the stomach and its position was verified by the water recovery test (11). Starting 45 min later, samples of the mixed gastric contents were aspirated just before and immediately after intragastric administration of 5–20 ml of a ^{99m}Tc-DTPA test solution (30 μCi/100 ml H_2O; pH 7.4; 37°C) and were centrifuged. The clear supernatant of each sample was assayed for ^{99m}Tc-DTPA concentrations using an Ultrogamma autogamma counter (LKB Instruments, Turku, Finland) and for titratable acidity using electrometric titration to pH 7.4 (Radiometer, Copenhagen, Denmark). These determinations were repeated every 10 min during the basal period and after intragastric instillation of an 80-ml water load containing ^{99m}Tc-DTPA (3 μCi/100 ml; pH 7.4; 37°C).

Intragastric volumes of fluid (V_1, V_2, ...) and amounts of ^{99m}Tc-DTPA (Tc_1, Tc_2, ...) were determined at the time of each sampling using the dilution principle (9,10,12,13). Fractional emptying rate (g) was then determined for each 10-min interval (t) between two dilutions, assuming that emptying was a first-order process (exponential) during a given 10-min interval and using the following equation:

$$g = -[\log_e (Tc_2/Tc_1)]/t.$$

Because g is allowed to vary from interval to interval, no general assumption has to be made regarding emptying

Table 1. Effect of Domperidone and Irradiation on Gastric Electrical Activity in Cycles per Minute (Mean ± SE)

	Control day		Irradiation day		
	Placebo	Domperidone	Placebo	Domperidone	2 days after irradiation
Fasting period	3.31 ± 0.10 (n = 12)	3.37 ± 0.12 (n = 9)	2.86 ± 0.19[a] (n = 5)	2.66 ± 0.18[a] (n = 5)	3.11 ± 0.09 (n = 11)
Postload period	3.19 ± 0.09 (n = 11)	3.15 ± 0.11 (n = 7)	2.60 ± 0.18[a] (n = 3)	2.5 ± 10.17[a] (n = 4)	3.03 ± 0.11 (n = 9)

[a] $p < 0.05$ compared with corresponding value on control day.

over the total duration of the experiment. Net fluid output (R_v) in milliliters per minute was then determined for the corresponding interval, assuming that it remained constant over the given interval and using the following equation:

$$R_v = [V_2 - V_1 \cdot \exp(-gt)] \cdot g[1 - \exp(-gt)].$$

Intragastric volumes of fluid and masses of ^{99m}Tc-DTPA were then recalculated, taking into account these first estimates of fractional emptying and fluid output, which were in turn recalculated. This iterative process was repeated until the improvement of the solution became < 1% per iteration. Having previously determined intragastric concentrations of acid (A_1, A_2, . . .), we then calculated net acid output (R_A) using the following equation:

$$R_A = [V_2 \cdot A_2 - V_1 \cdot A_1 \cdot \exp(-gt)] \cdot g[1 - \exp(-gt)].$$

These calculations were performed using a locally developed program and a PDP-10 computer (Division of Computer Research and Technology, National Institutes of Health, Bethesda, Md.). The assumptions involved have been described and discussed elsewhere (9,10) and are based on the original contributions by Hildes and Dunlop (12) and by George (13). In contrast to their method, however, the present technique allows correction for emptying and secretion occurring during the 1-min dye dilution interval and can be applied during fasting. On irradiation day, intervals with occurrence of vomiting were not taken into account for calculation of g, R_V, or R_A.

Plasma concentrations of iβ-END were determined at the start and at the end (i.e., 2 h after sham irradiation or true irradiation) of each study using a previously described radioimmunoassay (14). Briefly, the antibody used (C-55) recognizes the region of β-END$_{1-9}$ corresponding to amino acids 17 through 26 and, therefore, detects all β-END peptides, as well as β-lipotropin, on an equimolar basis. Addition of increasing amounts of dog plasma in the assay resulted in measureable amounts of iβ-END which paralleled β-END$_{1-9}$ standard (Peninsula Labs, Inc., San Carlos, Calif.).

The statistical significance of differences observed for each measurement of gastric function [e.g., fractional emptying rate (FER), acid output] was evaluated using a three-factor (treatment, time, and monkey) analysis of variance with repeated measures on the last two factors (9,10), the program LDU-040 (K.L. Dorn), and an IBM 370 computer (Division of Computer Research and Technology, National Institutes of Health, Bethesda, Md.).

Results

No vomiting or retching was observed on control days, i.e., after sham irradiation. On irradiation day, episodes of retching or vomiting, or both, were observed and recorded (Figure 1) in 5 of 6 monkeys in the placebo group and in all the monkeys in the domperidone group. In both treatment groups, these episodes started 29 ± 3 min (mean ± SE) and ended 71 ± 9 min after irradiation. During fasting, 1 monkey in each group exhibited retching alone and 9 had retching associated with vomiting (4 after placebo and 5 after domperidone); 4 monkeys vomited once, 2 vomited twice, 2 vomited three times, and 1 vomited four times. After intragastric administration of the water load, retching was never observed alone and only 6 of 12 monkeys had retching and vomiting; when present, vomiting occurred only once and always in monkeys who had already vomited during fasting. By 2 days after irradiation, vomiting occurred in only 1 monkey; this was at the end of the study and after most of the stomach contents had been aspirated.

Fasting gastric ECA is depicted in Figure 1; ECA was 3.31 ± 0.10 per minute on control days after the placebo and was not significantly altered by domperidone (Table 1). Electrical control activity was significantly decreased after irradiation, and returned to control level 2 days after irradiation (Figure 1 and Table 1). Electrical control activity tended to be lower after the water load but the difference was not statistically significant.

Values for the FER of liquids are shown in Table 2 and in Figure 2. On control days, the FER was stable during the fasting period but more than doubled after the water load compared with fasting; this response was not significantly affected by domperidone treatment. On irradiation day, fasting FER was suppressed as soon as the study started (20 ± 2 min after exposure) and was not significantly stimulated by either the water load or domperidone. As a result, there was virtually no emptying of the water load on irradiation day in the absence of vomiting (Figure 3). A significant ($p < 0.05$) correlation ($r = 0.60$) was

Table 2. Effect of Domperidone and Irradiation on Fractional Emptying Rate, Acid Output, and Fluid Output

	Control day		Irradiation day		
	Placebo	Domperidone	Placebo	Domperidone	2 days after irradiation
FER (% *min*)					
Fasting (1)	4.1 ± 1.3	3.0 ± 1.2	0.4 ± 0.3[a]	0.3 ± 0.3[a]	3.4 ± 1.5
Fasting (2)	5.5 ± 1.2	3.9 ± 1.3	0.3 ± 0.2[a]	0.6 ± 0.3[a]	3.3 ± 1.2
Postload	11.8 ± 1.8	11.3 ± 1.3	0.8 ± 0.2[a]	1.3 ± 0.4[a]	12.9 ± 2.2
AO (*μEq min*)					
Fasting (1)	8.5 ± 3.0	8.8 ± 3.3	5.4 ± 2.2	3.2 ± 1.0	15.2 ± 6.5
Fasting (2)	9.7 ± 3.8	8.1 ± 4.5	0.0 ± 0.0[a]	0.0 ± 0.0[a]	14.6 ± 5.0
Postload	24.4 ± 7.0	21.1 ± 8.4	1.6 ± 1.6[a]	0.0 ± 0.0[a]	27.8 ± 8.1
FO (*ml min*)					
Fasting (1)	0.21 ± 0.06	0.16 ± 0.04	0.40 ± 0.12	0.30 ± 0.06	0.24 ± 0.06
Fasting (2)	0.20 ± 0.04	0.14 ± 0.03	0.23 ± 0.06	0.27 ± 0.06	0.24 ± 0.06
Postload	0.30 ± 0.04	0.29 ± 0.04	0.12 ± 0.01	0.13 ± 0.02	0.23 ± 0.05

AO, acid output; FER, fractional emptying rate; FO, fluid output. Fasting (1) corresponds to the period 0–20 min after the start of the study; on the day of irradiation, this period was 20–40 min after exposure. Fasting (2) corresponds to the period 20–40 min after the start of the study; on the day of irradiation this period was 40–60 min after exposure. Values are mean ± SE. [a] $p < 0.05$ compared with corresponding value on control day.

found between gastric ECA and mean postload FER of the stomach, the best fit being obtained with a power curve ($ECA = 3.0 \times FER^{0.021}$).

Acid output was significantly stimulated after the load compared with fasting on control days (Figure 4); domperidone did not significantly modify either fasting or postload acid output. After irradiation, acid output was suppressed in all the monkeys who had secreted on control day; the suppression started 39 ± 4 min after irradiation, persisted after load stimulation, and was not affected by domperidone (Table 2). Interestingly, acid output was not abolished in the only monkey who did not retch or vomit after irradiation.

Fluid output was significantly stimulated after the load compared with fasting on control days. After irradiation, fasting fluid output tended to be increased compared with control days, but the difference was statistically significant only in the domperidone group. After the load, fluid output was significantly suppressed in all monkeys (Table 2).

As domperidone had no significant effect on emptying, acid output, or fluid output, either in the control state or after irradiation (Table 2), values were averaged for all 12 monkeys and are depicted in Figures 2–4. Two days after irradiation, all gastric parameters had returned to control day levels, even in the monkey who had vomited on that day.

As shown in Table 3, plasma levels of iβ-END were elevated markedly by domperidone and by irradiation with placebo; the effects of radiation and the drug were additive. Two days after irradiation, plasma concentrations of iβ-END returned to basal values. Plasma levels of iβ-END were significantly ($p < 0.05$) and inversely correlated with all gastric parameters (FER: r = 0.63; ECA: r = 0.61; acid output: r = 0.71).

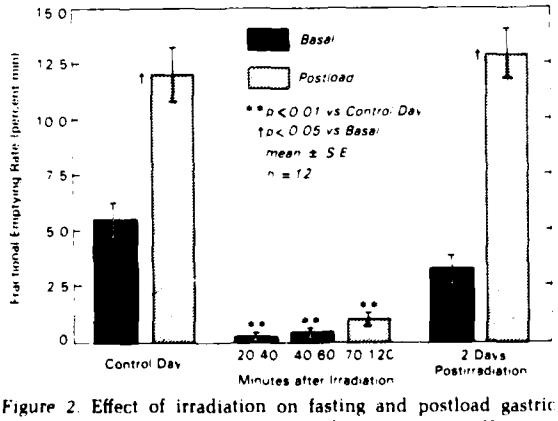

Figure 2. Effect of irradiation on fasting and postload gastric fractional emptying rate. Values are mean ± SE.

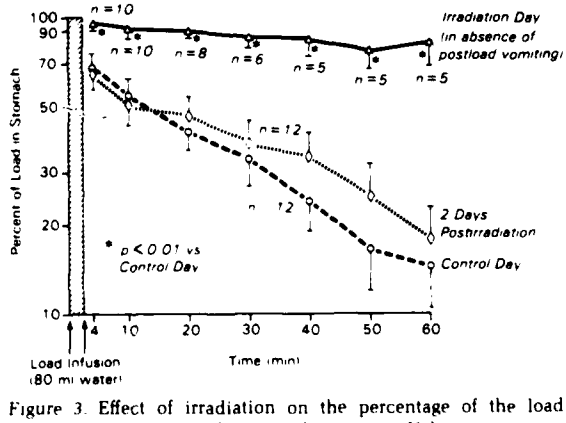

Figure 3. Effect of irradiation on the percentage of the load remaining in the stomach over time. Values are mean ± SE.

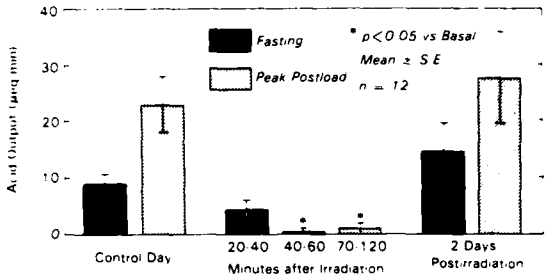

Figure 4. Effect of irradiation on basal and load-stimulated acid output. Values are mean ± SE.

Discussion

In the present studies, we report the precise and objective measurements of the immediate occurrence of retching and vomiting in rhesus monkeys exposed to total body irradiation, as well as the relation between these events, gastric function, and pituitary iβ-END secretion.

The visual distinction between retching and vomiting may be difficult in fasting monkeys, although it is easy in the presence of a large vomitus of food. Animals can either store a small vomitus into their cheek pouches and then swallow it, or they can emit some foamy saliva after a nonproductive retching. In the present studies, recording of skin potential helped in differentiating between these two types of events, demonstrating retching and vomiting in 9 of the 12 monkeys and retching alone in only 2 monkeys. This dose of 800 cGy has been selected because it is twice the ED_{50} for vomiting as previously determined by others for monkeys (1,8). Retching and vomiting started after a delay of ~30 min and disappeared after 70 min, which agrees with the observations of Middleton and Young (1) for similar doses of exposure, but markedly differ from a delay of almost an hour with doses between 400 and 550 cGy (1) and a delay of <5 min after a dose of 1200 cGy (8). Thus, the interval between irradiation and vomiting appears to be inversely proportional to the dose received.

The incidence of vomiting after irradiation appears to increase if monkeys are fed solid food 1–2 h before irradiation (8). In our study, however, a 16-h fast before irradiation does not appear to have reduced the incidence of this "radioemesis"; moreover, intragastric administration of a water load after irradiation is associated with only 6 vomiting episodes versus 18 during fasting, suggesting that the incidence of radioemesis is actually decreased by gastric distention with noncaloric liquids when irradiation is delivered at a high dose rate (500 cGy/min).

Gastric ECA may be recorded via skin electrodes as first described in 1922 (quoted in Reference 15). The frequency of this cutaneous electrogastrogram is correlated with the slow-wave frequency recorded from gastric serosal electrodes (6,7,16–18). In the present studies, the frequency of ECA was significantly decreased on the day of irradiation and had returned to basal values 2 days later; this observation has been confirmed by preliminary results obtained in monkeys with implanted gastric serosal electrodes (7). The radiation-induced decrease of ECA frequency accompanies a concurrent decrease of gastric FER both during fasting and after the load. This latter finding is similar to that observed in dogs (5,19) and in rats (20).

Our observations demonstrate that ionizing radiation has a different effect on gastric acid output and on nonparietal secretions. Immediately after irradiation, acid output is suppressed both during fasting and after a water load (Table 2 and Figure 4). This suppression of acid could be due to ultrastructural changes of parietal cells similar to those observed in the mouse within 30 min of exposure (21), but it is clearly different from the hypochlorhydria due to gastric atrophy that appears several weeks after irradiation (22–24). In contrast, fluid output is suppressed only after the water load, whereas it remains unchanged or even tends to increase during fasting (Table 2). Thus, fasting nonparietal fluid secretions appear to be increased immediately after irradiation, thereby masking the concurrent suppression of the parietal component of fluid output. As nonparietal secretions are not stimulated after a water load (9), no change of fluid output is expected during the postload period if acid output is suppressed. In fact, the significant decrease of fluid output after the water load indicates that the effect of irradiation on nonparietal secretions is biphasic, consisting of an initial stimulation followed in 40 min by an inhibition of fluid output. Two days later, however, both parietal and nonparietal secretions have returned to basal values.

The relation between radiation-induced emesis and gastric inhibition is unclear. As acid suppression starts at about the same time as vomiting and persists after its disappearance, these two symptoms may be closely related; this possibility is also sup-

Table 3. *Effect of Irradiation on Plasma Immunoreactive β-Endorphin in Picograms per Milliliter (Mean ± SE)*

Control day		125 min after irradiation		2 days after irradiation
Placebo	Domperidone	Placebo	Domperidone	
229 ± 48	881 ± 88[a]	1447 ± 228[b]	3389 ± 702[a,b]	159 ± 43

[a] $p < 0.05$ compared with placebo [b] $p < 0.01$ compared with control day.

ported by our anecdotal finding that acid output was unchanged after irradiation in the only monkey that did not retch or vomit. In contrast, radiation-induced suppression of gastric emptying and of ECA is observed even in the 2 monkeys that did not vomit; furthermore, in the animals that did vomit, gastric emptying suppression starts before, and persists after disappearance of, emesis. Thus, radiation-induced slowing of gastric emptying may appear independently from vomiting.

The mechanism of radiation-induced emesis and gastric inhibition is probably multifactorial. The central nervous system appears to play a pivotal role in these symptoms, as suggested by the rise of plasma iβ-END observed after irradiation. This rise is similar to that observed after exposure to physical stress (25,26) and could be responsible for the observed vomiting and gastric inhibition (27,28). It is probably due to the fact that irradiation activates the peripheral end of afferent nerves or, alternatively, causes the release of humoral or toxic substances. A direct effect of irradiation on the brain appears excluded by the observation that shielding of the chemoreceptor trigger zone does not prevent radiation-induced vomiting (15).

Our observation that, in the monkey, domperidone does not prevent vomiting induced by 800-cGy ^{60}Co total body irradiation, whereas it is effective in the dog (5), could be related to the two major relevant differences that are known to exist between these two animal models: the ED_{50} for radiation-induced vomiting is lower in the dog than in the monkey (3) and, in addition, the dopamine receptor agonist apomorphine causes vomiting in dogs but not in monkeys (29). Thus, the sensitivity of dopamine receptors to their agonists and antagonists could be lesser in monkeys than in dogs. Alternatively, the blood-brain barrier surrounding the vomiting center and the chemoreceptor trigger zone may be considerably more permeable to domperidone and apomorphine in the dog as compared with the monkey. The ability of domperidone to significantly increase circulating levels of iβ-END without altering vomiting or gastric function indicates that changes in blood-borne iβ-END *do not solely account for the effects of* radiation on gastric function. These findings, however, are consistent with the demonstration that dopaminergic receptor blockade results in the release of pituitary iβ-END in both dogs and rats (30,31); taken together, they suggest that dopaminergic inhibition of pituitary iβ-END release is a common feature among mammals.

In conclusion, radiation-induced emesis is accompanied by a suppression of gastric emptying and acid secretion. The concurrent slowing of gastric ECA suggests that an alteration of the motility of the stomach is responsible for the suppression of gastric emptying. The time of onset of each symptom after irradiation and the transiency of the acute prodromal syndrome to radiation sickness suggest the involvement of neural or neurohormonal mechanisms, or both, or a receptor inactivation (32). The release of pituitary iβ-END demonstrated by the present studies could mediate these effects and, in addition, clearly indicates an alteration of brain function. Thus, the central nervous system appears to play a pivotal role in the digestive symptoms that immediately follow total body irradiation.

References

1. Middleton GR, Young RW. Emesis in monkeys following exposure to ionizing radiation. Aviat Space Environ Med 1975;46:170–2.
2. Conard RA. Some effects of ionizing radiation on the physiology of the gastrointestinal tract: a review. Radiat Res 1956; 5:167–88.
3. Cordts RE. Animal-model studies of radiation-induced emesis and its control. USAF School of Aerospace Medicine 1982;SAM-TR-82-26.
4. Bond VP, Swift MN, Allen AC, Fishler MC. Sensitivity of abdomen of rat to x-irradiation. Am J Physiol 1950;161:323–30.
5. Dubois A, Jacobus JP, Grissom MP, Eng R, Conklin JL. Altered gastric emptying and prevention of radiation-induced vomiting in dogs. *Gastroenterology* 1984;86:444–8.
6. Smout AJPM, van der Schee EJ, Grashuis JL. What is measured in electrogastrography? Dig Dis Sci 1980;25:179–87.
7. Laporte JL, O'Connell L, Durakovic A, Sjogren R, Conklin JL, Dubois A. Cross correlation analysis of gastric motility following exposure to ionizing radiation in primates (abstr). Dig Dis Sci 1984;29:565A.
8. Mattson JL, Yochmowitz MG. Radiation-induced emesis in monkeys. Radiat Res 1980;82:191–9.
9. Dubois A, Natelson GH, van Eerdewegh P, Gardner JD. Gastric emptying and secretion in the rhesus monkey. Am J Physiol 1977;232:186–92.
10. Dubois A, van Eerdewegh P, Gardner JD. Gastric emptying and secretion in Zollinger-Ellison syndrome. J Clin Invest 1977;59:255–64.
11. Findlay JM, Prescott RJ, Strous W. Comparative evaluation of water recovery test and fluoroscopic screening in positioning a nasogastric tube during gastric secretory studies. Br Med J 1972;4:458–61.
12. Hildes JA, Dunlop DL. A method for estimating the rates of gastric secretion and emptying. Can J Med Sci 1951;29:83–9.
13. George JD. *New clinical method for measuring the rate of* gastric emptying: the double sampling test meal. Gut 1968; 9:247–52.
14. Mueller GP. Attenuated β-endorphin release in estrogen-treated rats. Proc Soc Exp Biol Med 1980;165:77–81.
15. Chinn HI, Wang SC. Locus of emetic action following irradiation. Proc Soc Exp Biol Med 1954;85:472–7.
16. Smout AJPM. Myoelectric activity of the stomach: gastroelectromyography and electrogastrography. thesis. Delft, Netherlands: Delft University Press; 1980.
17. Geldof H, van der Schee EJ, van Blankenstein M, et al. Gastric dysrhythmia: an electrogastrographic study. (abstr). Gastroenterology 1983;84:1163.
18. Kim MS, Lee YI, Park HI, Choi H. Role of prostaglandins on

experimental tachygastria in cats (abstr). Gastroenterology 1983;84:1208.
19. Conard RA. Effect of gamma radiation on gastric emptying time in the dog. J Appl Physiol 1956;9:234–6.
20. Hulse EV. Gastric emptying in rats after part-body irradiation. Int J Radiat Biol 1966;10:521–32.
21. Helander HF. Early effects of x-irradiation on the ultrastructure of gastric fundus glands. Radiat Res 1965;26:244–62.
22. Regaud C, Nogier T, Lacassagne A. Sur les effets redoutable des irradiations etendues de l'abdomen et sur les lesions du tube digestif determinees par les rayons de rontgen. Arch Elect Med 1912;21:321–34.
23. Ivy AC, Orndoff BH, Jacoby A, Whitlow JE. Studies of the effect of x-rays on glandular activity. III. The effect of x-rays on gastric secretion. Radiology 1923;1:39–46.
24. Palmer WL, Templeton F. The effect of radiation therapy on gastric secretion. JAMA 1939;112:1429–34.
25. Guillemin R, Vargo T, Rossier J, et al. β-Endorphin and adrenocorticotropin are secreted concomitantly by the pituitary gland. Science 1977;197:1367–9.
26. Rossier J, French E, Rivier C, Ling N, Guillemin R, Bloom F. Foot-shock induced stress increases β-endorphin in rat blood but not brain. Nature 1977;270:618–20.
27. Dubois A, Natelson BH. Habituation of gastric function suppression in monkeys after repeated free-operant avoidance sessions. Physiol Psychol 1978;6:524–8.
28. Shea-Donohue PT, Adams N, Arnold J, Dubois A. Effects of Met-enkephalin and naloxone on gastric emptying and secretion in rhesus monkeys. Am J Physiol 1983;245:G196–200.
29. Brizzee KR, Neal LM, Williams PM. The chemoreceptor trigger zone for emesis in the monkey. Am J Physiol 1955; 180:659–62.
30. Sharp B, Kasson B, Marshak D, et al. Domperidone elevates rat plasma β-endorphin-immunoreactivity when administered peripherally but not intracerebroventricularly. Life Sci 1982;31:981–5.
31. Sharp B, Ross R, Levin E, Sowers J. Dopamine regulates canine plasma β-immunoreactivity levels. Endocrinology 1982;110:1828–30.
32. Garvey TZ, Kempner ES, Steer CJ, et al. Molecular sizes of receptors for vasoactive intestinal peptide (VIP) and secretin determined by radiation inactivation (abstr). Gastroenterology 1982;82:1064.

RADIATION RESEARCH 103, 158–162 (1985)

Radiation Effects on Diamine Oxidase Activities in Intestine and Plasma of the Rat[1]

MELVIN J. ELY,[2] JAMES M. SPEICHER, GEORGE N. CATRAVAS, AND STEPHEN L. SNYDER

Biochemistry Department, Armed Forces Radiobiology Research Institute, Bethesda, Maryland 20814-5145

ELY, M. J., SPEICHER, J. M., CATRAVAS, G. N., AND SNYDER, S. L. Radiation Effects on Diamine Oxidase Activities in Intestine and Plasma of the Rat. *Radiat. Res.* **103**, 158–162 (1985).

Diamine oxidase (DAO; EC 1.4.3.6) activity was measured in plasma and in ileal tissue homogenates prepared from male Sprague–Dawley rats euthanized at 1–15 days after acute whole-body irradiation with 14.5-MeV electrons. Animals irradiated with 1 Gy showed no diminution in plasma and ileal DAO activities through Day 13 relative to nonirradiated controls. Animals irradiated with 5, 10, and 12 Gy displayed marked declines in ileal DAO activity, with levels reaching a nadir on Day 3. This was paralleled by a decrease in plasma DAO activity in all three dose groups. Recovery of ileal and plasma DAO levels was later seen as early as Day 4 in animals irradiated with 5- and 10-Gy doses, but animals receiving 12 Gy did not survive beyond Day 3. The relationship between radiation dose and levels of plasma and ileal DAO on Day 3, the time of maximum decrease at all doses, was also investigated. Ileal DAO activity decreased almost linearly between 2 and 8 Gy. Plasma DAO activity closely paralleled the dose dependency of the ileal levels. These data suggest that plasma DAO activity might be useful as a biologic marker of intestinal epithelial injury and recovery after acute radiation exposure.

INTRODUCTION

The levels of biological constituents found in the serum and urine of animals can be markedly altered following whole-body exposure to ionizing radiation (*1–3*). In some cases these alterations directly reflect radiation-induced biochemical damage at the molecular or subcellular level (*4, 5*), while changes observed in certain serum proteins most likely represent a nonspecific response to stress (*6*). Even though changes in metabolites and proteins in physiologic fluids are potential indicators of the extent of injury and of the total dose received, estimates of radiation trauma rely principally on clinical manifestation and hematologic changes (*7*). Furthermore, none of the biological indicators of radiation injury studied to date directly reflect the degree of mucosal injury and recovery following acute exposure. Also, they do

[1] Research was conducted according to the principles enunciated in the *Guide for the Care and Use of Laboratory Animals* prepared by the Institute of Laboratory Animal Resources, National Research Council.

[2] Present Address: Medical Division, USS FRANK CABLE, (AS-40), FPO Miami, FL 34086.

0033-7587/85 $3.00

not permit differentiation between concomitantly developing bone marrow hypoplasia and gastrointestinal damage. The ability to monitor the degree of damage to the intestinal epithelium (as distinct from other injury) is particularly important in assessing the status of an exposed individual, when one considers that (a) the intestinal epithelium is approximately as radiosensitive as bone marrow and (b) a close association exists between the functional efficiency of the gastrointestinal and hematopoietic systems and the development of the full acute radiation syndrome (*8, 9*).

Several recent investigations (*10–12*) have shown that levels of intestinal mucosal diamine oxidase [DAO; EC 1.4.3.6] decrease with progressive mucosal injury and increase with subsequent recovery, and that DAO activity in the plasma follows a parallel course. Thus changes in plasma DAO activity may be a relatively specific marker of intestinal injury and regeneration in the rat and in the human (*10, 11*). The present investigation was designed to assess whether the use of plasma DAO activity might be useful as a marker of the integrity of the intestinal epithelium after radiation exposure. Such a marker would make possible, through blood sampling, the clinical evaluation of radiation-induced gastrointestinal damage and the efficacy of measures designed to minimize that damage.

METHODS

Male Sprague–Dawley rats (Taconic Farms), 150–250 g, were irradiated with 14.5-MeV electrons delivered from the AFRRI linear accelerator. Pulse duration was 4 μsec, and pulses were delivered at a rate of 15/sec. Dose rate was approximately 7 cGy per pulse (60 Gy/min, 1 Gy = 100 rad). Dosimetry was accomplished by using a 0.05 cm^3 tissue-equivalent ion chamber whose calibration is traceable to the National Bureau of Standards. Animals were maintained throughout the experiment on Wayne Lab-Blox rat chow and acidified water *ad libitum*.

Animals were euthanized by cervical dislocation, and blood was withdrawn by draining through the vena cava into Vacutainer heparinized tubes. Plasma was obtained by centrifugation of the blood at 3000*g* for 20 min. The distal third of the small intestine, designated ileum, was removed. It was rinsed briefly and homogenized in 9 vol of ice-cold Sorensen's phosphate buffer, pH 7.4. The tissue homogenates were then centrifuged at 15,000*g* for 20 min to remove particulate matter. They were then stored, along with plasma, at −80°C until use. Protein was determined by the method of Lowry *et al.* (*13*).

The assay of DAO activity was based on the method of Okuyama and Kobayashi (*14*) as modified by Beaven and Shaff (*15*). Briefly, tissue homogenates and plasma samples were incubated with [^{3}H]putrescine (New England Nuclear Corp., Boston, MA; 27 pmole/liter μCi) in Sorensen's phosphate buffer (pH 7.4) for 1 and 3 hr, respectively, at 37°C. The concentration of putrescine was 1 m*M* for tissue homogenate assays and 0.01 m*M* for plasma assays; the final assay volume was 0.2 ml. At the end of the incubation, 0.2 ml of an aminoguanidine solution (4×10^{-5} *M*) in Sorensen's buffer was added to stop the reaction. The labeled product was extracted from the incubation mixture directly into 2.0 ml of a PPO–POPOP[3] and toluene scintillation mixture, and a 1.0-ml portion was assayed for radioactivity.

RESULTS AND DISCUSSION

Plasma DAO activity appears to come primarily from the small intestine in many mammalian species, including the rat and man (*10, 16*). In the rat, the mucosa is the site of highest DAO activity in the small intestine. This mucosal activity is associated with the mature villous tip absorptive cells rather than the proliferating crypt cells (*17*). Radiation damage to the small intestine is characterized by injury

[3] PPO = 2,5-diphenyloxazole; POPOP = 1,4-bis-2-(5-phenyloxazolyl)benzene.

to the crypt stem-cell populations, resulting in a decreased population of mature villous cells. As a result of this epithelial-cell attrition without renewal, one expects to observe a decline in DAO activity of both the intestinal mucosa and the plasma, thus paralleling the decrease in population of mature villous cells. Our results confirm this expectation.

Figure 1 shows the effect of acute radiation exposure on ileal mucosal and plasma DAO activities in the rat. No diminution in these DAO activities was observed within 13 days after irradiation with a dose of 1 Gy. Following a dose of 5 Gy, however, mucosal DAO levels fell markedly to less than 40% of basal levels by Day 3, with subsequent recovery by Day 5. This time course is similar to that observed for morphologic and physiological changes that indicate mucosal injury and recovery (*18, 19*). The loss and subsequent recovery of plasma DAO activity following a 5-Gy dose paralleled that of mucosal DAO activity. Although plasma DAO levels also reached a nadir on Day 3, complete recovery was not evident through the remainder of the 15-day observation period, with the maximum DAO activity at 80% of control levels on Day 9. A similar pattern was seen in animals irradiated with 10 Gy. Both ileal mucosal activities and plasma DAO activities reached a minimum on Day 3 and then gave signs of recovery through Day 6. Death of irradiated animals prevented observation beyond this time. Similarly, animals irradiated with 12 Gy failed to survive beyond Day 3, although the precipitous decline in levels of both mucosal and plasma DAO activity was again observed during these first 3 days postirradiation.

Figure 2 shows the relationship between radiation dose and levels of plasma and mucosal DAO activity on Day 3, the time of maximum decrease at all doses tested. Relative to nonirradiated control animals, mucosal DAO activities decreased almost linearly between 2 and 8 Gy (presumably reflecting increasing mucosal injury), after

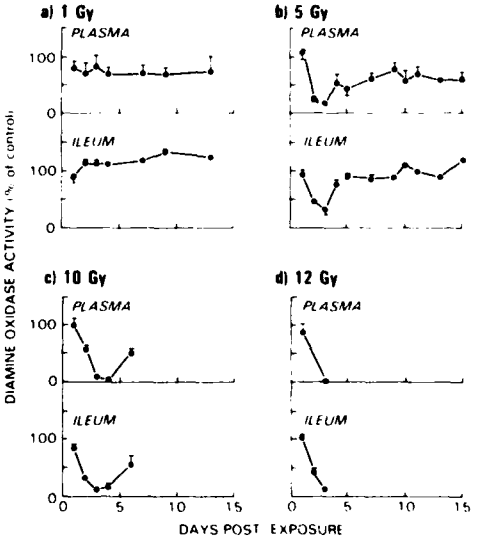

FIG. 1. Effect of acute radiation exposure on ileal and plasma DAO activities in the rat. Each point represents the mean of data from five animals; bars indicate ±1 SEM.

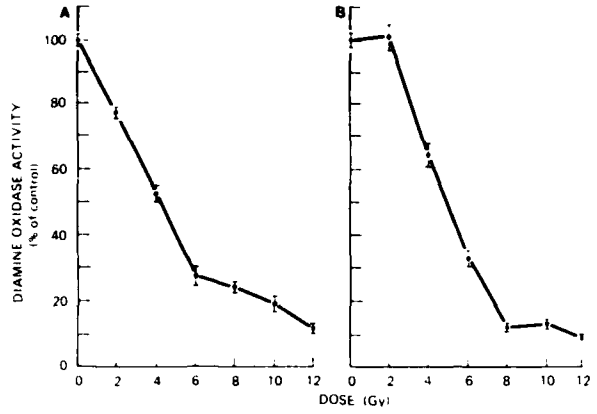

FIG. 2. Effect of increasing radiation doses on plasma (2A) and ileal (2B) DAO activities in the rat 3 days after exposure. Each point represents the mean of data from five animals; bars indicate ±1 SEM.

which no further decrease was observed. Except for the absence of a shoulder between 0 and 2 Gy, plasma DAO levels closely paralleled the dose dependency of the mucosal enzyme. The dose-dependent changes in DAO activity shown in Fig. 2 cannot be accounted for on the basis of loss of protein, since decreases in protein were observed only at the higher doses, and these appeared to be minimal. For example, the protein found in the gut homogenates decreased from a control value of 6.82 ± 0.10 mg/ml to 5.80 ± 0.20 mg/ml or 15% in samples obtained from rats exposed to 10 Gy. Likewise, protein found in plasma samples decreased by only 8% following exposure to 10 Gy.

These data suggest that DAO activity may serve as a useful plasma marker of mucosal integrity in the irradiated rat. Although the significance of these data for irradiated humans was not investigated, recent studies have shown the potential of plasma DAO activity as a useful marker in the human for studying intestinal mucosal toxicity of chemotherapy (*11*) and a number of pathological conditions involving the small intestine (*12, 20*). It seems likely that plasma DAO levels would reflect the integrity of intestinal mucosa in irradiated humans.

RECEIVED: January 15, 1985; REVISED: March 29, 1985

REFERENCES

1. H. M. PATT and A. M. BRUES, The pathological physiology of radiation injury in the mammal. II. Specific aspects of the physiology of radiation injury. In *Radiation Biology* (A. Hollaender, Ed.), Vol. I, pp. 959–1028. McGraw-Hill, New York/London, 1954. [See especially pp. 964–976.]
2. S. L. SNYDER, Radiation-induced alterations in serum and splenic lysosomal hydrolases of rat. *Radiat. Res.* **69**, 306–316 (1977).
3. M. DONLON, L. STEEL, E. A. HELGESON, A. SHIPP, and G. N. CATRAVAS, Radiation-induced alteration in prostaglandin excretion in the rat. *Life Sci.* **32**, 2631–2639 (1983).
4. J. PARIZEK, M. ARIENT, Z. DIENSTBIER, and J. SKODA, Deoxycytidine in urine as an indicator of changes after irradiation. *Nature* **182**, 721–722 (1958).
5. Z. DIENSTBIER and L. BURIE, Biochemical indicators of irradiation. In *13th International Congress of Radiation, Madrid, Spain*, Vol. I, pp. 604–607, 1974.

6. A. KOJ, Acute-phase reactants and lysosomal enzymes in the blood of rats with experimental inflammation or radiation injury. *Biologica* **18**, 275–286 (1970).
7. V. P. BOND, T. M. FLIEDNER, and E. P. CRONKITE, Evaluation and management of the heavily irradiated individual. *J. Nucl. Med.* **1**, 221–238 (1960).
8. Life Sciences Research Office Staff Report: *A Study of the Metabolic Aspects of Therapy of Radiation Injury in the Soldier.* Federation of American Societies for Experimental Biology, Bethesda, 1969.
9. V. ARENA, *Ionizing Radiation and Life*, pp. 414–431. Mosby, St. Louis, 1971.
10. G. D. LUK, T. M. BAYLESS, and S. B. BAYLIN, Diamine oxidase (Histaminase): A circulating marker for rat intestinal mucosal maturation and integrity. *J. Clin. Invest.* **66**, 66–70 (1980).
11. G. D. LUK, W. P. VAUGHAN, P. J. BURKE, and S. B. BAYLIN, Diamine oxidase as a plasma marker of rat intestinal mucosal injury and regeneration after administration of 1-β-D-arabinofuranosylcytosine. *Cancer Res.* **41**, 2334–2337 (1981).
12. R. HESTERBERG, J. KUSCHE, C.-D. STAHLKNECHT, and K.-D. FEUSSNER, The start of a programme for measuring diamine oxidase activity in biopsy specimens of human rectal mucosa. *Agents Actions* **11**, 33–37 (1981).
13. O. H. LOWRY, N. J. ROSEBROUGH, A. L. FARR, and R. J. RANDALL, Protein measurement with Folin phenol reagent. *J. Biol. Chem.* **193**, 265–275 (1951).
14. T. OKUYAMA and Y. KOBAYASHI, Determination of diamine oxidase activity by liquid scintillation counting. *Arch. Biochem. Biophys.* **95**, 242–250 (1961).
15. M. A. BEAVEN and R. E. SHAFF, Study of the relationship of histaminase and diamine oxidase activities in various rat tissues and plasma by sensitive isotopic assay procedures. *Biochem. Pharmacol.* **24**, 979–984 (1975).
16. F. BUFFONI, Histamine and related amine oxidases. *Pharmacol. Rev.* **18**, 1163–1199 (1966).
17. K. M. M. SHAKIR, S. MARGOLIS, and S. B. BAYLIN, Localization of histaminase (diamine oxidase) in rat small intestinal mucosa: Site of release by heparin. *Biochem. Pharmacol.* **26**, 2343–2347 (1977).
18. H. QUASTLER, The nature of intestinal radiation death. *Radiat. Res.* **4**, 303–320 (1956).
19. R. A. CONARD, Some effects of ionizing radiation on the physiology of the gastrointestinal tract: A review. *Radiat. Res.* **5**, 167–188 (1956).
20. J. KUSCHE, T. BIEGANSKI, R. HESTERBERG, C.-D. STAHLKNECHT, K.-D. FEUSSNER, I. STAHLENBERG, and W. LORENZ, The influence of carcinoma growth on diamine oxidase activity in human gastrointestinal tract. *Agents Actions* **10**, 110–113 (1980).

Wound-induced alterations in survival of ^{60}Co irradiated mice: importance of wound timing[1,2]

G. D. Ledney, E. D. Exum and W. E. Jackson III

Immunology Division, Experimental Hematology Department, Armed Forces Radiobiology Research Institute, Bethesda (Maryland 20814, USA), 24 April 1984

Summary. Wounding mice shortly before or shortly after lethal ^{60}Co irradiation enhances survival. Survival of wounded-irradiated mice may be due to enhanced hematopoietic recovery as measured by endogenous spleen colony (E-CFU-s) formation.

Key words. Trauma; radiation; combined injury; endogenous spleen colonies.

In previous publications[3-5] we established that skin-wound trauma 24 h prior to graded doses of ^{60}Co radiation resulted in survival of mice that ordinarily would die from radiation-induced hematopoietic failure. We also examined the repopulation of hematopoietic centers with early proliferative cells [colony forming unit-spleen-(CFU-s)] and committed progenitor cells [granulocyte-monocyte colony forming cell (GM-CFC) and monocyte-macrophage colony forming cell (M-CFC)] of sublethally irradiated-wounded mice.

While radiation has been employed in mice[6,7] and rats[8] in combination with surgical or wound trauma, the timing of wounding prior to or after whole body lethal radiation doses has not been comprehensively studied in both sexes of a single species. Our previous work[9] in combined injury (radiation wound trauma) and that of others dealing with the recovery from radiation injury[10] suggests the use of the endogenous-colony forming unit spleen (E-CFU-s) assay as a potential indicator of survival and recovery from radiation damage in mice. Additionally, wound trauma alone[11] perturbs the clonogenic cell compartments of the hematopoietic system. Since hematopoietic cells are involved in restoration after lethal radiation doses, we posited that wound timing relative to radiation exposure would effect survival from the combined injury. Therefore, in the present study we determined 1) the survival of mice wounded prior to or after lethal irradiation and 2) the number of E-CFU-s in mice wounded prior to or after lethal irradiation.

Materials and methods. Female and male (C57BL/6 X CBA)F1 Cum BR mice were obtained from Cumberland View Farms, Clinton, Tennessee. All mice were acclimated to laboratory conditions as previously described[11].

Between the hours of 10.00 and 14.00, groups of mice were given 4% skin surface wounds under light methoxyflurane anesthesia. The technique for wounding was previously described[11].

Whole-body irradiations of 40 rad/min (midline tissue) from bilaterally-positioned ^{60}Co elements were performed on mice placed in plexiglass restrainers. An ionization chamber calibrated against a National Bureau of Standards ionization chamber was used for dose determinations. Radiation exposures were performed between 10.00 and 14.00 h. Irradiations of traumatized animals were appropriately timed in relation to skin wounding (see figs 1 and 2).

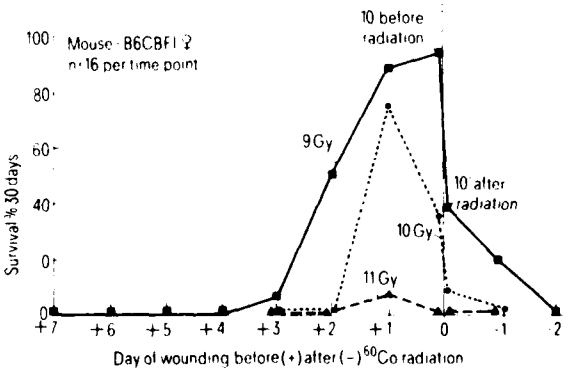

Figure 1. The 30-day survival percentages of wounded irradiated B6CBF1 female mice. At each time point indicated wounding was performed on 16 mice with the exception that 47 mice were injured 1 day after irradiation. All control-irradiated mice died (data not shown) with the exception that one mouse lived after 9.0 Gy. All control-wounded mice survived. 9.0 Gy ■—■; 10.0 Gy ●·····●; 11.0 Gy ▲ - - - ▲

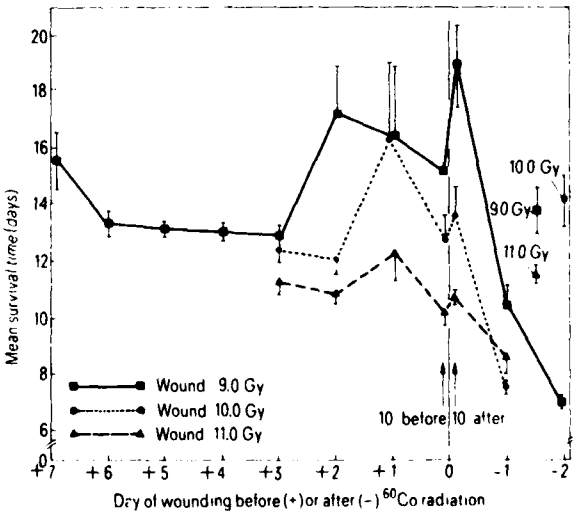

Figure 2. The mean survival times (days) of control irradiated and wounded-irradiated mice. These data reflect the survival of mice only within the 30-day observation period. See figure 1 legend for symbols.

In E-CFU-s studies, spleens were removed from mice 10 days after irradiation, placed in Bouin's solution for 4 h and the colonies counted (double-blind determinations). Presented in figure 3 are the mean values (± SEM) of two independent counts for each group of spleens.

30-day survival and E-CFU-s experiments were simultaneously performed at 9.0, 10.0, and 11.0 Gy on mouse groups given either 1) wound trauma and radiation, 2) radiation only or 3) wound trauma only. Approximately 700 mice were used in all three experiments. Survival percentages were based on groups of 16 mice each, while E-CFU-s studies were done with eight mice per group.

The survival data were analyzed as follows. The Kruskal-Wallis test [7] was used when all mice died within 30 days. The Cox F-test[8] was used when some mice within an experimental group survived (observations censored, i.e., terminated at 30 days). The chi-square test was used when comparing surviving proportions within radiation doses.

Results. Figure 1 illustrates the 30-day survival percentages of female mice wounded before or after irradiation. The mean survival times of mice dying within each of the treatment groups are depicted in figure 2.

At 9.0 Gy, wound injury performed 2 days, 1 day, 10 min before or 10 min after irradiation resulted in significant ($p < 0.01$) enhancement of survival. This was true for both survival times ($p < 0.01$) as measured by the Cox F-test and for survival percentages ($p < 0.01$ or $p < 0.05$) measured by the chi-square test. Importantly, wounding 1 day after irradiation (38 of 47 died) did not significantly contribute to the mortality percentage when compared to that of the irradiated controls (15 of 16 died). In mice given 10.0 Gy, injury sustained either 1 day or 10 min prior to irradiation produced a significant ($p < 0.01$ and $p < 0.05$, respectively) increase in survival percentage. Survival times were also significantly ($p < 0.01$) increased for injury 1 day before irradiation. Injury 1 day after 10.0 Gy significantly ($p < 0.01$) reduced the survival time from that observed for irradiated controls (14.2 ± 0.9 vs 7.6 ± 0.2 days). Injury either before or after 11.0 Gy had no significant positive or negative influence on survival percentages or survival times.

The results of E-CFU-s analysis for female mice are illustrated in figure 1. In all survival and E-CFU-s experiments, mice were irradiated simultaneously. E-CFU-s were detected after wound-irradiation time intervals and radiation doses that were associated with statistically significant increases in survival percentages or survival times. The single exception to this was when mice were wounded 10 min before 10 Gy. E-CFU-s were not detected even though survival was observed. In most instances where all the combined-injured animals died or where survival times were significantly decreased compared to irradiated controls, none or very few E-CFU-s colonies were found. However, in the case of mice wounded 1 day prior to 11.0 Gy where no enhancement of survival was found, E-CFU-s were present.

Discussion. The foregoing data support the contention that strategically timed wound trauma results in 1) an increase in the number of mice surviving lethal irradiation and 2) an increase in endogenous spleen colonies in irradiated mice which may account for the increased survival. Three important factors may be considered in interpreting our data. They are 1) sex differences in response to radiation, 2) wound contamination with bacteria and 3) mechanisms of action leading to survival or mortality.

First, the responses depicted graphically (figs 1–3) were obtained with female mice. In other experiments (data not shown) male mice of the same genetic lineage were used. Wounding before or after 9.0, 10.0, or 11.0 Gy ^{60}Co resulted in similar survival parameters. The main quantitative difference noted was that both survival percents and survival times were generally greater in male mice versus that found in female mice. This may be due to the radioresistance of male mice ($LD_{50/30}$ 8.8 Gy) compared to that of the female mice ($LD_{50/30}$ 7.9 Gy) in our laboratory (Ledney, *unpublished observations*). In E-CFU-s studies with male mice, wound trauma 24 h before and 10 min after 9.0–9.5 Gy resulted in significantly more colonies than that found in irradiated control mice. Thus, while male mice are more radioresistant, our data indicate that trauma-enhanced survival or mortality is similar in both sexes.

Secondly, it should be noted that all wounds can be potentially contaminated with bacteria. However, wound sepsis indicated by pus formation, edema, or lymph node swelling was not observed. Since irradiation depletes the antimicrobial defenses of the host, it is possible that wounding after exposure to radiation provides a portal of entry into the immune compromised host. The decreased survival fractions and survival times of mice wounded 1–2 days after irradiation are in accord with this idea. However, it is difficult to ascribe any beneficial or detrimental effect to wounds made (and potentially contaminated with bacteria) prior to radiation. Perhaps wounding prior to irradiation activates antibacterial defenses. Histologic examination of the wound site indicated granulocyte and macrophage infiltration into the margins of the wound. A 50% increase in peripheral blood granulocyte numbers was observed 1–2 days after trauma. These cellular events potentially enhance antibacterial activity. However, the beneficial value of such cellular responses would be abrogated by the subsequent radiation.

Lastly, the mechanism of action for the increases in survival or mortality are of paramount importance. These include the release of bacterial endotoxin and the elevation of prostaglandin (PGE) levels. In the combined injured animal, these mediators may be operating independently or concomitantly. Endotoxins are known modifiers of survival and hematopoietic responses in irradiated animals [9]. The two primary sources of endotoxin are the wound site and the intestinal tract [9]. Endotoxin given prior to irradiation has been demonstrated to afford a degree of radioprotection [9], but higher doses given after radiation enhances

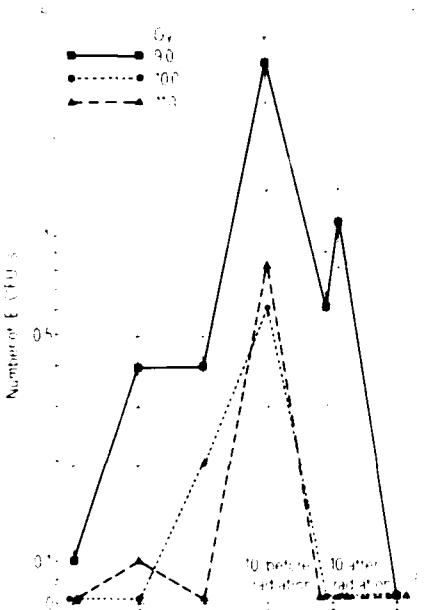

Figure 3. The number of endogenous colony forming units formed per spleen in wounded irradiated mice. The time points tested were based on the survival studies depicted in figure 2. No E-CFU-s were found in control irradiated mice or in control-wounded mice. The data presented in figures 1–3 were obtained from mice all exposed to radiation at the same time. See figure 1 legend for symbols.

mortality[16]. Prostaglandins are known modulators of hematopoiesis[17] and elevated levels are seen after both trauma[18] and radiation[19]. Thus, increased PGE_2 levels induced by trauma shortly before or shortly after radiation may enhance hematopoiesis and therefore survival, while increased amounts induced both by radiation and subsequent late trauma may result in death associated with sepsis[20]. We are currently directing our research efforts toward delineating the role of these biological modifiers in trauma-enhanced survival mortality with radiation exposure.

1 Supported by the Armed Forces Radiobiology Research Institute, Defense Nuclear Agency, under research Work Unit 00129. Views presented in this paper are those of the authors; no endorsement by the Defense Nuclear Agency has been given or should be inferred.

2 Research was conducted according to the principles enunciated in the 'Guide for the Care and Use of Laboratory Animals' prepared by the Institute of Laboratory Research, National Research Council.

3 Ledney, G. D., Stewart, D. A., Exum, E. D., and Sheehy, P. A., Acta radiol. oncol. *20* (1981) 29.

4 Ledney, G. D., Exum, E. D., and Sheehy, P. A., Experientia *37* (1981) 193.

5 Ledney, G. D., Exum, E. D., Stewart, D. A., Gelston, H. M., Jr. and Weinberg, S. R., Exp. Hemat. *10* (suppl. 12) (1982) 263.

6 Pachciarz, J. A., and Teague, P. O., Proc. Soc. exp. Biol. Med. *148* (1975) 1095.

7 Langendorff, H., Messerschmidt, O., and Melching, H., Strahlentherapie *125* (1964) 332.

8 Stromberg, L. W. R., Woodward, K. T., Mahin, D. T., and Donati, R. M., Ann. Surg. *167* (1968) 18.

9 Ledney, G. D., Gelston, H. M. Jr, Weinberg, S. R., and Exum, E. D., Experientia *38* (1982) 1228.

10 Boggs, S. S., Boggs D. R., Neil, G. L., and Sartiana, G., J. Lab. clin. Med. *82* (1973) 727.

11 Ledney, G. D., Stewart, D. A., Gruber, D. F., Gelston H. M. Jr, Exum, E. D., and Sheehy, P. A., J. surg. Res. *38* (1985) 55.

12 Statistical Methods for Survival Data Analysis, p. 133. Ed. E. T. Lee. Lifetime Learning Publications, Belmont, CA 1980.

13 Ainsworth, E. J., Larsen, R. M., Mitchell, F. A., and Taylor, J. F., in: Radiation Protection and Sensitization, Proc. 2nd int. Symp. on Radiosensitizing and Radioprotective Drugs, Rome 1969, p. 381. Eds H. L. Moroson and M. Quintilani. Taylor and Francis, London 1970.

14 Walker, R. I., and Porvaznik, M., Life Sci. *23* (1978) 2315.

15 Ledney, G. D., and Wilson, R., Proc. Soc. exp. Biol. Med. *118* (1965) 1062.

16 Walker, R. I., Ledney, G. D., and Bertok, L., J. Trauma *23* (1983) 225.

17 Kurland, J., and Moore, M. A., Exp. Hemat. *5* (1977) 357.

18 Wang, B. S., Heacock, E. H., and Mannick, J. A., Clin. Immun. Immunopath. *24* (1982) 161.

19 Steel, L. K., and Catravas, G. N., Int. J. Radiat. Biol. *42* (1982) 517.

20 Short, B. L., Gardiner, M., Walker, R. I., Jones, S. R., and Fletcher, J. R., in: Advances in Shock Research, vol. 6, p. 27. Eds W. Schumer, J. J. Spitzer and B. E. Marshall. A. R. Liss Inc., New York 1981.

0014-4754/85/050614-03$1.50 + 0.20/0

Physiology & Behavior, Vol. 35, pp. 249–253. Copyright Pergamon Press Ltd., 1985. Printed in the U.S.A.

Quaternary Naltrexone Reverses Morphine-Induced Behaviors

G. ANDREW MICKLEY,* KAREN E. STEVENS† AND JAMES A. GALBRAITH†

**Behavioral Sciences Department, Armed Forces Radiobiology Research Institute, Bethesda, MD 20814-5145 and †Department of Behavioral Sciences and Leadership, United States Air Force Academy Colorado Springs, CO 80840*

Received 13 April 1984

MICKLEY, G. A., K. E. STEVENS AND J. A. GALBRAITH. *Quaternary naltrexone reverses morphine-induced behaviors.* PHYSIOL. BEHAV 35(2)249–253, 1985.—This study explored the relative role of the peripheral and central nervous systems (CNS) in the production of morphine-induced behavioral changes. Toward this end we used a quaternary derivative of an opiate antagonist (naltrexone methobromide, NM) that presumably does not cross the blood-brain barrier. Naltrexone methobromide (20, 40 and 80 mg/kg, IP) was used to challenge the stereotypic locomotion, analgesia and elevated "Straub" tail response observed in C57BL/6J mice after a 30-mg/kg (IP) injection of morphine. The quaternary derivative of naltrexone reversed the locomotor hyperactivity, "Straub" tail and analgesia normally observed in the opiate-treated C57BL/6J mouse. The data reported here, if taken at face value, suggest an important role for peripheral opiate receptors in morphine-induced behavioral changes. However, these conclusions are contingent on further research to more fully evaluate NM's capacity to cross the blood-brain barrier of the C57BL/6J mouse.

Morphine Naltrexone methobromide Quaternary naltrexone Locomotion Analgesia
Tail erection CNS Peripheral nervous system Blood-brain barrier

THE discovery of the existence of central opiate receptors and opioid peptides (for review, see [22]) has led investigators to suggest several specific brain areas as mediators of a variety of opiate-induced behavioral alterations. For example, morphine analgesia [17,29], catalepsy [9, 11, 26, 27], locomotor changes [7, 17, 23, 25], and elevated straub tail reactions [13] are all apparently produced, at least in part, by brain neurons. The role of peripheral opiate receptors and endorphins in the production of these and other behaviors has been addressed only recently. Some of this work has been accomplished through the use of quaternary derivatives of opiate antagonists, which presumably do not cross the blood-brain barrier. In this regard it has been shown, for example, that methyl naloxone failed to alter morphine-induced antinociception unless administered in the cerebral ventricles of the rat [10]. Similarly, quaternary naltrexone did not block the stress-induced analgesia experienced by defeated mice [15]. Furthermore, methyl naltrexone, when given systemically, did not antagonize the discriminative stimulus effects of opiates; however, it did work peripherally to displace [^{3}H] etorphine from opiate receptors and reversed the effects of morphine on the isolated guinea-pig ileum [24]. Naltrexone has also been shown to be over 1500-fold more effective than quaternary naltrexone in reversing morphine-induced catalepsy [6].

In a further analysis, the present investigation sought to clarify the extent of peripheral opiate involvement in the production of several morphine-induced behaviors. Previous work [3, 16, 23] suggests that morphine (IP) produces a stereotypic locomotor activation (continuous movement, largely in one direction around the cage perimeter), analgesia and elevated "Straub" tail in the C57BL/6J mouse. In the present study, we challenged these behavioral responses with naltrexone methobromide (NM), which presumably has a primary action of peripheral opiate antagonism [2, 15, 24].

METHOD

Subjects

The subjects were male C57BL/6J mice (15–20 g) obtained from Jackson Laboratories (Bar Harbor, ME). Animals were initially housed in groups not exceeding 9 per cage (47 × 26 × 16 cm). However, subjects involved in locomotor activity testing were transferred to individual cages (30 × 19 × 13 cm) at least 24 hours before activity testing was begun. Mice were maintained on a 12-hour light-dark cycle (lights on 6:00 a.m.) in a temperature-controlled room (23° ± 1°C). Behavioral observations were made at the same time each day in order to avoid circadian variations. Purina laboratory chow and tap water were available ad lib except during behavioral measurements and drug injections.

Procedures

Two studies were conducted to assess the effect of a peripherally acting opiate antagonist on opiate-induced locomotor hyperactivity, elevated "Straub" tail and analgesia in the C57BL/6J mouse. The terms quaternary naltrexone and naltrexone methobromide (NM) are used interchangeably. In the first experiment, 60 mice received an injection (IP) of morphine sulfate (30 mg/kg), and 60 control animals received (IP) an equal volume of saline. Five minutes after these injections, locomotor activity was recorded during two successive 15-minute periods using the Automex D system of

Columbus Instruments (Columbus, OH). Half of the animals in the morphine and saline groups then received an injection of NM (20, 40 or 80 mg/kg, IP in 0.9% saline; N = 10/group). (These doses of quaternary naltrexone were chosen because *in vitro* and receptor-binding studies suggest that this peripherally acting opiate antagonist is apparently 20–80 times less potent than its tertiary counterpart [24]. A 1-mg/kg dose of naltrexone reverses mouse stress-induced analgesia [15].) The remaining subjects were injected with an equal volume of saline. After a 5-minute wait, locomotor activity was recorded for two additional 15-minute periods. During these final activity measurements, observations of tail position were also made. Twenty and 35 minutes after the second injection, two independent observers categorized the tail positions as (a) flaccid, (b) rigid but positioned horizontally, (c) rigid and elevated 5°–90° off the horizontal plane, or (d) rigid and elevated greater than 90° off the horizontal plane. Categories 3 and 4 are "Straub" tail reactions [3]. Observers were blind as to the drugged condition of each subject.

Analgesia was measured in a second experiment. Sixty mice received an injection of 30 mg/kg morphine sulfate (IP) and 60 control subjects received an equal volume of saline. Fifteen minutes after these initial injections, half of the animals in each group received an injection of NM (20, 40 or 80 mg/kg, IP; N = 10/group). The remaining mice received control injections of saline equal in volume to those of quaternary naltrexone. Five minutes later, analgesia was tested using the hot plate method [1]. Individual subjects were placed on a hot plate maintained at 50° ± 1°C. Two independent observers noted the time after placement when each mouse licked (a) forepaw(s) and (b) hindpaw(s). If paw licks did not readily occur, latency measurements were terminated after 120 seconds. The analgesic reaction of each mouse was measured only once.

RESULTS

High doses of quaternary naltrexone (40 and 80 mg/kg) reversed the locomotor hyperactivity and "Straub" tail reactions normally observed in the C57BL/6J mouse after an injection of morphine. Opiate analgesia was antagonized after a lower dose (20 mg/kg) of NM.

Locomotion and analgesia data were analyzed within a one-way ANOVA design. Separate ANOVAs compared the four treatment groups (Morphine + saline, morphine + NM, saline + saline, and saline + NM) at each antagonist dose and (in the case of locomotion) time period. Significant differences ($p < 0.001$) were further described through the use of Newman-Keuls post hoc tests [28].

Morphine's (30 mg/kg) locomotor-stimulating and "Straub" tail effects were observed within the first 5 minutes; they reached their peak within the first 30 minutes, and lasted approximately 2 hours. Subjects usually walked around the perimeter of the cage, and rarely changed direction. This was a reliable effect; it was seen in each replication and in each time period, beginning with the second 15-minute baseline interval (one-way ANOVAs, $F(36)$ ranging from 15.3 to 216.24, $p < 0.001$; Newman-Keuls post hoc tests, $p < 0.05$).

Baseline locomotor activity was similar for all morphine-injected subjects. However, after a challenging injection of either 40 or 80 mg/kg NM, locomotion decreased significantly as compared to controls (*first time period:* $F(36) = 30.85$, $p < 0.001$, and Newman-Keuls, $p < 0.05$, 40 mg/kg; $F(36) = 41.66$, $p < 0.001$, and Newman-Keuls, $p < 0.05$, 80 mg/kg; *second time period:* $F(36) = 29.84$, $p < 0.001$, and Newman-Keuls, $p < 0.05$, 40 mg/kg; $F(36) = 58.4$ $p < 0.001$, and Newman-Keuls, $p < 0.05$, 80 mg/kg). Mice receiving 40 mg/kg of NM often stopped their stereotypic activity; they groomed and exhibited slowed locomotion, rearing and sniffing. Subjects receiving 80 mg/kg NM showed these same changes although, for some periods of time, they were immobile. This high dose of NM reduced the morphine-induced locomotion to such an extent that, quantitatively, it could not be distinguished statistically from the spontaneous locomotion of saline control subjects (see Fig. 1). The lowest dose of NM used in this study did not reverse morphine hyperactivity. In fact, a significant increase was seen in

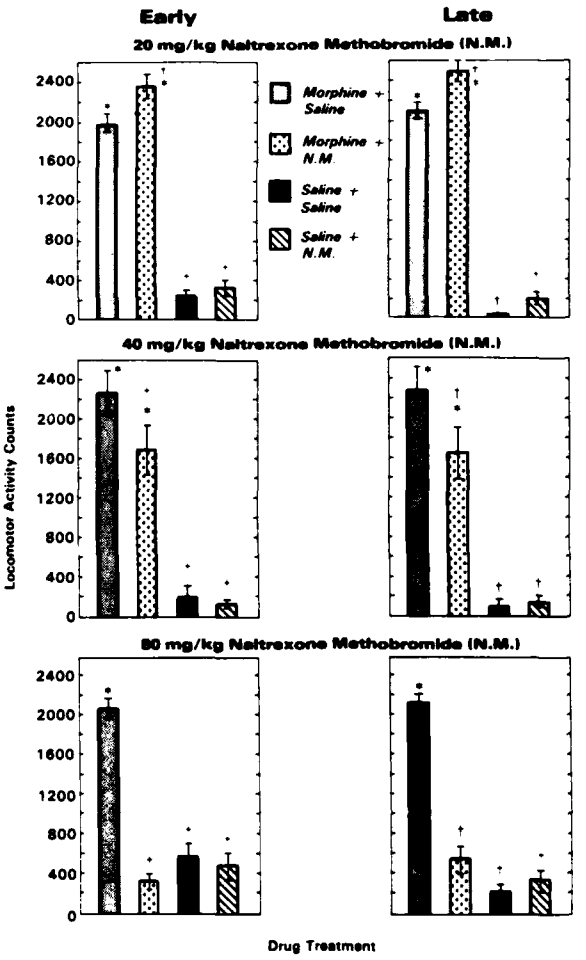

FIG. 1. Locomotor activity counts after an initial injection of either morphine (30 mg/kg) or saline followed by a challenging injection of either naltrexone methobromide (NM) (20, 40 or 80 mg/kg) or saline. Early (5–20 minutes after challenge injection) and late (20–35 minutes after challenge injection) activity observations are shown. Statistical comparisons indicate results of one-way ANOVAs and Newman-Keuls post hoc comparisons, $p < 0.05$; * = different from saline + saline control group; † = different from morphine + saline control group. Variance bars represent the standard errors of the means.

TABLE 1

PERCENT OF MORPHINE-TREATED (30 mg/kg) MICE EXHIBITING VARIOUS TAIL POSITIONS FOLLOWING SALINE OR NALTREXONE METHOBROMIDE (NM) CHALLENGE*

Drug Treatment/ Doses	N	First Observation†				Second Observation†			
		Flaccid	Rigid and Horizontal	Elevated 5° to 90°	Elevated greater than 90°	Flaccid	Rigid and Horizontal	Elevated 5° to 90°	Elevated greater than 90°
Morphine-saline	10	0	0	30	70	0	0	30	70
Morphine-NM (20 mg/kg)	10	0	0	90	10	0	10	80	10
Morphine-saline	10	0	0	10	90	0	0	10	90
Morphine-NM (40 mg/kg)	10	0	60	30	10	30	50	10	10
Morphine-saline	10	0	0	10	90	0	0	0	100
Morphine-NM (80 mg kg)	10	60	20	10	10	50	30	20	0

*All subjects that received first injections of saline (i.e., saline-saline or saline-NM) are omitted from this table since all had tail positions rated as flaccid.

†Two tail observations were made for each mouse: First = 20 minutes after challenge and Second = 35 minutes after challenge.

opiate-stimulated locomotion in both the time periods recorded after 20 mg/kg NM treatment (*first time period*: $F(36) = 113.42$, $p < 0.001$, and Newman-Keuls, $p < 0.05$; *second time period*: $F(36) = 216.24$; $p < 0.001$, and Newman-Keuls, $p < 0.05$).

Quaternary naltrexone alone apparently does not produce hypoactivity since post-hoc comparisons of locomotor activity counts between the saline-injected subjects and those receiving naltrexone methobromide revealed no statistically significant difference between these groups (Newman-Keuls, $p < 0.005$). This lack of statistical difference is apparently not due to total inactivity of the saline-injected animals. Although habituation to the testing environment did take place, the saline-injected animals were still sufficiently active in the 0.5-hour test period (average counts for all saline control groups = 228) to discern an even lower level of locomotor activity had it occurred in the naltrexone-treated mice.

All morphine-injected mice exhibited elevated "Straub" tails that were lowered significantly after treatment with 40 or 80 mg/kg NM (see Table 1). Tail positions were observed and categorized as previously described. However, for the purpose of data analysis, observations of tail positions were grouped as non-"Straub" tail reactions (either "flaccid" or "rigid and horizontal") or "Straub" tail reactions (elevated from 5° to >90° off the horizontal plane). Fisher exact probability tests were computed for each of the two observation times and doses of NM [21]. Morphine-induced "Straub" tail reactions were significantly antagonized after challenges of either 40 or 80 mg/kg of NM (all $p < 0.01$). Some of the most dramatic reactions to the opiate antagonist were observed after 80 mg kg. The majority of these morphine-injected subjects went from exhibiting tail positions that were almost parallel to the vertebral column to completely flaccid tails within 20 minutes. Although 20 mg/kg produced a slight lowering of the tails (see Table 1), this was not a statistically significant change within the present scheme of data analysis. All subjects that received first injections of control saline (i.e., either saline and then NM or saline and then saline had tail positions rated as "flaccid."

As expected, morphine-injected subjects were more analgesic than were the saline-injected controls. This analgesia has been shown to peak within 0.5 hour and to last at least 2 hours [20]. This response was observed on both the forepaw measure (20 mg/kg NM replication: $F(36) = 11.07$, $p < 0.001$; 40 mg/kg NM replication: $F(36) = 19.58$, $p < 0.001$, all Newman-Keuls $p < 0.05$) and the hind paw measure (20 mg kg NM replication: $F(36) = 48.33$, $p < 0.001$; 40 mg/kg NM replication: $F(36) = 39.29$, $p < 0.001$; 80 mg/kg NM replication: $F(36) = 9.17$, $p < 0.001$, and all Newman-Keuls, $p < 0.05$). See Fig. 2. This morphine analgesia could be reversed by an injection of either 20 or 40 mg/kg of NM (Newman-Keuls, $p < 0.05$). However, when 80 mg/kg NM was given, mice often developed tremors, limb stiffness and lethargic movements, which may have inhibited their paw licking.

DISCUSSION

Naltrexone methobromide effectively challenged morphine-induced locomotor hyperactivity, analgesia, and "Straub" tail erection in the C57BL/6J mouse. Previous studies have indicated that this quaternary opiate antagonist does not readily penetrate the blood-brain barrier [2, 10, 15, 24]. Taken in this context, the present data suggest that peripheral opiate receptors may mediate, at least in part, these morphine-induced behaviors. It has been well documented that seemingly central nervous system effects may sometimes be mediated by peripheral mechanisms (for review see [14]). These data do not, however, deny the already-demonstrated role of central neuronal mechanisms in the production of morphine-induced locomotion [7, 17, 23, 25], analgesia [17,29] and tail erection [13].

One of the doses of NM (20 mg/kg) used here did not reverse morphine-induced locomotion, but instead enhanced the stimulating effect of the opiate. This is unusual but is consistent with some other reports suggesting that some opiate antagonists (i.e., naloxone) can display opiate agonist activity in a number of behavioral and *in vitro* test systems (for review, see [19]).

In the present study, specific opiate-induced behaviors

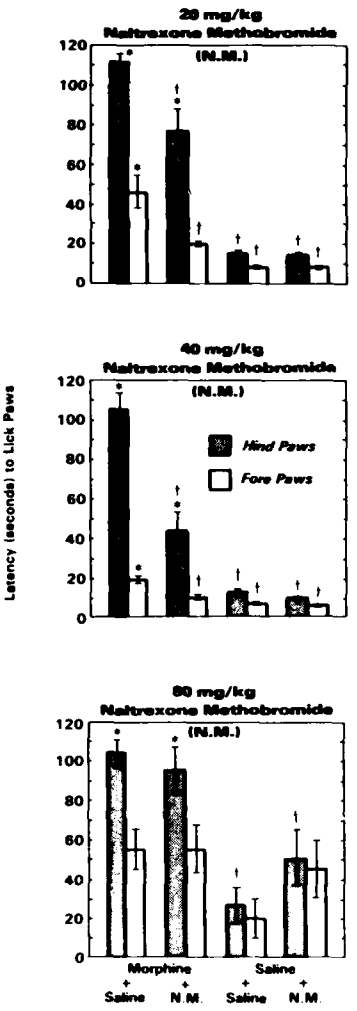

FIG. 2. Mean latency to lick forepaws and hind paws following an initial injection of morphine (30 mg/kg) or saline and then a challenging dose of either naltrexone methobromide (20, 40 or 80 mg/kg) or saline. Statistical comparisons indicate results of one way ANOVAs and Newman-Keuls post hoc comparisons, $p < 0.05$; * different from saline + saline control group; † different from morphine + saline control group. Variance bars represent the standard errors of the means.

were antagonized by different doses of NM. Morphine's analgesic effects were significantly attenuated by 20 mg/kg of NM whereas opiate-induced locomotion and "Straub" tail were essentially unchanged at this dose. These data support previous studies that highlighted the fact that the motor and analgesic effects observed in morphine-treated mice are clearly dissociated neurophysiologically and biochemically [16]. Similarly, the same dose of NM has been observed to reverse catalepsy [6] but not analgesia [18] of the rat.

Although morphine analgesia was effectively challenged by 20 and 40 mg/kg of NM this antagonism was not demonstrated after 80 mg/kg of the quaternary compound. These high-dosed animals exhibited tremors and rigidity which may have interfered with their capacity to lick their paws. Most of these subjects showed signs of pain sensation (e.g., jumping off the hot plate), but their failure to perform paw licks made them statistically indistinguishable from control morphine-injected mice (see Fig. 2). It may be the case that morphine-mediated antinociception was attenuated by quaternary naltrexone but the mice injected with 80 mg/kg NM were physically incapable of demonstrating this effect on the hot plate test.

The interpretation that peripheral opiate receptors may partially mediate morphine-induced locomotion, analgesia and "Straub" tail erection should not be made without some comment regarding the likelihood that quaternary naltrexone crossed the blood-brain barrier. The majority of the literature supports a primary peripheral action of NM. Still, Brown and colleagues [6] have suggested that quaternary naltrexone may be gradually leaking into the brain of rats after approximately 90 minutes. However, this explanation may not address naltrexone methobromide's apparent capacity to rapidly (within 5–35 minutes) reverse the morphine-induced locomotion, analgesia, and tail erection reported in the present study. In addition we found that early (within 15 minutes) reversal of morphine-induced locomotion by the antagonist is similar to that observed later (15–30 minutes postinjection). This suggests that leakage, if it occurred, must be quite fast. Finally, if the behavioral reversals reported here were caused by leakage of naltrexone methobromide into the central nervous system, then one might expect to see a gradual onset of antagonism, which would begin at the receptors located nearest the weak points of the blood-brain barrier [14]. The morphine-induced locomotion, analgesia, and tail erection responses measured in the present study are apparently mediated, at least partially, by quite different brain areas [5,13]. However, quaternary naltrexone reversed all of these behaviors within the same time period. These data are in consonance with those of others that suggest that the failure of naltrexone methobromide to antagonize heroin self-administration was consistent over a 3-hour period [12]. Thus, leakage of quaternary naltrexone into the CNS over time may not be the most likely explanation for the results presented here.

Another potential explanation of the present data is that quaternary naltrexone may metabolize into naltrexone [6] or some other opiate antagonist, and that it is this compound (which crosses the blood-brain barrier more readily) that antagonizes morphine's effects. Future studies are planned in an attempt to resolve these issues.

It should be recognized that the effects reported here may also be species dependent. Others have suggested that the blood-brain barrier may have different permeability characteristics in different mammals [4]. Some evidence suggests, for example, that quaternary naltrexone, at comparable doses, fails to produce centrally mediated symptoms of narcotic withdrawal in dogs or monkeys [18] but may [18] or may not [15] reverse mouse analgesia. The permeability of the mouse blood-brain barrier has yet to be fully described.

The present data may be interpreted as suggesting either (a) a role for peripheral opiate receptors in the production of morphine-induced locomotion, analgesia and "Straub" tail reactions, or (b) a CNS locus of action of naltrexone methobromide or its lipophilic metabolites. Future studies that measure the regional distribution of quaternary naltrexone and its breakdown products throughout the body should clarify these issues.

ACKNOWLEDGEMENTS

The authors wish to thank Robert L. Stewart, Joseph Dannelley, Paul Brenner, and Diane Pickle for their fine technical assistance during the course of these experiments. We wish to thank Dr. H. Merz for his contribution of naltrexone methobromide. We thank Mrs. Marion Golightly for her help in typing this manuscript and Ms. Junith VanDeusen for her editorial assistance. Research was conducted according to the principles enunciated in the "Guide for the Care and Use of Laboratory Animals" prepared by the Institute of Laboratory Animal Resources, National Research Council. This experiment was conducted, in part, while the first author was at the USAF Academy, and was supported by Defense Nuclear Agency (DNA) under research project U99QMXMK, 00041.

REFERENCES

1. Ankier, S. I. New hot plate tests to quantify antinociceptive and narcotic antagonist activities. *Eur J Pharmacol* **27:** 1–4, 1974.
2. Bianchi, G., R. Fiocchi, A. Tavani and L. Manara. Quaternary narcotic agonists' relative ability to prevent antinociception and gastrointestinal transit inhibition in morphine-treated rats as an index of peripheral selectivity. *Life Sci* **30:** 1875–1883, 1982.
3. Bilbey, D. L. J., H. Salem and M. H. Grossman. The anatomical basis of the straub phenomenon. *Br J Pharmacol* **15:** 540–543, 1960.
4. Bradbury, M. *The Concept of a Blood-Brain Barrier*. New York: John Wiley and Sons, 1979, pp. 116–136.
5. Brase, D. A., H. H. Loh and E. L. Way. Comparison of the effects of morphine on locomotor activity, analgesia and primary and protracted physical dependence in six mouse strains. *J Pharmacol Exp Ther* **201:** 368–374, 1977.
6. Brown, D. R., M. J. Robertson and L. I. Goldberg. Reversal of morphine-induced catalepsy in the rat by narcotic antagonists and their quaternary derivatives. *Neuropharmacology* **22:** 317–321, 1983.
7. Brown, R. G., D. C. Derrington and D. S. Segal. Comparison of opiate- and opioid-peptide-induced immobility. *Life Sci* **24:** 933–942, 1979.
8. Castellano, C. and A. Oliverio. A genetic analysis of morphine-induced running and analgesia in the mouse. *Psychopharmacologia* **41:** 197–200, 1975.
9. Dunstan, R., C. I. Broekkamp and K. G. Lloyd. Involvement of caudate nucleus, amygdala or reticular formation in neuroleptic and narcotic catalepsy. *Pharmacol Biochem Behav* **14:** 169–174, 1981.
10. Ferritti, P., G. Bianchi, A. Tavani and L. Manara. Inhibition of gastrointestinal transit and antinociceptive effects of morphine and FK 33-824 in rats are differently prevented by naloxone and its N-methyl quaternary analog. *Res Commun Subst Abuse* **2:** 1–11, 1981.
11. Koffer, K. B., S. Berney and O. Hornykiewicz. The role of the corpus striatum in neuroleptic- and narcotic-induced catalepsy. *Eur J Pharmacol* **47:** 81–86, 1978.
12. Koob, G. F., H. O. Pettit, A. Ettenberg and F. Bloom. Effects of opiate antagonists and their quaternary derivatives on heroin self-administration in the rat. *J Pharmacol Exp Ther* **229:** 481–486, 1984.
13. Lee, H. K., C. Y. Chai, M. J. Wayner, L. C. Kao and P. M. Chung. Mesencephalic central gray: Locus of morphine and electrical stimulation induced tail erection. *Pharmacol Biochem Behav* **9:** 221–226, 1978.
14. Meisenberg, G. and W. H. Simmons. Peptides and the blood-brain barrier. *Life Sci* **32:** 2611–2623, 1983.
15. Miczek, K. A., M. L. Thompson and C. Shuster. Opioid-like analgesia in defeated mice. *Science* **215:** 1520–1522, 1982.
16. Oliverio, A. and C. Castellano. Genotype-dependent sensitivity and tolerance to morphine and heroin: Dissociation between opiate induced running and analgesia in the mouse. *Psychopharmacologia* **39:** 13–22, 1974.
17. Oliverio, A. Genotype-dependent electroencephalographic behavioral and analgesic correlates of morphine: An analysis in normal mice and in mice with septal lesions. *Brain Res* **83:** 135–141, 1975.
18. Russell, J., P. Bass, L. I. Goldberg, C. R. Schuster and H. Merz. Antagonism of gut but not central effects of morphine with quaternary narcotic antagonists. *Eur J Pharmacol* **78:** 225–261, 1982.
19. Sawynok, J., C. Pinsky and F. S. LaBella. On the specificity of naloxone as an opiate antagonist. *Life Sci* **25:** 1621–1632, 1979.
20. Shuster, L., G. W. Webster, G. Yu and B. E. Eleftheriou. A genetic analysis of the response to morphine in mice: Analgesia and running. *Psychopharmacologia* **42:** 249–254, 1975.
21. Siegel, *Nonparametric Statistics for the Behavioral Sciences*. New York: McGraw-Hill Book Co., 1956, pp. 175–179.
22. Szara, S. Opiate receptors and endogenous opiates: Panorama of opiate research. *Prog Neuropsychopharmacol Biol Psychiatry* **6:** 3–15, 1982.
23. Teitelbaum, H., P. Giammatteo, and G. A. Mickley. Differential effects of localized lesions of n. Accumbens on morphine- and amphetamine-induced locomotor hyperactivity in the C57Bl. 6J mouse. *J Comp Physiol Psychol* **93:** 745–751, 1979.
24. Valentino, R. J., S. Herling, J. H. Woods, F. Medzihradsky and H. Merz. Quaternary naltrexone: Evidence for the central mediation of discriminative stimulus effects of narcotic agonists and antagonists. *J Pharmacol Exp Ther* **217:** 652–659, 1981.
25. Van Abeelen, J. H. F. and C. M. Van den Heuvel. Behavioral responses to novelty in two inbred mouse strains after intrahippocampal naloxone and morphine. *Behav Brain Res* **5:** 199–207, 1982.
26. Wilcox, R. E. and R. A. Levitt. Naloxone reversal of morphine catatonia: Role of caudate and periaqueductal gray. *Pharmacol Biochem Behav* **9:** 425–428, 1978.
27. Wilcox, R. E., M. Bozarth and R. A. Levitt. Reversal of morphine-induced catalepsy by naloxone microinjections into brain regions with high opiate receptor binding: A preliminary report. *Pharmacol Biochem Behav* **18:** 51–54, 1983.
28. Winer, B. J. *Statistical Principles in Experimental Design*. New York: McGraw-Hill Book Co., 1971, pp. 35–37, 262–283.
29. Yeung, J. C., T. L. Yaksh and T. A. Rudy. Effects of brain lesions on the antinociceptive properties of morphine in rats. *Clin Pharmacol Physiol* **2:** 261–268, 1975.

Ann. Rev. Phys. Chem. 1984. 35: 613–55

ELECTRONIC PROCESSES IN ORGANIC SOLIDS

Martin Pope

Radiation and Solid State Laboratory and the Department of Chemistry, New York University, New York, New York 10003

Charles E. Swenberg

Radiation Sciences Department, Armed Forces Radiobiology Research Institute, Bethesda, Maryland 20814

INTRODUCTION

In recent years, the number of studies of electronic processes in organic solids has assumed explosive proportions. In retrospect, it was inevitable. The increasing ability of organic chemists to design and synthesize molecules and structures almost to order has made it possible to provide an experimental testing ground for what were once figments of the imaginations of theorists. Thus excellent approximations of ideal one- and two-dimensional solids can be prepared with electrical properties varying from those of an insulator, to those of a superconductor. Disordered systems can be prepared with a large range of nearest-neighbor interaction energies, with and without additional trapping sites, making it possible to test almost any conceivable theory of energy or charge migration in a random or regular network. Increasingly sophisticated computer simulations are providing unusual insights into the microscopic details of dynamical processes, such as carrier or energy transport. These serve as a check on analytical theories and even a guide to indicate which assumptions are likely to be reasonable. The simulations can probe situations that are as yet not readily accessible to experiment, such as time domains in the femtosecond range. All of this new interest has been superimposed on what has been an orderly growth in a relatively isolated field, the study of the electrical and optical properties of polycyclic aromatic hydrocarbons

0066–426X/84/1101-0613$02.00

exemplified in anthracene. In the middle of 1982, our book appeared (1) in which most of the material to be presented herein approximately 40 pages was discussed in 821 pages and, at that, with apologies for significant omissions. It is thus obvious that this review represents an even more drastic condensation and omission of important work.

Books and reviews that have appeared since the beginning of 1982 include that edited by Mort & Pfister (2) dealing with triboelectricity, charge storage, piezoelectricity, pyroelectricity, energy transfer, photoconductivity, and polyacetylene. Organic semiconductors are discussed by Haddon et al (3). A wide ranging conference on the organic solid state was held in 1982 covering such topics as solid state photorearrangement, chemistry, semiconductivity, superconductivity, the polyacetylenes, electronic structure, and many others (4). Several lucid review articles have been written by Duke and his colleagues. These discuss conductivity (5), electronic structure (6, 7), and electronic excitation (8). The preparation of good crystals of pure materials is fundamental to the development of meaningful theory. Two books dealing with this subject are the recent work of Sloan & McGhie (9) and the earlier work of Karl (10).

Mention must be made of the remarkable results that are being observed by the combination of tunable lasers and supersonic molecular beams of isolated molecules in the study of intramolecular dynamics such as collision-free vibrational energy decay. A review of this important field is given by Smalley (11). The study of condensed phase molecular dynamics, including transport and trapping, has been reviewed by Fayer (12). The effect of pressure on molecular luminescence in solution is reviewed by Drickamer (13), and a critique of high pressure studies of molecular crystal spectra has been given by Berry et al (14). A review of luminescence in nucleic acids has been prepared by Callis (15). Additional references to reviews and books are made in the text.

In the course of this review we attempt to provide references to subjects that cannot be adequately covered due to severe space limitations. In addition, we make many references to our recent book (1).

EXCITON PROCESSES

Exciton Transport

Discussion is limited to exciton diffusion, percolation, and exciton annihilation; the reader may refer to recent reviews or papers for discussions of the effeet of electric fields on exciton transport (15a,b) polaritons (16–18), exciton-phonon interaction (18, 19), and exciton luminescence (19, 20, 20a,b). In ordered molecular crystals, exciton transport is generally characterized by a diffusion constant, D (1, p. 102 et seq). Sensitized

luminescence (21) produced by exciton diffusion to a suitable trap and delayed fluorescence resulting from exciton-exciton annihilation (1, pp. 135–47) have been used to determine D. In the usual interpretation, the exciton diffusion constant (D) is related to γ, the annihilation rate constant, and K, the exciton transfer rate, by the relationships $\gamma = v\gamma' = 8\pi R_d D$ and $K = \rho v K' = 4\pi R_c D$, where v is the volume per molecule of the crystal, ρ the relative guest concentration, and R_d and R_c are the effective radii for annihilation by another exciton and capture by a trap, respectively. Kenkre & Schmid (22) have shown that the use of the above relationships, which are derived from coagulation analysis, would yield the same values for the diffusion constant only under special conditions; values of D inferred from either γ or K could therefore be incorrect. A proper theoretical analysis of the experimental data can be obtained by noting that for trapping at a guest or defect site, the trapping time is the sum of the time to get to a trap, $1/M$, plus the time, $1/c$, needed for the (local) capture process to occur; M is the motion rate defined as (22)

$$M = \left\{ \int_0^\infty \exp(-t/\tau)\Psi_0(t)\, dt \right\}^{-1} \qquad 1.$$

where $\Psi_0(t)$ is the exciton self-propagator, and τ the exciton lifetime. For exciton annihilation a similar sum relationship holds, except that the mutual annihilation time, $1/b$, replaces the local capture time $1/c$. In terms of rates (γ' and K') the following general relationships have been shown to be valid (22):

$$(\gamma')^{-1} = M^{-1} + b^{-1}, (K')^{-1} = M^{-1} + c^{-1}. \qquad 2.$$

It is only in temperature regimes where either γ' or K' is dominant that information about the magnitude of D can be inferred. These formulae were applied by Kenkre & Schmid (22) to naphthalene and anthracene, where both γ' and K' are known over a broad temperature range. For the special case of incoherent three-dimensional motion, where $M = 4F$, F being the nearest neighbor transfer rate, a lower bound on the singlet exciton diffusion constant, $D = Fa^2/6$ can be inferred, where a is the nearest neighbor distance. In the particular case of the naphthalene singlet exciton, at $T = 300$ K, $D \geq 2.1 \times 10^{-5}$ cm^2 s^{-1}, while for anthracene $D \geq 4.3 \times 10^{-3}$ cm^2 s^{-1}. A similar type of analysis is possible for triplet excitons provided there are temperature domains where either $\gamma' > K'$ or $K' > \gamma'$; under these conditions, it may be inferred from Eq. 2 that $D > K'$ or $D > \gamma'$.

An important technique for measuring D, particularly for triplet excitons, involves the use of Ronchi rulings (23; 1, p. 173). It lends itself easily to the study of the anisotropy of D, and may be used to test for coherence in

exciton motion. Kenkre et al (24) have adopted the generalized master equation (GME) approach to derive expressions for steady state delayed fluorescence as a function of Ronchi ruling period that hold for any degree of coherence. The GME approach has also been adapted for use in sensitized luminescence studies (25).

Energy transport in mixed molecular crystals has attracted considerable attention, in part because these crystals, with their random distribution of components, provide useful models for testing theoretical concepts of disordered solids. The most extensively studied system has been the naphthalene-(guest)-perdeuteronaphthalene (host) mixed crystal doped with a third component, β-methylnaphthalene (BMN), present in concentrations generally less than 10^{-3} mol fraction (26). The third component has fluorescing levels sufficiently low to serve as a sensor or supertrap for excitons migrating among guest molecules. The experimental parameters are the time dependence and integrated intensities of the luminescence from both guests and supertraps, as a function of guest concentration. Measurements are performed at low temperatures ($\sim 4^{\circ}$K) so that the host sites act as barriers (antitraps) to energy transport among the guest molecules. For both triplet and singlet exciton transport in $C_{10}H_8$/$C_{10}D_8$/BMN the sensor emission depends in an almost step-function fashion upon guest concentration, (C_g), increasing rapidly over a narrow (critical) range (27; 1, pp. 125–34).

Several theoretical models have been suggested to account for these results, each of which has some validity. In the percolation model, the sharp transition is attributed to the formation of a minimal macroscopic connecting network of guest sites at the critcal guest concentration, C_c. Percolation analysis requires extensive computer simulations. Analytical solutions have been proposed by Blumen & Silbey (29) and by Loring & Fayer (30). Blumen & Silbey use a continuum kinetic equation formalism, and Loring and Fayer use a Green's function approach to solve the mixed-crystal kinetic master equation.

Several percolation models have been considered (26, 31, 32). *Static* percolation assumes that there is a cutoff on the allowable transfer distance and neglects dynamics within clusters; thus for any cluster containing a supertrap, the probability is unity for capturing a guest exciton that lands anywhere in the cluster. The latter approximation is called the *supertransfer limit* (26). If the supertransfer condition is relaxed so that not all excitons within a cluster containing a sensor are trapped because of limitations imposed by the finite lifetime of the exciton and its finite rate of transfer, then *quasistatic* percolation ensues. For singlet excitons, Gentry & Kopelman (31, 33) have shown that the quasistatic percolation model agrees with experiment at 1.8 K, but fails to account for data acquired at

4.2 K. On the öther hand, the two-dimensional continuum models of both Loring & Fayer (30) and Blumen & Silbey (29) are consistent with the experimental results at 4.2 K but not at 1.8 K. In the Loring & Fayer approximation (30) the trapping probability is given by $P = 1 - K_g\tilde{G}(0, \varepsilon = K_g)$, where K_g^{-1} is the guest lifetime, and $\tilde{G}$ is the Laplace transform of the time-dependent part of the system Green's function for the probability of finding excitons somewhere within the guest manifold. This relationship can account for the $T = 4.2$ K data only if the Förster distance (1, p. 100) $R_0 = 8$ Å and the transfer rate, W, has an octupole-octupole distance dependence, i.e. $W \propto R^{14}$. A weakness of the model is that these parameters imply a transfer rate of 5×10^9 s^{-1}, whereas expected nearest neighbor rates are the order of 10^{12} sec^{-1}. The lack of agreement with the 1.8 K data has been discussed by Gentry & Kopelman (33) and is attributed to the implicit assumption in the Loring & Fayer model of the equality of the forward and reverse transfer rates, $W_{ij} = W_{ji}$; this equality is known not to hold for naphthalene singlet excitons at low temperatures (34).

The Blumen & Silbey model (29) calculates the average probability for an exciton to land on a supertrap site and the average trapping time. Their results, in the absence of back transfer from the supertrap, are

$$K_{et}^{-1} \propto \{(C_s/C_g)C_g^{n/d}\} \quad 3.$$

$$P \propto \{1 + C_{1/2}/C_g\}^{-1} \quad 4.$$

where the energy transfer rate constant is K_{et}, the sensor concentration is C_s, the guest concentration is C_g and $C_{1/2}$ is that concentration at which $P = 0.5$; n is the multipole transfer exponent ($n = 14$ for octupole-octupole transfer) and d is the dimensionality of the system. Equation 4 provides an excellent fit to the 4.2 K data; however, it does not account for the sharpening of the critical transition upon lowering the temperature. Furthermore, recent time-dependent emission data of Parson & Kopelman (32) performed on the same mixed crystal system at 1.7 K demonstrate that the sensor emission profile is more rapid than expected from rate equation analysis (29) for guest concentrations near the transition regime (guest concentrations between 0.42 to 0.57 mol fraction).

The temperature and guest dependence of luminescence from the mixed crystal system $C_{10}H_8/C_{10}D_8$/BMN has also been studied by Brown et al (35), who found evidence for a transition from coherent triplet exciton motion at very low temperatures to hopping motion for $T > 10$ K. Transitions from band-like to hopping motion of triplet excitons have also been studied by Gentry & Kopelman (36).

In addition to protonated and deuterated isotopically mixed crystals, orientationally disordered solids (37, 38) are excellent model systems for

studying the static and dynamic properties of electronic excitations in disordered solids. In these systems local disorder is provided by the random distribution of orientations of the substituent groups, e.g. the chloride and bromide ligands of 1-bromo-4 chloronaphthalene (BCN) crystals. Orientational static disorder was studied by Morgan & El-Sayed (39), who measured the zero phonon $S_1 \rightarrow T_1$ transition at ≈ 4.2 K in BCN single crystals. The absorption line shape was Gaussian, which is characteristic of inhomogeneous broadening; the line width (HMHW) was ~ 32 cm^{-1}, which is approximately two orders of magnitude larger than the linewidths of the corresponding transition in single crystals of 1,4-dibromonaphthalene and 1,4-dichloronaphthalene. In addition, Morgan & El-Sayed (39) have shown how the temporal behavior of the phosphorescence emission at different laser excitation energies in the long wavelength region of the absorption band provides a measure of both the energy transfer rate and its mechanism.

Exciton Interactions

Excitons can interact with other excitons, and with carriers, defects, photons, phonons, and essentially any other entity that can be reached by a mobile electronically excited state (1, pp. 89–180). Exciton-exciton annihilation in neat molecular solids is characterized by an annihilation rate constant γ. The limitation of the assumption that the depletion of excitons (n) due to bimolecular annihilation is given simply by $-\gamma n^2$ has been reviewed by Kenkre (25). The role of boundaries and domain (or cluster) size on exciton kinetic rates is of considerable current interest [see Hatlee & Kozak (40) and references quoted]; confinement to small domains is expected to enhance the number of collisions with other excitons, defects, or traps. In the particular case of tetracene triplet excitons created in pairs in small tetracene domains by singlet exciton fission, confinement results in an increase in the fluorescence yield and singlet exciton lifetime as the domain size decreases (41).

Mixed crystals are good model systems for the study of size effects on exciton reactions. Recently Klymko & Kopelman (42) have shown that when guest cluster formation occurs, the delayed fluorescence (D) resulting from guest-guest exciton annihilation is no longer proportional to the square of the guest phosphorescence (P), even at low triplet exciton concentrations. Using mixed $C_{10}H_8/C_{10}D_8$ crystals with dopant levels of 0.1% to 20% $C_{10}H_8$ they found $D \propto P^x$, where x is a function of excitation intensity, time after excitation, and guest concentration. Values of x ranged from 2 to ~ 30 at $T = 1.7$ K and increased monotonically with decreasing naphthalene concentration. As noted by the authors, these results are inexplicable in terms of standard diffusion kinetics (43). Klymko &

Kopelman (44) interpret their data in terms of fractal kinetics, which is appropriate for bimolecular processes in small domains. A discussion of fractal properties is beyond the scope of this review; see Alexander & Orbach (45) and DeGennes (46) for more information.

Excitons interact with carriers (1, pp. 164 et seq), and in the process of interacting, it may happen that a transient intermediate state is produced between the exciton and its collision partner. More recently the bound exciton + hole (excitonic ion) case was treated by Schilling & Mattis (47, 48), who call the ion a trion as initially suggested by Thomas & Rice (49). Here, the exciton could be either the Frenkel exciton or the Wannier exciton. The case of N excitons and one hole was solved by the same authors (48). Excitonic ions with Frenkel exciton parentage were discussed by Singh (50, 51) and ions based on excitons intermediate between Frenkel and Wannier excitons were treated by Gumbs & Mavroyannis (52). Experimental evidence for the existence of excitonic ions in benzene solid films is given by Sanche et al (53). Excitons interacting with trapped electrons was discussed by Agranovich & Zakhidov (54), who deduced an attractive interaction, which is the order of $e^2\Delta\alpha/2\varepsilon r$, where $\Delta\alpha$ is the change in the molecular polarizability of the excited molecule, $\sim 10^{-23}$ cm^3, r is the separation of the charge e from the exciton, and ε is the local dielectric constant.

One intriguing possibility that has not yet been ruled out theoretically is that of a Bose-Einstein condensation of Frenkel excitons in organic crystals, particularly triplet excitons (55); attempts are being made to detect this phenomenon, or at least the formation of exciton aggregates. A review of these experiments, particularly in the Soviet Union, is given by Brikenshtein et al (56).

Exciton Trapping

Trapping of excitons at either impurity or guest sites has been a subject of considerable study because of the insight gained on the mechanism of exciton diffusion (21, 25). Studies by Powell and co-workers (21) had suggested that the exciton transfer rate K was time-dependent, in significant departure from earlier results obtained in sensitized luminescence experiments (57). A careful study of the time-dependence of K has recently been made by in tetracene-doped anthracene by Braun et al (58). They demonstrated that for temperatures between 1.6 and 300 K and over a dopant concentration range of 10^{-6} to 2.3×10^{-3} mol fraction, that K was time-independent at least for times greater than a few picoseconds. This is in agreement with previously reported studies of Campillo et al (59) and Al-Obardi et al (60).

A recent study of singlet exciton trapping in the system *p*-terphenyl

(host)/tetracene (guest) (61) also showed that the transfer rate from host to host was time-independent but, more interestingly, that it was thermally activated. It was concluded that the energy of activation was to be associated with singlet exciton motion on the host lattice sites, and that the transfer from host to host was facilitated by a phonon-assisted increase in co-planarity of their donor and acceptor molecules (62). This phenomenon is reminiscent of that observed by Meyer et al (63) described herein. The concentration of sites at which an increase in co-planarity might be facilitated (predimer or incipent dimer) can reach 10^{-3} mol fraction (64).

The theory of trapping of excitons at guest sites in the presence of low trap concentrations has been considered by several authors (64–67). An analytic theory that accounts for the guest and host fluorescence yield for all guest concentrations has recently been given by Kenkre (68) and Kenkre & Parris (69), who use the general master equation (GME) governing excitation transfer (1, p. 108). They gave explicit expressions for both guest and host luminescence yield as a function of trap concentration (69).

In addition to exciton trapping at impurities and guests that have lower excited state energies than host molecules, it is also possible for self-trapping to occur in the host lattice (69a). Self-trapping of Frenkel excitons in homomolecular aromatic organic crystals was unlikely, according to Toyozawa & Shinozuka (70). However, under certain circumstances, the formation of an excimer that lies energetically beneath the exciton band may be viewed as a self-trapped exciton (1, pp. 85–89, 257–67).

The association of broad excimer-like luminescence with the existence of a self-trapped state necessitates (*a*) simultaneous observation of both free exciton and excimer luminescence, (*b*) an activated temperature dependence of the emission bands, i.e. the existence of a small energy barrier between the free state and the self-trapped state, and (*c*) the association of the emission of the trapped state with the intrinsic property of the crystal and not with defects. Previously reported excimer emission in β-9-10 dichloroanthracene (71), initially identified with a self-trapped exciton luminescence, is now known (72) not to satisfy the above criteria, since the monomer emission arises from defects. This conclusion was reached after it was found that crystal annealing greatly reduced the monomer emission. Thus, in this case, excimer formation was not a thermally activated process.

Evidence of exciton self-trapping in α-perylene was initially provided by von Freydorf et al (73), who observed a weakly structured emission (called the *Y*-emission) at low temperature (at slightly higher energy than the broad excimer fluorescence band) that had a long first-order decay time (≈ 38 ns). In β-perylene crystals the temperature dependence of the luminescence spectrum provides evidence for at least two types of self-trapped states: at least one of them is in thermal equilibrium with free

excitons (74). Additional evidence for self-trapping in both crystal phases comes from the work of Matsui et al (75).

SPECTROSCOPY

Lineshape Analysis

A theoretical analysis of EPR, NMR, and optical lineshape data can provide a wealth of information about structural and dynamical properties of solids. The inhomogeneous linewidth of optical lines is determined primarily by the degree of static disorder, and for this reason it is sometimes used as an indicator of the structural quality of crystalline materials. The homogeneous linewidth reflects intrinsic properties such as lifetime effects (T_1) (76) and the coupling strength of a particular excited electronic state to the local dynamical (phonon) modes (T_2). The homogeneous linewidth of optical transitions is not an easily accessible parameter; however, studies of fluorescence line-narrowing (77), hole-burning (78), fluorescence saturation (79), and optical coherence such as the photon-echo (80) and stimulated photon-echo (81) are methods that can yield the homogeneous linewidth of a particular vibronic state [see supersonic studies of (82, 82a)]. Hole-burning spectroscopy is a static method for investigating the dynamics of molecular vibronic states. In non-photochemical hole burning (NPHB) a particular set of molecules tuned to the laser frequency are excited but not chemically altered. The excited chromophore produces a change in its microenvironment, converting it rapidly to a new structural arrangement before deactivation; this decreases the number of chromophores having excitation energies at the laser frequency and increases the number of chromophores having excitation energies at other frequencies. The net result is that a hole is burned in the absorption band; the profile can be probed by measuring the fluorescence excitation spectra. When spectral diffusion processes are negligible, the hole shape is Lorentzian and its shape will be a measure of the true homogeneous lineshape [FWHM $= (\pi T_2)^{-1}$].

NPHB has been observed in a wide variety of amorphous matrices at low temperatures (83). Jankowiak & Bässler (84, 85) studied NPHB in tetracene ($\sim 10^{-5}$ mol fraction) incorporated into amorphous anthracene at 4 K. Holes burned at $T \approx 2.5$ K at $\lambda = 491.5$ nm show a pronounced zero-phonon hole and two almost symmetric one-phonon sideband holes; in some materials multiple phonon sidebands can be detected (86, 87). The ratio of the zero- to the one-phonon sideband intensities gave an electron-phonon coupling constant of ~ 0.9 and a phonon energy of $\approx 40\ cm^{-1}$ for those phonons which interact most strongly with the electronic state. The holes disappeared after annealing at 40 K for one hour. The homogeneous linewidth Γ (at FWMH) of the zero-phonon hole varied with temperature

as $\Gamma(T) = \Gamma_0 + aT^2$ where $\Gamma_0 \approx 4.0\,\text{cm}^{-1}$; this corresponds to a dephasing time on the order of 2.5 ps, which is 3×10^3 times faster than the radiative decay of tetracene in solution [for a study of vibrational dephasing in naphthalene, see (87a)]. The temperature dependence was rationalized in terms of the Reineker & Morawitz theory (88), which considers a distribution of tunneling states (TLS) coupled to the matrix acoustic phonons.

In photochemical hole burning, a photochemical process, such as proton-transfer (detachment), occurs; the photoproducts in general have absorption bands that lie outside those of the inhomogeneous band of the reactant; and if the photochemistry is irreversible, there will be no loss in the integrated hole intensity with time.

Fluorescence saturation methods have recently been applied by Treshchalov & Rozman (79) to determine the homogeneous linewidths of the first two inhomogeneously broadened vibronic states (400 cm^{-1} and 1400 cm^{-1} phonons) of molecular anthracene, at 10^{-5} mol fraction in naphthalene. The technique involves a measurement of the fluorescence intensity (F) as a function of the excitation intensity (I_n) and is applicable to guest molecules that are photochemically stable. For both steady-state and pulse excitation conditions, $F \propto I_n$ in the low intensity regime. At high excitation intensities $F \propto \sqrt{I_n}$. Treshchalov & Rozman (79) reported an energy relaxation time T_1 equal to 40 and 25 ps for the 400 and 1400 cm^{-1} vibrational modes of anthracene; for comparison we note that in a fluorene host, hot luminescence spectral measurement gave 28 and 22 ps, respectively, for these states (90).

The introduction of femtosecond time-resolution capabilities into the field of spectroscopy will probably provide the ultimate measure of relaxation dynamics. So far, the shortest-lived molecular process that has been directly time-resolved is the decay of the Rydberg $3R_g$ state in gas-phase benzene; this is 70 ± 20 fs, as measured by Wiesenfeld & Greene (91). The decay mechanism was not established, but may involve transitions directly into the high vibrational levels of the ground state. This time scale is so short that intermolecular collisions could be neglected. The ionization rate is comparable to the relaxation rate.

Photoelectron Spectroscopy

With the advent of synchrotron light sources, the energy region between far UV and X-ray has been made accessible to experimenters. A discussion of the principles of this light source and a description of recent photoemission experiments on phthalocyanines (Pc) is given by Koch & Gürtler (92). An examination of photoelectron energy distribution curves in Zn-Pc shows that the excitation of 3*d* to 4*s* states in the metal Pc is enhanced relative to

that in the free metal atom because 4*s* states in the metal Pc are transferred from the metal site to the ligand, increasing the availability of empty 4*s* states for occupation from 3*d* levels. In a similar way it was found that there is a smaller number of empty 4*s* states in Cu-Pc than in a Zn-Pc, because the $3d \rightarrow 4s$ transitions are stronger in the Zn-Pc. This hybridization of metal 3*d* electrons with the π-electron structure of phthalocyanine ligand is particularly important in understanding the high conductivity of the porphyrinic molecular metals (93). In many studies of photoemission, the three-stage model of Berglund & Spicer is used (1, p. 533) because of its simplicity. A good discussion of this model has appeared, using anthracene data, showing that structural defects must be taken into consideration (94).

A singularly clear and powerful demonstration of the utility of photoelectron spectroscopy coupled with the application of a simple theoretical model to determine the electronic structure of solids, particularly polymers, continues to emerge from the laboratory of C. B. Duke. A CNDO/S3 (complete neglect of differential overlap, self-consistent field method) model, originally developed to rationalize the photoemission and UV absorption spectra from polyacenes, was extended (95) to include infinite (periodic) macromolecules, as for example polyacetylene. In a companion paper (96) this method was used to rationalize the ultraviolet absorption and emission spectra of pyrrole and polypyrrole. In the calculation, it was found by varying the nymber of pyrrole units in the polymer that some of the essential features of the polypyrrole photoemission spectrum appeared when 4 to 6 pyrrole units were connected, implying that the photoemission hole state extends over at least 4 to 6 pyrrole units, or ~ 14 Å or more. In a similar way, it was found that a bonding $\pi \rightarrow \pi^*$ transition extending over at least 4 pyrrole units is responsible for the 3.0 eV peak in the absorption spectrum. By simulating the twisting of the pyrrole units, it was found that there would be no major changes in the photoemission or absorption spectra relative to that of a planar molecule, so no information about twisting may be deduced from the spectra. In another paper (97) the electronic structure of poly(*p*-phenylene) (PPP), poly(*p*-phenylene vinylene) (PPV), and poly(*p*-xylylene) (PPX), as well as the previously studied polyacetylene and polypyrrole was calculated. [For ab initio calculations, see (97a).]

CARRIER GENERATION MECHANISMS

Intrinsic

Among the homomolecular polynuclear aromatic hydrocarbons (PAH) compounds, anthracene has long been the hydrogen-atom for theoretical calculations. As one proceeds from naphthalene to pentacene, for example,

the optical absorption spectrum shows a significant increase in the contribution of states that have ionic character (98). This increase in ionic character is paralleled by an increase in the quantum efficiency of photogeneration. However, there is not yet unanimity on the association of this increased ionic character with a specific mode of ionization.

One hypothesis has it that carrier generation requires the excitation of a precursor Frenkel exciton that dissociates when its energy is degenerate with that of a pair of free carriers. This process is referred to as *autoionization* (AI). It does not follow that all AI transitions lead to completely uncorrelated carrier pairs. The electron thermalization distance is ~60 Å (1, p. 489). Thus, most electrons that are created inside the solid will thermalize within the Coulomb capture radius of the geminate positive ion, forming a transient charge-transfer (CT) state that can either decay to the ground state or dissociate by the absorption of ambient energy. For excitation energies exceeding that of crystal ionization, electrons are photoemitted with the maximum kinetic energy (100, 101) as calculated by the Einstein photoelectric equation, or with kinetic energies diminished by amounts equal to the energy of excitation of the remaining positive ion. This is proof that no intermediate CT state is necessary for free carrier generation.

However, there is strong experimental and theoretical evidence that direct optical excitation to a CT state takes place in homomolecular solids (102, 103), particularly in the more highly colored members of the polyacene family and particularly for excitation energies less than that of the band gap. The proposition that direct CT generation was the primary mechanism for photoconductivity in most, if not all, PAH crystals was put forth in a series of theoretical papers by Bounds & Siebrand (102, 103) and more recently by Bounds, Petelenz & Siebrand (BPS) (104, 105).

The fundamental premise of the theoretical work of (BPS) (based on anthracene) is that the direct excitation of the CT exciton is made possible by the coupling of this low oscillator strength state, with that of the high oscillator strength ($f \approx 1$)$S_3(^1B_u)$ Frenkel state located at 4.63 eV. In anthracene the S_3 state is about 0.5 eV higher in energy than the anthracene band gap $E_g \approx 4.1$ eV, and all optical excitations in the energy region up to 4.63 eV would produce CT states (albeit, vibrationally excited); in other words, there would be an energy of activation for photoconductivity due to the dissociation of the intermediate CT state even when the optical energy $h\nu > E_g$; this is observed (106). The energy E_{CT} of CT states of varying separation distance between the charges was calculated quantum mechanically by BPS; the CT energies were capable of being described qualitatively by a simple Rydberg-like expression of the form

$$E_{CT}(n) = E_g - \mu e^4 \, 8(h\varepsilon\varepsilon_0 n)^2 \qquad 5.$$

where μ is the effective mass of the electron-hole pair, $\varepsilon\varepsilon_0$ the dielectric constant parameters, and n is a principal quantum number, related to the distance r between electron and hole. The $E_{CT}(n)$ values can be related to the different activation energies $E_a(h\nu)$ found for carrier generation by light of energy $h\nu$ by the equation $E_a = E_g - E_{CT}(n)$. The explicit assumption is made here that while it is possible to excite vibrational states of CT excitons for each value of E_n, only the 0–0 vibrational state is available for thermal dissociation, the excess energy being dissipated in a time shorter than that for dissociation or recombination. The agreement between theory and experiment (107) for the E_a values is good, but not so good for the quantum efficiencies of carrier generation $\phi_0(h\nu)$. It was possible for BPS to estimate the contribution of CT states to the overall absorption spectrum; in anthracene this contribution was small but significant, while in tetracene and pentacene, the CT contribution was dominant.

Considerable experimental support for the CT exciton mechanisms for carrier generation has been provided by work on electric field modulated absorption spectroscopy in pentacene (108, 1, p. 574). Similar studies were made on anthracene by Sębastian et al (109), although it proved to be more difficult to detect the CT states. These authors correlated the energies of the peaks that were attributed to the CT exciton electroabsorption spectra with the size of the CT exciton using a Coulombic equation. The extrapolated value of E_g proved to be 4.4 eV, in contrast with the accepted value of about 4.1 eV; they justified this discrepancy by identifying their CT values with the vertical (Franck-Condon) transitions from a Frenkel ground state to vibrationally excited CT states. Furthermore, in opposition to a basic premise of the BPS treatment, they postulated that the excess vibrational energy for any particular CT state could be used to separate further the members of the ion-pair state. This postulate, in a sense, combines the processes of direct CT exciton generation with the ballistic carrier separation mechanism that is implied in the AI mechanism. The identification of the structures found by Sebastian et al (109) in the electroabsorption spectrum with CT states of different separations r_{CT} has been questioned by Siebrand & Zgierski (109a). These authors calculated the spectrum of CT states in anthracene and attributed the structure observed by Sebastian et al (109) to the vibrational overtones of the nearest-neighbor CT state (110). A resolution of the discrepancies between theory and experiment is not yet at hand.

The AI mechanisms of ionization coupled with the ballistic model of electron-hole separation has been discussed in detail by Silinsh et al (111), who studied tetracene and pentacene. Here, AI steps are succeeded by the escape of the hot electrons into the lattice, where they thermalize by acoustic phonon scattering, producing the series of bound CT states. Using a rather simple scattering theory, Silinsh et al (111) calculated the optical

energy dependence of the thermalization distances, $r_0(h\nu)$, which in turn correspond to specific separations of CT states. They found good agreement between their calculated and experimental values. Calculations were also made of the photoconductivity quantum efficiency, and agreement was found between calculated (using ballistic theory and a modified Onsager theory) and measured values in the energy region $E(h\nu) > E_g$. In the region $E(h\nu) \sim E_g$, they found a discrepancy that they attributed to a contribution from direct CT state absorption. In the higher regions of photon energy, they found another discrepancy that they attributed to excitation to a different AI state.

In addition to the cases considered above there is another interesting experimental result in which it appears that the efficiency of photoconduction is independent of photon energy (112). This work was carried out with X-metal-free phthalocyanine crystals embedded in a polymeric matrix. It was found that all the ionization proceeded from the first excited singlet state, S_1.

Summarizing the results presented herein regarding the relative roles of AI and direct CT exciton formation, it appears that there are materials and energy ranges in which one or the other, or both, mechanisms prevail; this point has been made by Silinsh et al (111). The actual determination of the relative roles of AI and direct CT exciton formation might be resolvable if photocurrent rise time measurements could be made. This suggestion was made by Bounds et al (105).

Extrinsic

Carrier injection by means of a suitably chosen electrode is a convenient and widely used method for producing a mobile carrier density in organic compounds (1, pp. 273 et seq). The time-resolved study of the injection process, which makes it possible to expose its microscopic details, can be facilitated by the fact that the rate constant for the recombination of the injected carrier with the electrode can be made arbitrarily small by choosing an electrolyte as the injection electrode. Using this fact, Eichhorn et al (113) have carried out the first time-resolved measurement of the escape of charge carriers by diffusional motion out of a Coulombic well near the injecting electrode. This well is created by the attraction of the injected carrier to its image in the electrode. The complete model consisted of a hole injected into the top layer of molecules in the crystal, which could recombine with the electrode with a rate constant k_{rec}, or decay to a trap level with a rate constant k_{tr}. The trapped hole could either recombine with the electrode with a rate constant $k_{t(rec)}$ or be activated back into the free state with a rate constant k_d. The rate of escape of the electron out of its Coulombic well was k_{es}. A fairly good agreement with experiment was

found using 4 Å as the effective boundary distance from which carrier injection proceeded, and the values $k_d = 5 \times 10^7\ s^{-1}$, $k_{t(rec)} = 4 \times 10^7\ s^{-1}$, $k_{tr} = 3 \times 10^8\ s^{-1}$, $k_{rec} \approx 0$. Other conclusions that were made were that the hole mobility in the c' direction was independent of electric field up to at least $5 \times 10^5\ V\ cm^{-1}$ and also at $1 \times 10^6\ V\ cm^{-1}$ (114). The recombination was assumed to be nongeminate, and to involve an OH^- ion. There is a problem with this assumption because the energy required to discharge an OH^- ion in a neutral aqueous solution is ≈ 6.8 eV, referenced to the vacuum zero (115), whereas only 5.8 eV are available as a result of the discharge of the anthracene hole. Chemical attack by a water molecule is a more likely route for this process.

CARRIER RECOMBINATION

Time Independent (Theory)

The Onsager theory of geminate recombination (116, 117) was designed as a steady state solution for a pair of oppositely charged geminate particles moving in a condensed phase continuum in the presence of an external electric field. Nevertheless, it has been widely and rather successfully used to interpret the electric field dependence of the quantum yield of photogenerated carriers in crystals, where the carriers undoubtedly are moving on a discrete lattice (118) (see 1, pp. 481 et seq). Recently, the Onsager continuum theory was extended to include the transient case (119), and the original Onsager assumption of a point-sink at $r = 0$ was refined into a recombination sphere of finite radius and recombination velocity (120). A seminal theory has recently been introduced by Rackovsky & Scher (121a) in which the problem of geminate recombination in a face-centered cubic (fcc) lattice is treated as a random walk on lattice sites in the presence of both an external field and a Coulomb field. The solution is given in terms of lattice Green's functions, modified by the presence of an applied electric field. In this model, one carrier is fixed at the origin and the other, oppositely charged, carrier moves on the lattice in accordance with a function $\psi(1, t)$ that gives the probability per unit time that it will leave a site 1 in a given direction. This function is determined by relative transition rates to the neighbors, and the transition rates in turn are determined by variables such as wavefunction overlap, energetic differences, and electron-vibration interactions. An important factor is the role of competing processes, such as the decay rate of the electronically excited precursors to the ion-pair state that dissociates. What emerges from this treatment will have profound effects on the interpretation of experiments using the Onsager formalism. The Onsager theory has two parameters that are specific to the system under study. These are the electron thermalization

distance r_0, and the initial quantum yield of geminate pair generation ϕ_0. These parameters can be evaluated if an assumption is made regarding the initial distribution of geminate pair distances (1, pp. 489 et seq). Scher & Rackovsky show that depending on the relative magnitudes of some molecular parameters described in Figure 1 and using a *fixed* initial distribution of charges (hence, a fixed r_0), the values of ϕ_0 that would have been calculated using the Onsager formalism on the yield versus field plots can be considerably different from each other. Thus, consider the calculation shown in Figure 1 illustrating the photogeneration efficiency η dependence on reduced electric field strength. Here $\varepsilon_{ex} = E_{ex}/kT$ where E_{ex} is the difference in energy between the first electronically excited state at the origin and the state consisting of a hole at the origin and an excess electron at a nearest neighbor. This could be a few tenths of an eV. The term χ is the strength of the Coulomb field between the carriers in the geminate pair, R gives the ratio of the relaxation rate of the initially excited state to the rate of intermolecular charge transfer, and the reduced field strength $\gamma = eFa/2kT$ where F is the electric field and the lattice spacing is a. Notice that in the top two curves, only ε_{ex} has changed; this could be produced for example by local energy fluctuations, which would be significant in the case of

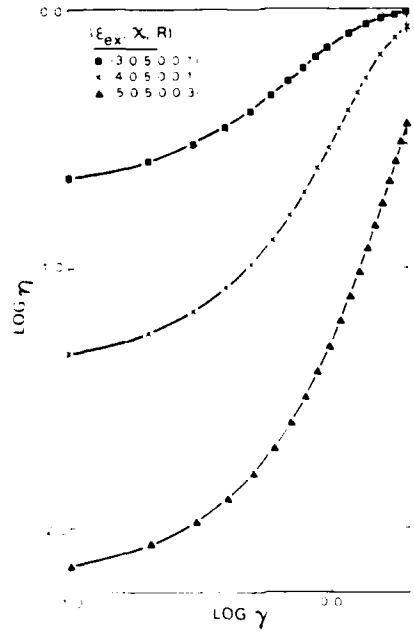

Figure 1 Log-log plot of the photogeneration efficiency η vs the reduced field strength γ illustrating the effect of varying ε_{ex} with χ and R essentially fixed. From Scher & Rackowsky (121).

molecularly doped polymers. In this calculation, the initial distribution is fixed (i.e. the average value of r_0 is *constant*). At low fields, it may be seen that for the lower value of ε_{ex}, η has decreased by an order of magnitude. If the Onsager formalism were used then for the same value of ϕ_0 the apparent value of r_0 would have to be altered in order to compensate for the differences in η. For a greater ε_{ex}, and a slightly larger value of R, η changes by another factor of 10, r_0 would have to change even more, and no saturation is evident at high field, in contrast with what is seen for the top curve.

Another important experiment is the measurement of the temperature dependence of the yield. According to the Onsager theory, the temperature dependence of η at zero field should follow an Arrhenius relationship in which the activation energy is $E_a = e^2/4\pi\varepsilon\varepsilon_0 r_0$. In the notation of Scher & Rackovsky, this would read $E_a = a\chi kT/2r_0$, or $r_0/a = \chi kT/2E_a$. This prediction is not realized. When R is large, a linear Arrhenius plot is obtained but with E_a a function of applied field. When R is small there is no linear plot.

In addition to the analytical treatment of Scher & Rackovsky, a Monte Carlo simulation was carried out by Ries et al (122) of field and temperature assisted dissociation on a perfectly isotropic 3D lattice, and perfectly linear (1D) systems. It was found that for a perfectly 1D system, the zero-field intercept of the dissociation probability would be zero, and the extent to which this intercept is not zero is a measure of the degree of anisotropy of the carrier motion. The power of the simulation approach is that any degree of anisotropy between 1D and 3D can easily be inserted.

An important, and not self-evident, assumption made in the simulations is that of field-independent hopping rates in 1D and 3D systems, i.e. the field does not affect either the initial pair distribution, or the prefactor to the expression containing the barrier height (which is modified by the field). For intersite hopping energies $< kT$, the Onsager result emerges.

An important test of the field dependence of the hopping rates was made by Seiferheld et al (123) using crystalline polydiacetylenes (see 1, pp. 673–99 for a description of these compounds) as model compounds. These compounds (PTS and DCH) are formed by the solid-state polymerization of crystalline acetylenic monomers, as a result of which a highly crystalline solid is formed composed of long conjugated polymeric chains held together by van der Waals forces. The strong covalent forces along the chain and the weak van der Waals forces between the chains lead to a markedly anisotropic electrical behavior. This makes these crystals good examples of quasi-1D systems. The degree of anisotropy may be quantified by means of the ratio $\mu_{\parallel}/\mu_{\perp}$, which are respectively, the mobilities parallel

and transverse to the molecular chain. The deduced ratio for the microscopic anisotropy was $>10^5$ in opposition to the value of $\sim 10^3$ indicated by current flow measurements (125, 126). The conclusion that the anisotropy is so high follows from an application of the Onsager theory of geminate recombination as modified for true 1D behavior. In a true 1D system, in the absence of an external electric field, the degree of dissociation of a hole-electron pair must be zero (127) because a particle executing a random walk on a 1D lattice must return to the origin with unit probability. In the present case, the experimental results are in accordance with the Onsager theory for a 1D system for applied fields down to 30 V/cm. Furthermore, according to a computer simulation carried out by Ries et al (122), the low-field intercept of the dissociation yield is a direct measure of the mobility anisotropy, i.e. $\lim_{F\to 0}\phi^{esc}(F) \propto \mu_\perp/\mu_\parallel$, where ϕ^{esc} is the probability of an electron escaping geminate recombination at the applied field F; no deviation from the Onsager 1D behavior appeared even when $\phi^{esc}(F) < 10^{-4}$.

Another important conclusion of this paper follows from the low-field agreement with the predictions of the Onsager 1D theory. According to the computer simulation results (122) the Onsager equations will be followed as long as the mean free path of the carrier between scattering events is comparable to the distance between lattice sites (≤ 10Å). The low-field agreement with the Onsager predictions then imply that diffusive transport in PTS and DCH is accompanied by strong scattering. However, for DCH, a mean free path of ≈ 100 Å for carrier scattering follows from an $m^* = 0.05\, m_e$ (128) and a scattering time of 8×10^{-14} s. This apparent contradiction may be removed by the application of theoretical findings of Movaghar & Cade (129, 130), who have shown that carrier transport in PTS occurs via localized polaron states whose mean free path for scattering could be about the distance between polymer repeat units. During the initial hole-electron formation, during which the Onsager formalism is not operative, the electron could travel in the wide conduction band for a distance of about 100 Å before falling into a polaron state. This distance could be associated with the thermalization distance, which is calculated by ~ 65 Å from other results.

The proposal that a polaron state is created in $\sim 10^{-14}$ s has other important ramifications. According to Donovan & Wilson (131), electron mean free paths are ~ 1 μm in length, and the electron mobility is $>2 \times 10^5$ cm^2 V^{-1} s^{-1}. If the mean free paths are so long, then geminate recombination should not be observed, whereas it is. The high mobilities (132) also become puzzling. This paradox was resolved by Movaghar et al (133), who showed that standard linear response theory as applied to transport was not applicable in these 1D systems.

A most significant result is that at high-field ($F > 10^4$ V cm^{-1}) the anticipated saturation does not occur. This failure to saturate had already been noticed in anthracene by Geacintov & Pope (134). Seiferheld et al (123) concluded that their results can only be explained by a primary ionization yield ϕ_0 that is field dependent.

Time Independent (In Polymers)

Evidence for exciton fusion as a mechanism for the intrinsic generation of free carriers in molecularly doped polymers has been reported by Orlowski & Scher (135, 136). The system studied consisted of solid solutions of the amine TTA [tri-(*p*-tolyl)amine] in the polymer Lexan (bisphenol-A-polycarbonate) in concentration between 30 and 40% by weight. Bulk (as distinguished from surface) photoconductivity was induced in 10 μm thick films. The singlet exciton decays by intersystem crossing ($\Phi_{isc} \approx 0.95$) to the lowest triplet state (T) of TTA. The phosphorescence of TTA peaks at 2.8 eV, so two triplet excitons can supply 5–6 eV; this is sufficient to induce photoionization. It was found that the photogeneration yield, q/A, varied smoothly as the light intensity I^2 at low light intensity, as I at high light intensity, and at some intermediate value in between. With an increase in field strength F from 5 V/μm to 20 V/μm, q/A increased by a factor of about 250 at $I = 10^{13}$ photons cm^{-2}, and in general the I dependence itself was F dependent. The scheme used to explain the results was as follows:

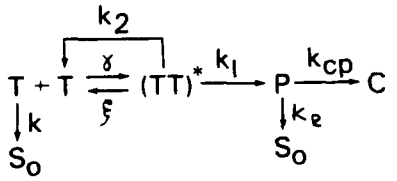

$(TT)^* = T^*$ is an associated triplet-pair state, S_0 is the ground electronic state, and C is the hole on the TTA molecule generated at the rate K_{CP} from P which is a charge-separated state in which the polymer contributes an acceptor state. The constant γ refers to the diffusion-limited process of triplet exciton fusion, and ξ applies to the diffusion-limited separation of T^*; K_1 refers to the creation of P, K_2 describes the annihilation of T^* to produce T and S_0, and K_R represents the recombination of hole and electrons to produce a ground state. The quantity η_{eff} is to be compared with the quantum yield obtained from data representing the linear response of q/A to I, and γ_{eff} corresponds to what would be measured as the diffusion-limited rate constant for triplet-triplet fusion to produce T^*. It was found that γ_{eff} increased from 0.16×10^{-12} cm^3 s^{-1} at $F = 0$, to

160×10^{-12} cm^3 s^{-1} at $F = 20 \times 10^4$ V cm^{-1}. At $F = 5 \times 10^4$ V cm^{-1}, η_{eff} was 1×10^{-4}, while at $F = 38 \times 10^4$ V cm^{-1}, η_{eff} was 24×10^{-4}.

The Onsager field effect found in many systems (1, pp. 484–95) applies to the relative magnitudes of K_{CP} and K_R, with P given by some initial efficiency ϕ_0, and says nothing about any of the other quantities in the schematic diagram. However, the Onsager theory cannot explain the magnitude of the observed results even if ϕ_0 is made field dependent (111). The picture that emerges is that the T^* state is probably a configuration consisting of a mixture of a triplet exciton pair, an excited S^* state, an excited charge-transfer complex and some other configurations as well. The electric field would have the effect of increasing the tunneling rate of the CT state to the P state, thus enhancing the value of γ_{eff}. The assignment of CT character to the intermediate triplet-pair state has been made in the past (137, 138). In systems in which singlet excitons play a dominant role in photoionizations, an extension of this mechanism would propose the existence of an intermediate S^* state that has CT character; the electric field should have a similar effect in this system and, indeed, had already been recognized by others (139, 140), who found this field effect on the ratio of carrier generation yield to fluorescence yield. Popovic (140) studied X-metal free phthalocyanene powders dispersed in Lexan. He concluded that the electric field increased the rate of dissociation of the lowest-lying excited singlet state S_1 into a CT state, which subsequently dissociated thermally, assisted by the external field. His work also provided an example of a case in which the same S_1 state acted as a precursor to CT state formation even though the initially excited state was higher in energy.

It has now become clear from the work of Popovic (140), Scher & Orlowski (135, 136), Silinsh and co-workers (141), and Rackovsky & Scher (121a) that the field dependence of photocarrier generation in organic molecular solids is not capable of being interpreted entirely by the continuum Onsager model (116, 117). Depending on the energy of photoexcitation, a state is produced in these materials that has a complex character including, for example, singlet-singlet (142), triplet-triplet (143), and a considerable charge-transfer component. The effect of the high external field is to shift the character of the intermediate state to one that is more ionic, and easier to ionize. Following the dissociation of the intermediate state, the usual Onsager formalism applies.

Time Dependent

Monte Carlo computer simulations of physical processes have also played a major role in the elucidation of the time-dependent geminate recombination. This is particularly important because it is difficult to carry out experiments in the picosecond time scale. The time dependence of geminate

recombination was simulated by Ries, Schönherr, Bässler, and Silver (144) and compared with the analytical solution given for the isotropic continuum model by Hong & Noolandi (HN) (119, 120) and Hong, Noolandi & Street (145). The simulation was not restricted to the isotropic continuum case, but considered 1, 2, and 3D motion on a discrete lattice of variable size and graininess. One of the conclusions of HN was that at long times, the survival probability of a geminate pair in 3-D follows a $t^{-3/2}$ decay law. That is, according to HN,

$$R^{3D}(t \gg \tau_0) = r_c \exp(-r_c/r_0)/(4\pi D t^3)^{1/2}$$

where

$$\tau_0 = r_c^2/4D, \qquad r_0 = e^2/4\pi\varepsilon\varepsilon_0 kT$$

and r_c is the Coulomb capture radius, D is the diffusion coefficient, R^{3D} is the geminate recombination rate in 3D. The simulation indicates that the $t^{-3/2}$ behavior, if realizable at all in an actual experiment, would be observed only when the signal amplitude (as for example, that for recombination luminescence) has decayed to 10^{-4} of its peak value. For practical situations, the exponent x of the decay function t^{-x} is $> 3/2$; the value of x will depend also on the dielectric constant of the medium (through r_c) and the dimensionality of the motion. In anthracene, $r_c/r_0 \approx 8$ (118), whereas for α-Si, where $\varepsilon = 11.5$ (compared to $\bar{\varepsilon} = 3.2$ for anthracene), r_c/r_0 is small enough so that the HN theory works well in explaining the α-Si luminescence decay rate (121).

Another startling result of the simulation is that in the first decade of the decay process ($t > \tau_0$) the simulated decay rate exceeds the HN results if extrapolated to short time limits. Thus, by using the HN theory to rationalize an observed recombination luminescence life time, one would have to use an inordinately large diffusion coefficient. The simulated and analytic results converge when the number of surviving particles has decayed to 10^{-6} of its peak value. Again, the HN theory predicts that for $t \gg \tau_0$

$$N^{3D} = \exp(-r_c/r_0)|1 + r_c/(4\pi D t)^{1/2}|$$

where N^{3D} is the fraction of surviving pairs, whereas the simulation results show a more complex function of time.

Another parameter that was varied in the simulation was the frequency of the final jump to the recombination center. This is particularly relevant because of the accumulating experimental evidence for the existence of a long-lived electron-hole pair state in organic crystals (142, 146–152). So far no attempts have been made to rationalize such behavior theoretically. Ordinarily one would expect the final recombination step to be rapid.

Although no picosecond time-resolved geminate recombination studies have been made on anthracene or its homologs, Braun & Scott (152) did carry out such a study on a hexane solution of anthracene at a concentration of 4.5×10^{15} cm^{-3}. At room temperature, the decay rate of photogenerated geminate cation-electron pairs is characterized by a first half-life of no more than 9 ps. The recombination process is strongly nonexponential, as would be predicted by the theory of Hong & Noolandi (120) and the recent work of Ries et al (144). Thus, the second half-life is 28 ps and the third half-life is 125 ps. The work in liquids indicates that geminate recombination can be rapid. However, there are conditions under which the final jump can be slow. To explore the consequences of such a situation, Ries et al (144) generated a "waiting factor" f_W for the final jump such that the inverse probability of the final step is $t_{rec} = f_W \tau_0$, where τ_0 is the hop time for an isoenergetic or exoenergetic jump. Thus, if the final recombination took place at a defect site, there might be an energetic barrier U_B to overcome, to which could be related an $f_W = \exp(U_B/kT)$. Carriers trapped in defect sites may exhibit abnormally long dwell times (see this review under CARRIER TRAPPING).

CARRIER TRANSPORT

In Molecular Crystals

Carrier transport in van der Waals molecular crystals, such as anthracene and naphthalene, has been the subject of intensive study during the last several years. The adequacy of band theory as a proper framework for interpreting experiments had been questioned as a result of its failure to explain electron mobility in the c' direction in anthracene and naphthalene. For a review of pertinent experimental data and theoretical models prior to 1982 see (1, pp. 337–78). A collection of data on mobilities in organic molecular crystals was published by Schein & Brown (153). In this review, we present the most recent experimental data and theoretical model. Requiring explanation are (*a*) the band-to-hopping transition observed (154) in naphthalene at $T \approx 100$ K for electron transport (μ^-) along the c' crystallographic direction, and (*b*) the almost complete lack of temperature dependence in μ^- in anthracene from 78–479 K (155) and in naphthalene from 100–325 K (156).

In contrast to electrons, hole transport (μ^+) characteristics are in accordance with band theory predictions (1, p. 349); μ^+ increases with decreasing temperature in the temperature region, in which shallow trapping is not dominant. Because of the weak intermolecular interactions in van der Waals crystals, the nearest-neighbor transfer energies, which are on the order of 10^{-2} eV (157, 158), are comparable to the conduction band

broadening due to dynamic disorder; strong dynamic disorder tends to localize carriers. A major theoretical problem has been to isolate the dominant terms in the complete transport Hamiltonian, which so far has been intractable. Sumi (159–162), in a series of papers, assumed that μ^- was dominated by electron-libron scattering. A recent analysis of mobility data suggests that a more conventional approach is fully capable of accounting for the temperature dependence of the electron mobility for $T < 100$ K. Specifically Andersen et al (163) have demonstrated that a Boltzmann equation analysis with longitudinal acoustic phonon-electron scattering can account quantitatively for the electron mobility in all crystallographic directions, in which case $\mu \propto T^{-3/2}$. Figure 2 illustrates how well $\mu \propto T^{-3/2}$ fits the experimental data. The lack of a temperature dependence in μ for $T > 100$ K is, however, still unexplained. Furthermore, as noted by Andersen et al (163), there is still the difficulty of reconciling the conventional band picture with the short mean free path (λ) of the carriers in the c' direction at temperatures $40 \leq T \leq 100$ K ($\lambda \approx a$).

Although saturation of the electron velocity along the c' direction has not been observed (164), field-dependent hole mobilities for F parallel to the a-axis at low temperatures have been reported by Warta & Karl (165).

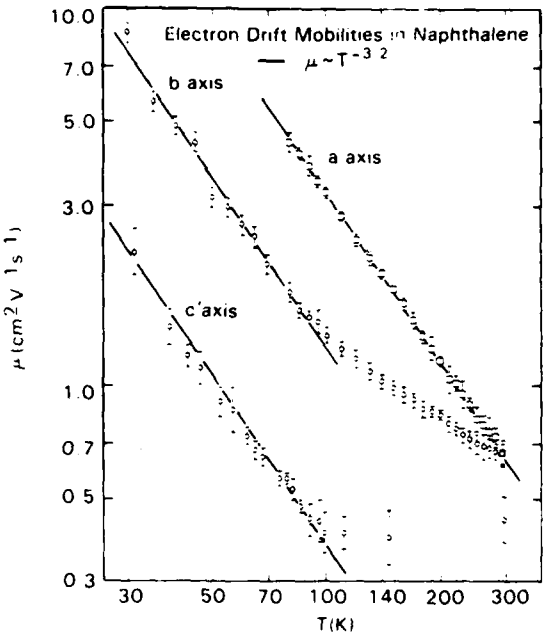

Figure 2 Measured electron drift mobilities along the a, b, and c′ directions in naphthalene as a function of temperature. From Anderson, Duke & Kenkre (163).

Presumably the freezing out of phonon modes at low temperatures enhances the carrier mean free path sufficiently so that momentum states near the edge of the Brillouin zone are significantly occupied.

In Poly-π-electron Polymers

Interest in the electrical conductivity of polymers is high and will certainly become greater with time. Several conferences have been devoted almost entirely to the subject of these poly-π-electron polymers (166, 167). A review of polyacetylene has been given by Etemad et al (168). Doped polyacetylenes have conductivities that are metallic ($\sim 1000\ \Omega^{-1}\ cm^{-1}$) and they have been fashioned into *p-n* junctions (169). In this review, we discuss only two polymeric systems that consist of long chains of conjugated molecules; these are the polyacetylenes and the polydiacetylenes, which have been the model systems used for the study of carrier transport.

POLYACETYLENES The polymer polyacetylene has received the greatest attention both theoretically and experimentally due, partly because it is the simplest conjugated polymer and also because the *trans* form can support mobile solitons. A *soliton* is an uncharged defect or a kink in the *trans*-polyacetylene (*t*-PA) chain consisting of two single bonds adjacent to each other, instead of the usual single and double bond alternation. This kink, or soliton, has one unpaired electron associated with it and is free to move along the *t*-PA chain. A charged soliton would have no unpaired electrons, and would not exhibit electron spin. No soliton exists in *cis*-polyacetylene (1, pp. 701, 780).

Structural changes usually associated with the *cis*- to *trans*-thermal isomerization have been observed in polyacetylene by Robin et al (170), who used synchrotron X-radiation (1.34 Å); the isomerization process was found to proceed homogeneously throughout the polymer and not in isolated amorphous or selected crystallite regions. That doping also induces a *cis*-to-*trans* isomerization has been demonstrated by Hoffman et al (171). The soliton has an EPR Lorentzian line-shape with a linewidth less than 1 Gauss (172, 173); that is suggestive of motional narrowing at least at room temperature since estimated linewidths from hyperfine interactions with neighboring protons is expected to be approximately 23 Gauss (174, 175). The observation of an Overhauser effect (176) is consistent with the paramagnetic defect being highly mobile. Furthermore ENDOR studies (177, 178) show a coalescing of the two-line spectrum into a single line on increasing the temperature. The ENDOR 2-line spectrum has been shown by Heeger & Schrieffer (179) to express the qualitative features of a mobile soliton. Evidence for solitons, independent of optical studies (180), has been provided by elastic tunneling conductance measurements (181).

A direct measurement of the time evolution of a photogenerated electron-hole state into charged kink-antikink states in *cis*- and *trans*-PA has been made by Shank et al (182). They showed that the electron-hole state decays in less than 1.5×10^{-13} s. This result supports the theoretical calculation of Su & Schrieffer (182a). From the decay curve of the charged kink state in *cis*-PA, it appears that the photogenerated state converts into a metastable state with a lifetime greater than 10 μsec. The long lifetime for recombination in *cis*-PA is reminiscent of that found in the polyacenes (146–151). In *t*-PA, the recombination is complete in ~200 ps, in which nearest neighbor jump times of $\sim 10^{-13}$ s at 300 K and 10^{-12} s at 20 K were calculated.

Soliton theory has been quite successful in explaining a wide variety of physical properties in *cis*- and *trans*-PA. Some of the subtle difficulties with the soliton theory in explaining EPR and NMR measurements and photo-induced changes in optical absorption have recently been summarized by Baeriswyl (183). We note here only the problem in explaining the transport characteristics. The Kivelson theory (184) of phonon-assisted hopping between charged and neutral solitons, although quite successful in making specific predictions regarding conductivity as a function of temperature, frequency, and concentration, is not without difficulties. The theory requires the presence of both neutral and charged solitons and is valid only at low concentrations, in the regime where $Y < 0.005$. This assumption is hard to reconcile with the observation of spinless conductivity at high dopant levels (at 2% dopant, all neutral solitons have been converted to charged solitons). Furthermore, spinless conductivity is not a unique property of *trans*-polyacetylene; it has been observed in poly(*p*-phenylene) (PPP) and for this polymer it is known that solitons cannot exist since the benzenoid form is significantly more stable than the quinoid form, i.e. PPP does not possess a degenerate ground state. In fact, PPP doped with AsF_5 has been reported to have a conductivity comparable to that of doped-PA ($\sim 500\ \Omega^{-1}\ cm^{-1}$ at dopant levels of 0.42 mole of AsF_5 per mole of monomer (185)). Thus, a theory of spinless conductivity that is based solely on charged solitons, even for *trans*-$(CH)_x$ is considered highly artificial.

A more promising model for spinless conductivity is the polaron-bipolaron theory of Bredas, Chance & Silbey (186, 187). This model does not exclude solitons: in factor neutral solitons are the main extrinsic defects in undoped *trans*-$(CH)_x$. In $(CH)_x$ the polaron is viewed as a pair consisting of a free radical (neutral soliton) and an ion (charged soliton) with an estimated binding energy of 0.05 eV, a value quite comparable to the pair binding energy of 0.03 eV calculated for PPP. An antisoliton is the mating kink to a soliton. An antisoliton will annihilate a soliton, producing a defect-free chain. An antipolaron is a combination of a charged soliton and

a neutral antisoliton. The evolution of states within the gap as a function of dopant concentration can be summarized as follows: Low doping introduces both bonding and antibonding localized polaron states within the gap. At higher doping levels the localized polaron states coalesce to form two polaron bands. In PA the interaction of a polaron with an antipolaron of the same charge results in two free charged solitons. This process occurs only for PA since the neutral soliton-antisoliton pair annihilates and the degenerate ground state allows the charged solitons to move apart. In PPP and other conducting polymers that lack a degenerate ground state, the two charged defects cannot separate and bipolaron formation ensues. Bipolarons are correlated charged soliton-charged antisoliton pairs. At even higher dopant concentrations bipolaron bands are formed. Evidence to support the existence of bipolarons and a polaron band in doped-PPP has been provided by electron energy loss spectroscopy (188).

Within the bipolaron model of transport, the neutral solitons that are required on neighboring chains are produced by the formation on a neighboring polymer chain of a virtual neutral soliton-antisoliton pair. After the charged portion of the bipolaron jumps to the virtual soliton-antisoliton pair on a neighboring chain, the residual soliton-antisoliton pair annihilates. This mechanism requires only a small activation energy, is applicable not only to *trans*-$(CH)_x$ but also to other conducting polymers, and does not eliminate the phonon-assisted interchain hopping mechanism of Kivelson in *trans*-$(CH)_x$ in dopant regimes where sufficient neutral solitons are available.

First principle calculations have shown that as in PPP, polaron states form within the band gap in polypyrrole at low doping levels (189). Optical absorption due to polarons in polyacetylene and in other polymers (polypyrroles, poly-paraphenylenes) has been considered theoretically by Bredas et al (186) and Fesser, Bishop & Campbell (190). Experimental support for bonding and antibonding polaron states in the low dopant limit in *t*-PA is reported by Etemad et al (191). It appears that in *t*-PA both polarons and solitons coexist at low doping concentrations and are the current carriers, whereas in polymers lacking a degenerate ground state and thereby precluding soliton formation, polarons are the exclusive carriers.

POLYDIACETYLENE The unusual features of carrier transport in PDA-TS are the apparent saturation of the drift velocity v_d at $\sim 2 \times 10^5$ cm s^{-1} down to fields as low as 1 V cm^{-1} [giving a lower bound for $\mu \approx 2 \times 10^5$ cm^2 V^{-1} s^{-1} (131)] and the photocurrent decay rate following a short light flash; this decaying photocurrent $I(t)$ obeys a relationship of the form $t^{-\alpha}$ where $\alpha \sim 1$ over 6 decades in time (10^{-6} s to 1 s) (144). This decay law is often found in amorphous materials, whereas in PDA-TS one would

expect very few scattering or recombination centers. Additional experiments by the authors in the time domain for which $I(t) \propto t^{-\alpha}$ shows that v_d is still field independent and $\alpha \sim 0.85$.

According to Seiferheld, Ries & Bässler (123), the anomalously high carrier mobility ($\mu \approx 10^5$ cm^2 V^{-1} s^{-1}) deduced for PDA-TS (131) is inconsistent with the strong scattering required to explain their successful use of the Onsager 1D carrier recombination formalism. The paper by Movaghar et al (133) resolves these difficulties and shows that there need be no qualitative conflict between the results of Donovan & Wilson (131) and those of Seiferheld et al (123).

The explanation for all of the observed results lies in the breakdown of linear response theory as applied to transport problems in a broad class of 1D systems (192). A model is used that is suitable for materials like PDA-TS, with its low concentration of crystal defects. Using the 1D diffusion theory of Alexander et al (193) one may deduce a time (t) dependent current $j(t)$ relationship of the form

$$j(t) \sim ea\eta t^{-\alpha(2-\alpha)}, \qquad t \to \infty. \tag{6.}$$

Here η is the applied reduced electric field and need not be defined here other than to state that for small fields, $2\eta = eFa/kT$, where a is the lattice spacing. However, as explained by Movaghar et al (192), linear-response theory breaks down in the long time domain and therefore Eq. 6 is wrong. The correct form for $j(t)$ at long times is

$$j(t) \sim 2ea\eta W_0^{1-\alpha} C(\alpha)/|2\eta t^{\alpha}| \tag{7.}$$

where $C(\alpha)$ is constant and W_0 is the hopping rate in a defect free 1D chain. Since $j(t)$ is proportional to the carrier drift velocity v_d, then according to Eq. 7 and the definition of η, v_d will vary sublinearly with the electric field. Furthermore, since $\alpha \sim 1$, it follows that the drift velocity will be almost independent at F.

The authors make the important point that behavior of the type described by Eq. 7 should appear in a wide class of 1D transport problems. Thus, for PDA-TS, the authors derived, for $t > t_c$

$$v_d(t, \eta) \sim (2x\eta C(\alpha, x)/x) W_0^{1-\alpha}/|2\eta t|^{\alpha} \tag{8.}$$

where x is the fraction of jumps that are difficult and t_c is the time required for the carrier to drift to a defect; $t_c \sim (2\eta x W_0)^{-1}$. Equation 8 applies to the PDA-TS experiments where $\alpha = 0.85$, and $v_d \propto F^{0.15}$, which looks like a saturated drift velocity. In addition, the photocurrent will decay as $t^{-\alpha}$ until carrier recombination (or collection at the electrode) takes place. It can be also shown that a lower bound for the mobility along the regular portion of

the chain will be $\mu_f > 10^8 a/2xF$. If v_d remains saturated at 2×10^5 cm s^{-1} down to $F = 1$ V cm^{-1}, as stated by Donovan & Wilson (131), then $\mu_f > 2 \times 10^5$ cm^2 V^{-1} s^{-1}. Thus, with $a = 1.2$ Å x could be $\sim 10^{-5}$ or fewer than 1 defect per 10^5 Å; this was also stated by Donovan & Wilson (131). Using the data of Seiferheld et al (123), who only went down to $F = 50$ V cm^{-1}, and taking $v_d = 2 \times 10^5$ cm s^{-1}, one gets $\mu_f \sim 10^3$ cm^2 V^{-1} s^{-1} and $x \sim 10^{-5}$, which is still a high mobility. Another interesting calculation is the time required to cross half the sample length, or $L_0/2$. This turns out to be

$$t_0 = (2\eta W_0)^{-1}(L_0 x/2a)^{1/(1-\alpha)}. \qquad 9.$$

With $v_d = 2 \times 10^5$ cm s^{-1}, $F = 1$ V cm^{-1}, $L_0 = 0.3$ cm, $\alpha = 0.85$, $a \sim 5$ Å, and $x = 10^{-5}$, then $t_0 \sim 10^{-2}$ s. For $x = 10^{-4}$, one obtains $t_0 \sim 10^5$ s. Thus, t_0 is extraordinarily sensitive to x and α. It is possible to increase x by creating radiation-induced defects; this has been done and very long relaxation times have indeed been observed (194).

In Amorphous Systems

As mentioned above, the introduction of computer modeling as a quasi-experimental technique is having a profound effect on the course of both experimental and theoretical studies. Consider the study of carrier transport in amorphous systems, of which polymeric conductors are a prime example. In amorphous systems, carrier transport clearly is by hopping. It has been shown by Bässler (195) and Schönherr et al (196) that by assuming a Gaussian distribution of hopping site energies, a wave function overlap factor $\exp(-2\alpha r)$, where r is the distance between neighboring sites, and a Boltzmann factor to accommodate hops to energetically unfavorable sites, one obtains the following: a temperature dependent trap-free mobility of the form $\mu(T) = \mu_x \exp\{-(T_0/T)^2\}$ where μ_x is the ideal mobility in the absence of disorder, and a field dependent mobility of the form $\mu(F) = \mu(0)\exp(F/F_0)$. The field dependence is of interest because it shows that no charged traps need be invoked to explain a field dependent mobility (1, p. 78); such a field dependence had already been observed, and charged traps had been conjectured (197). In a series of experiments (198) carried out with hole-transporting solid solution of a phenylmethane derivative in a plastic matrix, complete agreement was found between experiment and simulation, without invoking charged traps. As for the temperature dependence of the mobility in amorphous systems, this was studied experimentally by Lange & Bässler (199), who used amorphous tetracene films. The use of amorphous films of an otherwise crystalline material permits a study of the effects of disorder without changing chemical composition. Tetracene films deposited on substrate

held at 120–180 K are amorphous. A trap-free mobility obeys a relationship of the form $\mu(T) = \mu_x \exp\{-(T_0/T)^2\}$, where $\mu_x \approx 0.4$ to $0.8\ cm^2\ V^{-1}\ s^{-1}$, validating the Monte Carlo computer simulation. The Gaussian width given by Γ_0 is ≈ 0.1 eV, and is a function of sample preparation temperature T_F and hence of the degree of disorder. Important results of this paper are that the Gaussian width is a consequence of disorder-induced splitting of the transport band into a distribution of localized site energies; this effect is larger than that produced by the dielectric relaxation of the environment around a carrier. The success of the computer simulation strengthens support in its assumptions, and provides an alternate explanation for the results reported by Mort & Pfister (200).

Another interesting result was the observation of an almost temperature independent trapping time, although μ varied by more than an order of magnitude. Their explanation is based on the notion of trapping at an incipient dimer site. The density-of-states' profile in tetracene as deduced in these experiments exhibit a 0.1 eV width; this is in contrast with widths of 0.5 to 1 eV found in photoelectron spectra of molecular glasses (6). An explanation may be found in the differences between the processes of photoemission (which depends not only on the inhomogeneous broadening of the valence states, but lifetime broadening of the final state) and transport. In addition, transport probes the volume density of state distribution, whereas photoemission is essentially a surface phenomenon and the polarization energy changes markedly in this region (201, 202; see also 1, p. 63).

Another example of the power of a computer simulation is that carried out by Silver et al (203), who showed that while a Gaussian distribution of hopping site energies gives little dispersion, an exponential energy distribution gives rise to dispersive transport indistinguishable from multiple trapping. This introduces another mechanism for the interpretation of experimental results.

CARRIER TRAPPING

Experimental Techniques

A general technique for the determination of the concentration, energetic distribution, and composition of carrier trapping sites in organic solids does not yet exist. It remains as a challenge, and the rewards for solving the problem are great, since relatively small concentrations of traps radically modify the transport properties of the carriers. Present techniques include space charge limited currents (SCLC), thermally stimulated currents (TSC), optical detrapping, and electric field detrapping (1, pp. 267 et seq).

An important comparison of the results obtained on trapping states by

SCLC and TSC was made by Taure et al (204). They studied thin films of tetracene (Tc) and pentacene (Pc) in the form of oriented crystallites. The SCLC results were consistent with the existence of at least two sets of shallow traps of Gaussian distribution: In Tc the binding energy of one was $E_t = 0.1$ eV, with a distribution parameter ranging from $\sigma = 0.08$ to 0.14 eV in different samples, and a total trap density $N_c = \approx 4 \times 10^{15}$ cm^{-3}; for the other, $E_t \approx 0.3$ eV, $\sigma = 0.05$ to 0.1 eV and $N_t \approx 10^{14}$ cm^{-3}. The TSC results were in fair agreement with those of SCLC as shown in Figure 3, but gave higher resolution and probed deeper traps. Trapping cross-sections for the hole traps in Pc and Tc range from 10^{-16} to 10^{-14} cm^2 for the energy range 0.2 to 0.5 eV, and are about 10^{14} cm^2 for deep electron traps in Pc.

Some recent work involving the use of thermally stimulated currents (TSC) is that of Samoc et al (205), which also contains many references to important work in this field. This paper tests a recent theory of Plans et al (206) that deals with the field and sample thickness dependence of the peak at T_m, the temperature of the maximum that appears in the TSC glow curve. Samoc et al (205) added phenothiazine in a concentration of 5×10^{-5} mol fraction to anthracene. Using their technique, they found that phenothiazine created a hole trap centered at 0.62 eV above the valence band and that there was sufficient distribution of energy around this value to induce dispersive transport in the doped material. This trap depth may be

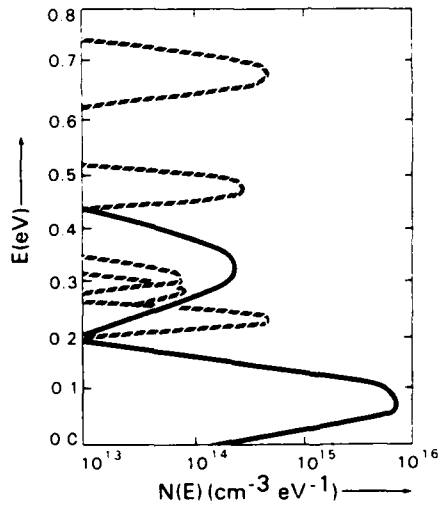

Figure 3 Density of electron trapping states $N(E)$ in pentacene layers as a function of trap depth E as determined by SCLS (*solid curves*) and TSC (*dashed curves*) techniques. From Taure et al (204).

compared with the value of 0.57 eV deduced by Karl et al (207) from photoemission studies.

An experimental technique for studying multiple deep trapping levels using only a single thermal scan was developed by Yoshie & Kamihara (208), and several intuitively appealing theoretical treatments of multiple trapping have appeared (209, 210). In these papers, an exponential distribution of traps with relatively fixed parameters was assumed. In a recent paper, Monroe & Kastner (211) relax these restrictions by allowing variation in capture cross-section, release times, trap distribution, and energy. The final result is a classification scheme in which the current transients may fall into any of five basic types; this scheme may be used as a diagnostic tool to identify the relevant trapping parameters operative in the experimental situation. The analytical results of Monroe & Kastner can also serve as a check on the results of increasing popular computer simulations. Mention should also be made of another comprehensive treatment of multiple trapping in amorphous systems by Arkhipov et al (212).

An interesting aspect of electron trapping was exposed by Meyer et al (63). They found that the electron trapping lifetime for transport in the c' direction over a range of temperatures (81–374 K) and applied electric fields (10^3 to 4.7×10^4 V cm^{-1}) was activated, and that this activation energy is independent of the field. The activation energies, E_a, ranged from 30 to 84 meV on crystals all prepared from the same sample, indicating that the behavior is extrinsic. The electron transport in the c' direction was not shallow-trap controlled; it was nearly independent of temperature. The authors conclude that the most likely source of the activation energy was the cross-section of capture. A parallel experiment was carried out by Arnold & Hassan (213), who measured the effect of pressure on the triplet exciton lifetime in anthracene. They found that the cross-section of capture was increased markedly (by a factor of four, in going from 1 atm to 6.4 kbar), without changing the trap concentration. Arnold & Hassan concluded that specific mechanical defects, referred to as preexcimer sites, were the source of these traps, and that triplet excimers were formed at these sites. They attributed the pressure effect to the creation of a more favorable intermolecular orientation. The role of predimer or incipient dimer sites as trapping centers was discussed by Pope & Kallmann (214; 1, pp. 283 et seq) and the existence of such sites was supported by the work of Thomas et al (215) and was also discussed by Lange and Bässler (199) and, at great length, by Williams & Thomas (216; 1, pp. 50–53). More recently, Zboinski (217) has examined the possibility that a deep trap can be created by the localization of a carrier at a pair of approximately parallel anthracene molecules.

A novel explanation of what can account for apparently deep ($\sim$0.7 eV) traps in pure molecular crystals has been presented by Petelenz (218). In pure crystals, one can account for shallow ($\sim$0.3 eV) traps by the increase in polarization energy surrounding a defect in the crystal lattice. However, one cannot use lattice distortions to explain a trap of depth $\sim$0.7 eV. Petelenz points out that the detrapping of a trapped electron involves not only supplying the binding energy E_t of the trap, but the electron must transfer itself away from the trap in a time short compared to the vibrational relaxation time of the excess electron. This requirement is the same as that for autoionization of a neutral state. In a sample calculation, Petelenz showed that detrapping could be accomplished by exciting vibrational degrees of freedom, rather than the carrier itself. He also showed that for a trap only 10^{-3} eV deep by virtue of lattice distortion, the apparent detrapping energy could be $\geq$0.75 eV due to the requirement of exciting effective vibrational modes.

Field Effects

One of the many differences between 3D systems and those of lesser dimensionality (1, p. 617) is the electric field-dependent reduction in the charge carrier trapping time in the 1 and 2D systems. In a 3D system, trapping is generally a first-order process with a time-independent rate constant. This is a consequence of the trapping probability increasing linearly with the number of new sites visited. The number of new sites visited by a randomly diffusing particle varies as n in 3D, $n/\ln(n)$ in 2D, and $n^{1/2}$ in 1D, where n is the number of steps taken (1, p. 122). If the hopping rate is constant, then the trapping rate will become time dependent in 2D and 1D motion. Movaghar et al (219, 220) showed analytically that in a 1D system, at long times, the relaxation of an excitation follows an $\exp[-(t/\tau)^{1/3}]$ law. This law was shown to apply to 1D trapping kinetics by Hunt et al (221) in a disordered polydiacetylene polymer, which shall be referred to as PDA-10H; this polymer contains a pendant CH_2OH group in every repeat unit of four carbon lengths. This paper reports the first measurement of a 1D relaxation law. The specific phenomenon is the decay of a transient photocurrent pulse in the PDA-10H in the time range 1 to 2 $\times 10^4$ s. Although the more widely studied PTS has an exceedingly low dislocation density (222), the concentration of deep traps is $\sim$1 per mm of polymer chain (131) in PDA-10H; due to the presence of extensive hydrogen bonding between the CH_2OH groups, there is a closer packing and greater internal strain in the final crystal, which is not as perfect as the PTS single crystals. A sample was excited by a square wave pulse of light and it was found that the decay follows an $\exp(-bt^{1/3})$ law.

In the presence of an electric field, the motion of the particle will be anisotropic and thus, in a 1D system, more new sites are likely to be visited than would otherwise be encountered. This implies that the trapping rate will increase with field strength. This effect was first observed by Haarer & Möhwald (223; 1, p. 616), in the charge-transfer complex phenanthrene-pyromellitic acid dianhydride. An exact solution of the time dependence of the trapping probability in the presence of an electric field F was derived by B. Movaghar, B. Pohlmann, and D. Würtz (MPW) (unpublished). They showed that as $t \rightarrow \infty$, a simple exponential law should be approached, the free carrier concentration decay time going as F^{-2} below a critical field F_c, and as F^{-1} above F_c. This theory was tested by Seiferheld et al (194), who used PTS; this polymer is an excellent model for a 1D crystal because its mobility anisotropy ratio $\mu_{\parallel}/\mu_{\perp}$ is $\sim 10^5$, where $\mu_{\parallel}$ is the mobility along the chain and $\mu_{\perp}$ is the mobility transverse to the chain direction. The PTS polymer is also unusual because it contains essentially no recombination centers for carriers (131), so the decay of a transient carrier population is governed by the kinetics of hopping and detrapping from traps of ~ 0.7 eV and discharge at the electrodes. In this experiment, traps and recombination centers were produced in a PTS crystal by bombardment with 100 KeV He^+ ions. It was found that at long times, and for fields of $\leq 1.7 \times 10^3$ V cm^{-1}, the current relaxation went as $\exp[-(t/\tau_1)^{1/3}]$. As the field increased, the long time relaxation curve became steeper, approaching a simple exponential, $\exp[-(t/\tau_2)]$. Moreover, τ_2 varied as F^{-2} below $F_c \approx 10^4$ V cm^{-1} and as F^{-1} above F_c. The effective carrier jump rate W can be calculated from τ_1, giving ~ 1 s^{-1}; this implies that the trap depth is ≈ 0.8 eV.

SUPERCONDUCTIVITY

The dramatic discovery of superconductivity in organic crystals was made by Bechgaard et al (225) and Jerome et al (226) in a family of isostructural compounds of the general formula $(TMTSF)_2X$ (also referred to as Bechgaard salts) where X is an anion (ClO_4^-, TaF_6^-, AsF_6^-, SbF_6^-, and ReO_4^-) and the cation is tetramethyltetraseleno-fulvalene. Only the ClO_4^- derivative exhibits superconductivity at atmospheric pressure; this occurs at a critical temperature $T_c \approx 1$ K. The other compounds all require the application of external pressure (8–12 kbar). Reviews of this field have been written by Jerome & Schulz (227) and by Friedel & Jerome (228). In addition, the proceedings of two conferences are particularly useful (229).

In the search for a general mechanism for superconductivity in organic materials, attention has been focused on the unit cell volume V_c and on the

interstack Se–Se distances (230). As has been found to be the case with the highly conducting ion-radical salts of the TTF-TCNQ class (1, pp. 581–91), the nearly planar, almost parallel TMTSF molecules are arranged in stacks along the *a* crystal axis (1, p. 638). In addition, the TMTSF molecules in neighboring stacks are sufficiently close to each other along the *b* direction so that infinite sheets are formed in the *ab* plane, separated by columns of anions. The short interstack, and intrastack Se–Se distances ($d < 4.0$ Å; this is less than the van der Waals radius sum for Se–Se) lead to strong interactions that result in the high conductivity in these materials. As the temperature is lowered from 298 to 125 K, anisotropic structural changes take place in which the interstack distances can decrease almost twice as much as the intrastack distances (231). A linear correlation was found between the unit cell volume, V_c, and the average interstack Se–Se distance (d_{avg}); this is shown in Figure 4. The correlation shows ClO_4^-, FSO_3^-, and BF_4^- salts clustering around the minimum values for V_c and d_{avg}, with almost identical values for d_{avg}. This suggests that these compounds will have a similar Se atom network geometry and similar low temperature electrical properties barring the onset of anion ordering (232); such ordering introduces a new crystal symmetry, and is considered to be a prerequisite for the attainment of superconductivity in $(TMTSF)_2ClO_4$ (233), in direct opposition to previous beliefs. In addition, those compounds requiring external pressure to achieve superconductivity have d_{avg} values greater than $d_{avg}(ClO_4^-)$. One may therefore venture to predict the anion size most likely to produce the desired V_{cp} (V_{cp} = predicted cell volume V_c). These results suggest that good results should be obtainable with those anions whose sizes are comparable to ClO_4^-; these include not only BF_4^-

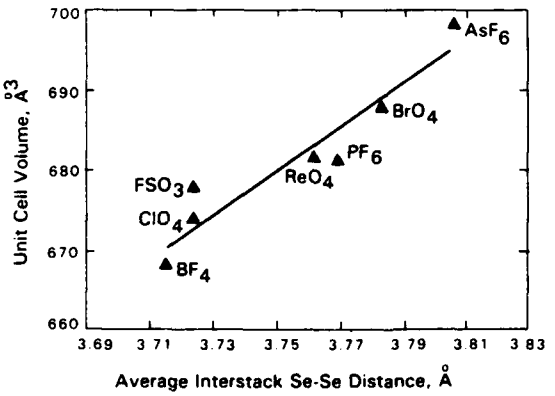

Figure 4 Plot of observed unit cell volume (V_c) vs the average interstack Se–Se distance for various $(TMTSF)_2X$ metals at 125 K. From Williams et al (231).

and FSO_3^-, but anion alloys embodying all possible combinations of these two anions.

Most organic molecules in crystals that exhibit metallic conductivity are planar, of D_{2h} symmetry, and pack in parallel layers in a stack, along which the conductivity is a maximum (1, pp. 588 et seq). In this quasi-1D crystal, it would therefore be expected that there would be intrastack bonding in this direction; this expectation is supported by the observation that in the organic metal TTF-TCNQ, the TCNQ-TCNQ distances are ≈ 3.17 Å as compared with 3.45 Å in the pure TCNQ crystal. In the case of the superconductors in the $(TMTSF)_2X$ family, it has been concluded that Se–Se bonding within a stack and between stacks creates a quasi-2D structure, which is chiefly responsible for the high conductivity. This conclusion was tested by making X-ray diffraction studies on perfect crystals of $(TMTSF)_2AsF_6$ prepared by Wudl (234). An accumulation of electron density was found above and below the TMTSF molecular plane in the region between the Se atoms, implying that there is bonding between the TMTSF molecules within the stack, probably as a result of the Se atom interactions. In addition, there was considerable electron density between Se atoms at the edge of adjacent stacks in the stacking direction. This could be evidence of a one-dimensional conduction band. In view of the substantial conductivity observed in the direction (*b* axis) perpendicular to the stacking axis (*a*) of the TMTSF molecules, electron density was looked for between Se atoms in neighboring stacks. An electron density was found between the Se atoms at the edge of adjacent stacks, but surprisingly, only between Se atoms with the longest interstack distance, ~ 4.15 Å. This was predicted by Grant (235). The continuum of electron density from Se to Se between the stacks may represent a conduction band. Thus, there exists a bonding originating from the Se atoms, between molecules within and between the stacks of $(TMTSF)_2AsF_6$ and $(TMTSF)_2PF_6$.

In the search for other superconducting compounds a new, and only the second, family of organic conductors was discovered (235a) based on the substitution of S for Se in the cation. The newly discovered compound is called $(BEDT\text{-}TTF)_4\ (ReO_4)_2$ where the cation is bis(ethylenedithiolo)-tetrathiafulvalene, and the anion is the perrhenate ion. This compound becomes superconductive above 4 kbar for $T_c \approx 2$ K. A metal-insulator transition takes place at a pressure < 7 kbar, and it may be associated with an anion rearrangement. These BEDT-salts have a variety of crystal structures and stoichiometries (236), in distinction to the Bechgaard salts, so it may be easier to locate the origin of superconductivity in these materials. These discoveries are particularly valuable because the mechanism for organic superconductivity is still poorly understood. One arduously sought for goal is to find a compound that has a high T_c.

MISCELLANEOUS

In this section, we would like to mention work that cannot be adequately discussed due to space limitations.

An example of the power of picosecond spectroscopy to unravel mechanisms of chemical and biological reactions is given in a review article by Rentzepis (237). In the wings stands the even more potent tool of femtosecond spectroscopy, as outlined by Shank & Greene (238). Optical pulses as short as 30 fs have been attained, which is shorter than some vibrational periods. One can anticipate the use of such pulses to follow the evolution of energy transfer in a coherent fashion between two degenerate states. Another impressive experiment showing the fission of a singly excited state into multiple excitonic states from which quantum yields and autoionization efficiencies are obtained has been carried out by Klein (239).

A discussion of electroluminescence in organic crystals is given by Kalinowski (240); the effect of pressure and temperature on the luminescence of tetracene single crystals was also studied by Kalinowski et al (241). In this latter study, a surprising feature of earlier work on tetracene was reexamined; this was the observation of an unusually large Stokes red shift (~ 500 cm^{-1}) between the 0–0 fluorescence and absorption transitions, whereas in anthracene it is 100–200 cm^{-1}. It now appears that this shift is an artifact caused by the compensation of the red shift resulting from the temperature modification of the exciton state and a blue shift caused by decreased overlap of the fluorescence and absorption spectrum. The Stokes shift of the reabsorption free 0–0 transition at 528 nm is 260 cm^{-1}, in good agreement with the value 280 cm^{-1} found at 4.2 K (242).

A recent review of the important subject of energy transfer has been given by Klöpffer (243). This review discusses basic concepts, measuring techniques, and results, mainly in polymeric systems. In the same book is an excellent discussion of triboelectricity in organic materials (244). This subject has not yet been put on a sound theoretical footing because of the enormous experimental difficulties in creating reproducible contacting surfaces. Important insights have been provided by Duke (245) and Duke & Fabish (246). Triboelectricity and triboluminescence may one day be studied in a more straightforward manner in outer space. Triboluminescence is thought to arise from the creation and annihilation of mobile cracks (247, 248), which in piezoelectric crystals can result in the creation of oppositely charged neighboring surfaces. The intense electric field at the tips of the cracks may facilitate charge recombination. In Mort & Pfister's book, a review of piezoelectricity and pyroelectricity by Wada (249) brings the field up to date from the last reviews prepared by Kepler (250) and Davies (251).

In the first of a series of photoconductivity experiments on PDA-TS crystals, Donovan & Wilson (131) found that the low field mobility was high, $\mu > 2 \times 10^5$ cm^2 V^{-1} s^{-1} and that the drift velocity saturated at a low value $v_s = 2 \times 10^5$ cm s^{-1} even for fields down to 1 V cm^{-1}. On the other hand, Spannring & Bässler (252) measured SCLC in PDA-DCH using ohmic electrodes; they found that $J \propto V^2$ for $F < 26$ V cm^{-1}, $v_d \propto F$, and $\mu = 6 \times 10^3$ cm^2 V^{-1} s^{-1}. This large discrepancy has been removed by the development of a SCLC theory for 1D materials. The conclusions are as follows:

1. A trap-limited SCLC shows a $J \propto V^2$ dependence even if v_s is saturated.
2. If F increases, then for some critical value F_c if $F > F_c$ the SCLC will become trap-free instead of trap-limited if v_d is saturated.
3. A trap-free SCLC in a 1D material shows a $J \propto V$ dependence if v_d is saturated.

With these findings, the discrepancies between the Donovan & Wilson results and those of Spannring & Bässler can be reconciled. The properly interpreted data of Spannring & Bässler yield a calculated μ for PDA-DCH of 1.6×10^5 cm^2 V^{-1} s^{-1}, very similar to that in PDA-TS.

CONCLUSIONS

This has been an active period for this field and promises to become even more so. The enormous skill of the organic chemist is being harnessed for the creation of a cornucopia of compounds with novel electronic properties. The discovery of superconductivity in more than one type of ion-radical salt greatly increases the prospects of determining the mechanism(s) of superconductivity, and hence of synthesizing compounds of higher transition temperature. The synthesis of compounds that behave as quasi 1- and 2D materials has provided a field day for theorists who can now find exact solutions to transport problems. The use of computer simulations has assumed major proportions,[1] and is already dominating fields such as amorphous solids, in which transport takes place by hopping. The continued development of ultra-short laser pulses of precisely defined wavelength has made possible the excitation of specific vibrational modes, and the study of their intrinsic relaxation rates; homogeneous linewidths are being measured and the mechanisms of line broadening elaborated.

Carrier generation in the homomolecular polyacenes has become much

[1] Journals devoted to a discussion of simulation techniques include *Mathematics and Computers in Simulation*, published by North Holland, and *Simulation*, published by Society of Computer Simulation.

better understood with the recognition of the importance of direct optical excitation of charge-separated (CT) states, and of precursors to CT states. It was certainly satisfying to view the evidence that at least at low temperatures, all carrier transport processes in anthracene and undoubtedly in essentially all of the polyacenes, is understandable in terms of a band theory of mobility. There is still the problem of the almost zero temperature dependence of electron mobility in the c' direction in anthracene, but this should give way before the next review of this field. The development of a generalized master equation (GME) approach to the study of exciton transport has revealed instances in which significant errors have been made in interpreting experimental data. The study of carrier recombination was enlivened by the discovery of novel high field effects that point to the existence of a field sensitive process for producing CT states, and by indications that the evaluation of the thermalization distance and the initial ionization yield from Onsager theory is a more delicate operation than previously thought. This latter conclusion followed upon the development of analytical and computer simulation techniques for following the recombination of geminate carriers on a discrete lattice.

The surface has not been scratched in the study of electronic processes in organic solids.

ACKNOWLEDGMENTS

One of us (M. P.) wishes to acknowledge support of the Department of Energy. We have benefitted from correspondence with H. Bässler, C. B. Duke, A. J. Epstein, and W. Siebrand. We express our appreciation to Ms. M. Menzel and Ms. A. Lunsford for their cheerful and indefatigable typing effort.

Literature Cited

1. Pope, M., Swenberg, C. E. 1982. *Electronic Processes in Organic Crystals*. New York: Clarendon Press, Oxford. 821 pp.
2. Mort, J., Pfister, G., eds. 1982. *Electronic Properties of Polymers*. New York: Wiley
3. Haddon, R. C., Kaplan, M. L., Wudl, F. 1982. In *Kirk-Othmer Encyclopedia of Chemical Technology*, 20:674–98. New York: Wiley. 3rd ed.
4. Adler, G., ed. 1983. *Proc. 6th Int. Conf. on Chem. of Organic Solid State. Mol. Cryst. Liquid Cryst.*, Vols. 93, 96
5. Duke, C. B. 1982. *Festkorperprobleme* 22:21–34
6. Duke, C. B. 1982. In *Extended Linear Chain Compounds*, ed. J. S. Miller, 2:59–125. New York: Plenum
7. Ford, W. K., Duke, C. B. 1983. See Ref. 4, 93:327–54
8. Duke, C. B. 1983. In *Electronic Excitations and Interaction. Processes in Organic Molecular Aggregates*, ed. P. Reineker, H. Haken, H. C. Wolf. 49:14–19. Berlin Heidelberg New York: Springer-Verlag
9. Sloan, G. J., McGhie, A. R. 1984. *Melt*

Crystallization Techniques. New York: Wiley
10. Karl, N. 1980. *Crystals: Growth Properties and Applications*, pp. 1–100. Berlin: Springer-Verlag
11. Smalley, R. E. 1983. *Ann. Rev. Phys. Chem.* 34:129–53
12. Fayer, M. D. 1982. *Ann. Rev. Phys. Chem.* 33:63–87
13. Drickamer, H. G. 1982. *Ann. Rev. Phys. Chem.* 33:25–47
14. Berry, D. E., Tompkins, R. C., Williams, F. 1982. *J. Chem. Phys.* 76:3362–70
15. Callis, P. R. 1983. *Ann. Rev. Phys. Chem.* 34:329–57
15a. Hanson, D. M. 1983. In *Molecular Electronic Devices*, ed. F. L. Carter, pp. 89–111. New York: Dekker
15b. Hanson, D. M., Patel, J. S., Winkler, I. C., Morrobel-Sosa, N. 1983. In *Spectroscopy and Excitation Dynamics of Condensed Molecular Systems*, ed. V. M. Agranovich, R. M. Hochstrasser, pp. 621–79. Amsterdam: North Holland
16. Johnson, C. K., Small, G. J. 1982. In *Excited States*, ed. E. C. Lim, 6:97–216. New York: Academic
17. Turlet, J. M., Kottis, P., Philpott, M. R. 1983. *Adv. Chem. Phys.* 54:303–468
18. Agranovich, V. M., Hochstrasser, R. M. 1983. *Spectroscopy and Excitation Dynamics of Condensed Molecular Systems*. Amsterdam: North Holland
19. Agranovich, V. M. 1982. *Electronic Excitation and Energy Transfer*. Amsterdam: North Holland
20. Knox, R. S. 1983. In *Collective Excitations in Solids*, ed. B. DiBartolo, pp. 183–245. New York: Plenum Press
20a. Aaviskoo, J., Liidja, G., Saari, P. 1982. *Phys. Status Solidi B* 110:69–73
20b. Saari, P., Rebane, K. 1981. *J. Phys. Colloq.* 42(C6):502–4
21. Powell, R. C., Soos, Z. G. 1975. *J. Lumin.* 11:1–45
22. Kenkre, V. M., Schmid, D. 1983. *Chem. Phys. Lett.* 94:603–8
23. Ern, V., Avakian, P., Merrifield, R. E. 1966. *Phys. Rev.* 148:862–67
24. Kenkre, V. M., Fort, A., Ern, V. 1983. *Chem. Phys. Lett.* 96:658–66
25. Kenkre, V. M. 1982. In *Exciton Dynamics in Molecular Crystals and Aggregates*, ed. G. Hohler. Berlin: Springer-Verlag
26. Kopelman, R. 1976. In *Topics in Applied Physics*, ed. F. K. Fong, 15:297–346. Berlin: Springer-Verlag
27. Kopelman, R., Monberg, E. M., Ochs, F. W., Prasad, P. 1975. *Phys. Rev. Lett.* 34:1506–9
28. Deleted in proof
29. Blumen, A., Silbey, R. 1979. *J. Chem. Phys.* 70:3707–14
30. Loring, R. F., Fayer, M. D. 1982. *Chem. Phys.* 70:139–47
31. Gentry, S. T., Kopelman, R. 1982. *Chem. Phys. Lett.* 93:264–66
32. Parson, R. P., Kopelman, R. 1982. *Chem. Phys. Lett.* 87:528–32
33. Gentry, S. T., Kopelman, R. 1983. *J. Chem. Phys.* 78:373–82
34. Monberg, E. M., Kopelman, R. 1980. *Mol. Cryst. Liquid Cryst.* 57:271–312
35. Brown, R., Lemaistre, J. P., Megel, J., Pee, P., Dupuy, F., Kottis, P. 1982. *J. Chem. Phys.* 76:5719–26
36. Gentry, S. T., Kopelman, R. 1983. *Phys. Rev. B* 27:2579–82
37. Prasad, P. M., Morgan, J. R., El-Sayed, M. A. 1981. *J. Phys. Chem.* 85:3569–71
38. Morgan, J. R., El-Sayed, M. A. 1983. *J. Phys. Chem.* 87:383–85
39. Morgan, J. R., El-Sayed, M. A. 1983. *J. Phys. Chem.* 87:2178–85
40. Hatlee, M. D., Kozak, J. J. 1981. *Phys. Rev. B* 23:1713–18
41. Arnold, S., Alfano, R. R., Pope, M., Yo, H. P., Selsby, R., Tharrats, J., Swenberg, C. E. 1976. *J. Chem. Phys.* 64:5104–14
42. Klymko, P. W., Kopelman, R. 1982. *J. Phys. Chem.* 86:3686–88
43. Blumen, A., Klafter, J., Silbey, R. 1980. *J. Chem. Phys.* 72:5320–32
44. Klymko, P. W., Kopelman, R. 1983. *J. Phys. Chem.* 87:4565–67
45. Alexander, S., Orbach, R. 1982. *J. Phys. Lett.* 43:L625–L631
46. DeGennes, P. G. 1983. *C.R. Acad. Sci. Paris* 296(2):881–85
47. Schilling, R., Mattis, D. C. 1982. *Phys. Rev. Lett.* 49:808–11
48. Schilling, R., Mattis, D. C. 1983. *Phys. Rev. B* 27:3318–23
49. Thomas, G. A., Rice, T. M. 1977. *Solid State Commun.* 23:359–63
50. Singh, J. 1981. *Phys. Status Solidi B* 1036:423–28
51. Singh, J. 1981. *J. Chem. Phys.* 75:4603–11
52. Gumbs, G., Mavroyannis, C. 1982. *Solid State Commun.* 41:237–40
53. Sanche, L., Bader, G. B., Caron, L. 1982. *J. Chem. Phys.* 76:4017–27; 77:3166–70
54. Agranovich, V. M., Zakhidov, A. A. 1979. *Chem. Phys. Lett.* 68:86–89
55. Sugakov, V. I. 1979. *Sov. Phys. Solid State* 21:332–35
56. Brikenshtein, V. Kh., Benderskii, V. A., Filippov, P. G. 1983. *Phys. Status Solidi B* 117:9–39

57. Wolf, H. C. 1967. In *Advances in Atomic and Molecular Physics*, Vol. 3. New York: Academic
58. Braun, A., Mayer, U., Auweter, H., Wolf, H. C., Schmid, D. 1982. *Z. Naturforsch. Teil A* 37:1013–1023
59. Campillo, A. J., Shapiro, S. L., Swenberg, C. E. 1977. *Chem. Phys. Lett.* 52:11–15
60. Al-Obaidi, S. J., Birks, J. B., Birch, D. J. S., Hallam, A., Imhoff, R. E. 1978. *J. Phys. B* 11:2301–11
61. Davies, M. J., Jones, A. C., Williams, J. O., Munn, R. W. 1983. *J. Phys. Chem.* 87:541–43
62. Shinohara, H., Kotani, M. 1980. *Bull Chem. Soc. Jpn.* 53:3171–75
63. Meyer, K. E., Schein, L. B., Anderson, R. W., Narang, R. S., McGhie, A. R. 1983. *Mol. Cryst. Liquid Cryst.* 101:199–218
64. Crisp, G. M., Walmsley, S. H. 1982. *Chem. Phys.* 68:213–22
65. Huber, D. L. 1980. *Phys. Rev. B* 22:1714–21; 24:1083–86
66. Kenkre, V. M., Wong, Y. M. 1981. *Phys. Rev. B* 23:3748–55
67. Lakatos-Lindenberg, K., Hemenger, R. P., Pearlstein, R. M. 1972. *J. Chem. Phys.* 56:4852–67
68. Kenkre, V. M. 1982. *Chem. Phys. Lett.* 93:260–63
69. Kenkre, V. M., Parris, P. E. 1983. *Phys. Rev. B* 27:3221–34
69a. Khizhnyakov, V. V., Sherman, A. V. 1980. *Sov. Phys. Sol. State* 32:1904–9
70. Toyozawa, Y., Shinozuka, Y. 1980. *J. Phys. Soc. Jpn.* 48:472–78
71. Mayer, U., Auweter, H., Braun, A., Wolf, H. C., Schmid, D. 1981. *Chem. Phys.* 59:449–65
72. Ludmer, Z., Berkovic, G. E., Zeiri, L., Muhle, W., Wolf, H. C. 1982. *Chem. Phys. Lett.* 90:245–46
73. Von Freydorf, E., Kinder, J., Michel-Beyerle, M. E. 1978. *Chem. Phys.* 27:199–209
74. Matsui, A., Nishimura, H. 1982. *J. Phys. Soc. Jpn.* 51:1711–12
75. Matsui, A., Mizuno, K., Iemura, M. 1982. *J. Phys. Soc. Jpn.* 51:1871–77
76. Berk, N. F., Rosenthal, J., Yarmus, L. 1983. *Phys. Rev. B* 28:4963–69
77. Szabo, A. 1971. *Phys. Rev. Lett.* 27:323–26
78. DeVries, H., Wiersma, D. A. 1976. *Phys. Rev. Lett.* 36:91–94
79. Treshchalov, A. B., Rozman, M. G. 1983. *Opt. Commun.* 47:262–67
80. Olson, R. W., Patterson, F. G., Lee, H. W. H., Fayer, M. D. 1981. *Chem. Phys. Lett.* 77:403–7
81. Hessenlink, W. H., Wiersma, D. A. 1978. *Chem. Phys. Lett.* 50:51–56
82. Amirav, A., Even, O., Jortner, J. 1982. *J. Phys. Chem.* 86:3345–58
82a. Godzik, K., Hays, T. R., Henkre, W. E., Selzle, H. L., Schlag, E. W. 1982. In *Laser Chemistry* 1:59–75. London: Harwood Headem Press
83. Small, G. J. 1982. In *Molecular Spectroscopy:* volume of *Modern Problems in Solid State Physics*, ed. V. M. Agranovich, A. A. Maradudin. Amsterdam: North-Holland
84. Jankowiak, R., Bässler, H. 1983. *Chem. Phys. Lett.* 95:124–28
85. Jankowiak, R., Bässler, H. 1983. *Chem. Phys. Lett.* 95:310–14
86. Jankowiak, R., Bässler, H. 1983. *Chem. Phys. Lett.* 101:274–78
87. Olson, R. W., Lee, H. W. H., Patterson, F. G., Fayer, M. D., Shelby, R. M., Burum, D. P., Macfarlane, R. M. 1982. *J. Chem. Phys.* 77:2283–89
87a. Hess, L. A., Prasad, P. N. 1983. *J. Chem. Phys.* 78:626–31
88. Reineker, R., Morawitz, H. 1982. *Chem. Phys. Lett.* 86:359–64
89. Deleted in proof
90. Freiberg, A., Saari, P. 1983. *IEEE J. Quantum Electron.* QE19:622–30
91. Wiesenfeld, J. M., Greene, B. I. 1983. *Phys. Rev. Lett.* 51:1754–58
92. Koch, E. E., Gürtler, P. 1983. In *Photophysics and Photochemistry in the Vacuum UV*, ed. S. P. McGlynn, G. L. Findley, R. H. Huebner. Dordrecht, Holland: Reidel
93. Hoffman, B. M., Ibero, J. A. 1983. *Acc. Chem. Res.* 16:15–21
94. Zagrubskii, A. A., Petrov, V. V., Lovcjus, V. A. 1981. *Izv. Akad. Nauk. Lat. SSR Fiz. Tver. Tela.* 5:29–33
95. Ford, W. K., Duke, C. B., Patson, A. 1982. *J. Chem. Phys.* 77:4564–72
96. Ford, W. K., Duke, C. B., Salaneck, W. R. 1982. *J. Chem. Phys.* 77: 5030–39
97. Duke, C. B., Ford, W. K. 1983. *Int. J. Quant. Chem.* 17:597–608
97a. Ladik, J. 1981. In *Theoretical Chemistry*, ed. C. Thomson, 4:49-ff. London: R. Soc. Chem. London Butterworths
98. Rice, S. A., Jortner, J. 1967. In *Physics and Chemistry of the Organic State*, ed. D. Fox, M. M. Labes, A. Weissberger, 3:201–497. New York: Wiley
99. Deleted in proof
100. Pope, M., Kallmann, H., Giachino, J. 1965. *J. Chem. Phys.* 42:2540–43
101. Vilesov, F. I., Zagrubskii, A. A., Garbuzov, D. Z. 1964. *Sov. Phys. Sol. State* 5:1460–64

102. Bounds, P. J., Siebrand, W. 1980. *Chem. Phys. Lett.* 75:414–18
103. Bounds, P. J., Siebrand, W. 1982. *Chem. Phys. Lett.* 85:496–98
104. Bounds, P. J., Petelenz, P., Siebrand, W. 1981. *Chem. Phys.* 63:303–20
105. Bounds, P. J., Petelenz, P., Siebrand, W. 1982. *Chem. Phys. Lett.* 89:1–3
106. Chance, R. R., Braun, C. L. 1976. *J. Chem. Phys.* 64:3573–81
107. Kato, K., Braun, C. L. 1976. *J. Chem. Phys.* 72:172–76
108. Sebastian, L., Weiser, G., Bässler, H. 1981. *Chem. Phys.* 61:125–35
109. Sebastian, L., Weiser, G., Peter, G., Bässler, H. 1983. *Chem. Phys.* 75:103–14
109a. Siebrand, W., Zgierski, M. Z. 1983. In *Electronic Excitations and Interaction Processes in Organic Molecular Aggregates*, ed. P. Reineker, H. Haken, H. C. Wolf, pp. 136–44. Berlin: Springer-Verlag
110. Hinchliffe, A., Munn, R. W., Siebrand, W. 1983. *J. Phys. Chem.* 87:3837–39
111. Silinsh, E. A., Kolesnikov, V. A., Muzikante, I. J., Balode, D. R. 1982. *Phys. Status Solidi* 113b:379–93
112. Popovic, Z. D., Sharp, J. H. 1977. *J. Chem. Phys.* 66:5076–82
113. Eichhorn, M., Willig, F., Charle, K. P., Bitterling, K. 1982. *J. Chem. Phys.* 76:4648–56
114. Eichhorn, M. 1982. PhD thesis. Technical Univ., Berlin
115. Slotnick, K. 1983. PhD thesis. New York: Univ., New York
116. Onsager, L. 1934. *J. Chem. Phys.* 2:599–615
117. Onsager, L. 1938. *Phys. Rev.* 54:554–57
118. Chance, R. R., Braun, C. L. 1976. *J. Chem. Phys.* 64:3573–81
119. Hong, K. M., Noolandi, J. 1978. *J. Chem. Phys.* 69:5026–39
120. Noolandi, J., Hong, K. M. 1979. *J. Chem. Phys.* 70:3230–36
121. Scher, H., Rackovsky, S. 1984. *J. Chem. Phys.* In press
121a. Rackovsky, S., Scher, H. 1984. *Phys. Rev. Lett.* 52:453–56
122. Ries, B., Schönherr, G., Bässler, H., Silver, M. 1983. *Philos. Mag.* 48:87–106
123. Seiferheld, U., Ries, B., Bässler, H. 1983. *J. Phys. C Solid State Phys.* 16:5189–5201
124. Deleted in proof
125. Lochner, K., Reimer, B., Bässler, H. 1976. *Chem. Phys. Lett.* 41:388–90
126. Siddiqui, A. S., Wilson, E. G. 1979. *J. Phys. C Solid State Phys.* 12:4237–43
127. Haberkorn, R., Michel-Beyerle, M. E. 1973. *Chem. Phys. Lett.* 23:128–30
128. Sebastian, L., Weiser, G. 1981. *Phys. Rev. Lett.* 46:1156–59
129. Movaghar, B., Cade, N. A. 1982. *J. Phys. C Solid State Phys.* 15:L807–L813
130. Cade, N. A., Movaghar, B. 1983. *J. Phys. C Solid State Phys.* 16:539–50
131. Donovan, K., Wilson, E. G. 1981. *Philos. Mag. B* 44:9–29
132. Spannring, W., Bässler, H. 1979. *Ber. Bunsenges Phys. Chem.* 83:433–36
133. Movaghar, B., Murray, D., Donovan, K. J., Wilson, E. G. 1984. *J. Phys. C* 17:1247–55
134. Geacintov, N. E., Pope, M. 1971. In *Proc. 3rd Int. Conf. Photoconductivity*, ed. E. M. Pell, pp. 289–95. New York: Pergamon
135. Orlowski, T. E., Scher, H. 1983. *Phys. Rev. B* 27:7691–7702
136. Scher, H., Orlowski, T. E. 1983. *Phys. Rev. Lett.* 50:775–78
137. Jortner, J., Choi, S. I., Katz, J. L., Rice, S. A. 1963. *Phys. Rev. Lett.* 11:323–26
138. Petelenz, P. 1980. *Chem. Phys. Lett.* 76:186–89
139. Yokoyama, M., Matsubara, A., Shimiokihara, S., Mikawa, H. 1982. *Polymer J.* 14:73–75
140. Popovic, Z. D. 1983. *J. Chem. Phys.* 78:1552–58
141. Silinsh, E. A., Kolesnikov, V. A., Muzikante, I. J., Balode, D. R., Gailis, A. K. 1981. *Izv. Akad. Nauk. Latv. SSR Ser. Fiz. Tekhn. Nauk.* 5:14–28
142. Klein, J., Martin, P., Voltz, R. 1981. *J. Lumin.* 24/25:99–102
143. Moller, W., Pope, M. 1973. *J. Chem. Phys.* 59:2760–61
144. Ries, B., Schönherr, G., Bässler, H., Silver, M. 1983. *Philos. Mag. B* 48:87–106
145. Hong, K. M., Noolandi, J., Street, R. A. 1981. *Phys. Rev. B* 23:2967–76
146. Pope, M., Burgos, J. 1966. *Mol. Cryst.* 1:395–415
147. Altwegg, L., Pope, M., Fowlkes, W. 1984. *Chem. Phys.* 86:471–82
148. Fünfschilling, J., Samoc, M., Williams, D. F. 1983. *Chem. Phys. Lett.* 96:157–60
149. Klein, G., Carvalho, M. J. 1977. *Chem. Phys. Lett.* 51:409–12
150. Popovic, Z. D. 1983. *Chem. Phys. Lett.* 100:227–29
151. Altwegg, L., Davidovich, M. A., Fünfschilling, J., Zschokke-Gränacher, I. 1978. *Phys. Lett. Rev. B* 18:4444–53
152. Braun, C. L., Scott, T. W. 1983. *J. Phys. Chem.* 87:4776–78
153. Schein, L. B., Brown, D. W. 1982. *Mol. Cryst. Liquid Cryst.* 87:1–12

154. Schein, L. B., Duke, C. B., McGhie, A. R. 1978. *Phys. Rev. Lett.* 40:197–200
155. Schein, L. B. 1977. *Chem. Phys. Lett.* 48:571–75
156. Schein, L. B., McGhie, A. R. 1979. *Phys. Rev. B* 20:1631–39
157. Katz, J. L., Rice, S. A., Choi, S., Jortner, J. 1963. *J. Chem. Phys.* 39:1683–97
158. Silbey, R., Jortner, J., Rice, S. A., Vala, M. T. Jr. 1965. *J. Chem. Phys.* 42:733–37
159. Sumi, H. 1978. *Solid State Commun.* 28:309–12; 29:495–99
160. Sumi, H. 1979. *J. Chem. Phys.* 70:3775–85
161. Sumi, H. 1979. *J. Chem. Phys.* 71:3403–11
162. Sumi, H. 1979. *J. Chem. Phys.* 75:2987–93
163. Andersen, J. D., Duke, C. B., Kenkre, V. M. 1983. *Phys. Rev. Lett.* 51:2202–5
164. Schein, L. B., Narang, R. S., Anderson, R. W., Meyer, K. E., McGhie, A. R. 1983. *Chem. Phys. Lett.* 100:37–40
165. Warta, W., Karl, N. 1982. *10th Mol. Cryst. Symp.*, St. Jovette, Canada
166. Epstein, A. J., Conwell, E. M., eds. 1981/82. *Proc. Int. Conf. on Low Dimensional Conductors, Mol. Cryst. Liquid Cryst.* Vols. 77, 79, 81, 83, 85, 86
167. *Int. Conf. sur la Phys. Chem. des Polymeres et Conductors*, 1983. *J. Physique* 44: Coll. C-3
168. Etemad, S., Heeger, A. J., MacDiarmid, A. G. 1982. *Ann. Rev. Phys. Chem.* 33:443–69
169. Nigrey, P. J., MacDiarmid, A. G., Heeger, A. J. 1982. *Mol. Cryst. Liquid Cryst.* 81:309–17
170. Robin, P., Pouget, J. P., Comes, R., Gibson, H. W., Epstein, A. J. 1983. *Phys. Rev. B* 27:3938–94
171. Hoffman, D. M., Gibson, H. W., Epstein, A. J., Tanner, D. B. 1983. *Phys. Rev. B* 27:1454–57
172. Francois, B., Bernard, M., Andre, J. J. 1981. *J. Chem. Phys.* 75:4142–52
173. Weinberger, B. R., Ehrenfreund, E., Pron, A., Heeger, A. J., MacDiarmid, A. G. 1983. *J. Chem. Phys.* 72:4749–55
174. Weinberger, B. R., Kaufer, J., Heeger, A. J., Pron, J., MacDiarmid, A. G. 1979. *Phys. Rev. B* 20:223–30
175. Roth, S., Eichinger, K., Menke, K. 1984. In *Quantum Chemistry of Polymers*, ed. J. Ladik, M. André, pp. 165–90. Dordrecht: Reidel
176. Nechtschein, M., Devreux, F., Greene, R. L., Clarke, T. C., Street, G. B. 1980. *Phys. Rev. Lett.* 44:356–59
177. Thomann, H., Dalton, L. R., Tomkiewicz, Y., Shiren, N. S., Clarke, T. C. 1983. *Phys. Rev. Lett.* 50:533–36
178. Kuroda, S., Schrieffer, J. R. 1983. *Solid State Commun.* 43:591–94
179. Heeger, A. J., Schrieffer, J. R. 1983. *Solid State Commun.* 48:207–10
180. Suzuki, N., Ozaki, M., Etemad, S., Heeger, A. J., MacDiarmid, A. G. 1980. *Phys. Rev. Lett.* 45:1209–13
181. Leo, V., Gusman, G., Deltour, R. 1982. *Phys. Rev. R B* 26:3285–88
182. Shank, C. V., Yen, R., Fork, R. L., Orenstein, J., Baker, G. L. 1982. *Phys. Rev. Lett.* 49:1660–63
182a. Su, W. P., Schrieffer, J. R. 1980. *Proc. Natl. Acad. Sci. USA* 77:5626–29
183. Baeriswyl, D. 1983. *Helv. Phys. Acta* 56:639–53
184. Kivelson, S. 1981. *Phys. Rev. Lett.* 47:1549–53; 1982. *Phys. Rev. B* 25:3798–3821
185. Shacklette, L. W., Chance, R. R., Ivory, D. M., Miller, G. G., Baughman, R. H. 1980. *Synth. Metals* 1:307–20
186. Brédas, J. L., Chance, R. R., Silbey, R. 1982. *Phys. Rev. B* 26:5843–54
187. Brédas, J. L., Chance, R. R., Silbey, R. 1982. *Mol. Cryst. Liquid Cryst.* 77:319–32
188. Crecelius, G., Stamm, M., Fink, J., Ritsko, J. J. 1983. *Phys. Rev. Lett.* 50:498–500
189. Brédas, J. L., Themans, B., Andre, J. M. 1983. *Phys. Rev. B* 27:7827–30
190. Fesser, K., Bishop, A. R., Campbell, D. L. 1983. *Phys. Rev. B* 27:4804–25
191. Etemad, S., Feldblum, A., MacDiarmid, A. G., Chung, T. C., Heeger, A. J. 1983. *J. Phys. Coll.* 44(C3):413–22
192. Movaghar, B., Murray, D., Pohlmann, B. Würtz, D. 1984. *J. Phys. C* 17:1677–83
193. Alexander, S., Bernesconi, J., Schneider, W. R. 1981. *Rev. Mod. Phys.* 53(2):175–98
194. Seiferheld, U., Bässler, H., Movaghar, B. 1983. *Phys. Rev. Lett.* 51:813–16
195. Bässler, H. 1981. *Phys. Status Solidi B* 107:9–53
196. Schönherr, G., Bässler, H., Silver, M. 1981. *Philos. Mag. B* 44:369–81
197. Hirsch, J. 1974. *Phys. Status Solidi A* 25:575–80
198. Bässler, H., Schönherr, G., Abkowitz, M., Pai, P. M. 1982. *Phys. Rev. B* 26:3105–13
199. Lange, J., Bässler, H. 1982. *Phys. Status Solidi B* 114:561–69
200. Mort, J., Pfister, G. 1982. In *Electronic Properties of Polymers*, ed. J. Mort, G. Pfister, pp. 215–65. New York: Wiley
201. Salaneck, W. R. 1978. *Phys. Rev. Lett.* 40:60–63
202. Duke, C. B., Fabish, T. J., Paton, A. 1977. *Chem. Phys. Lett.* 49:133–36
203. Silver, M., Schönherr, G., Bässler, H. 1982. *Phys. Rev. Lett.* 48:352–55
204. Taure, L. F., Silinsh, E. A., Muzikante, I. J., Rampens, A. J. 1983. In *Tagungsband*

Organische Festkorpen. Brandenburg: DPR
205. Samoc, M., Samoc, A., Sworakowski, J., Karl, N. 1983. *J. Phys. C Solid State Phys.* 16:171–80
206. Plans, J., Zielinski, M., Kryszewski, M. 1981. *Phys. Rev. B* 23:6557–69
207. Karl, N., Sato, N., Seki, K., Inokuchi, H. 1983. *J. Chem. Phys.* 77:4870–78
208. Yoshie, O., Kamihara, M. 1983. *J. Appl. Phys. Jpn.* 22:629–35
209. Tiedje, T., Rose, A. 1981. *Solid State Commun.* 37:49–52
210. Orenstein, J., Kastner, M. A. 1981. *Solid State Commun.* 40:85–89
211. Monroe, D., Kastner, M. A. 1983. *Philos. Mag. B* 47:605–20
212. Arkhipov, V. I., Popova, J. A., Rudenko, A. I. 1983. *Philos. Mag. B* 48:401–10 and references therein
213. Arnold, S., Hassan, N. 1983. *J. Chem. Phys.* 78:5606–11
214. Pope, M., Kallmann, H. 1972. *Isr. J. Chem.* 10:269–86
215. Thomas, J. M., Evans, E. L., Williams, J. O. 1972. *Proc. R. Soc. Ser. A* 331:417–27
216. Williams, J. O., Thomas, J. M. 1973. In *Surface and Defect Properties of Solids*, pp. 229–49. Vol. 2, *Specialist Periodical Report*. London: Chemical Society
217. Zboinski, Z. 1983. *Chem. Phys.* 75:297–304
218. Petelenz, P. 1981. *Mat. Sci.* 7:285–90
219. Movaghar, B., Sauer, G. W., Wurtz, D., Huber, D. L. 1981. *Solid State Commun.* 39:1179–82
220. Movaghar, B., Sauer, G. W., Wurtz, D. 1982. *J. Stat. Phys.* 27:473–85
221. Hunt, I., Bloor, D., Movaghar, B. 1983. *J. Phys. C Solid State* 16:2623–28
222. Dudley, M., Sherwood, J. N., Bloor, D., Ando, D. J. 1982. *J. Mat. Sci. Lett.* 1:479–81
223. Haarer, D., Möhwald, H. 1975. *Phys. Rev. Lett.* 34:1447–50
224. Deleted in proof
225. Bechgaard, K., Jacobsen, C. S., Mortensen, K., Pedersen, H. J., Thorup, N. 1980. *Solid State Commun.* 33:1119–25
226. Jerome, D., Mazaud, A., Ribault, M., Bechgaard, K. 1980. *J. Phys. Paris Lett.* 41:L95–L98
227. Jerome, D., Schulz, H. J. 1982. *Adv. Phys.* 31:229–490
228. Friedel, J., Jerome, D. 1982. *Contemp. Phys.* 23:583–624
229. Colloq. Iht. CNR sur la Phys. et la Chem. des Metaux Synthetique et Organiques. 1983. *J. Phys. Colloq.* 44(C.3)
230. Williams, J. M., Beno, M. A., Sullivan, J. C., Banovetz, L. M., Braam, J. M., Blackman, G. S., Carlson, C. D., Greer, D. L., Loesing, D. M. 1983. *J. Am. Chem. Soc.* 105:643–45
231. Williams, J. M., Beno, M. A., Appelman, E. H., Wickel, F., Aharon-Shalom, E., Nalewajek, D. 1982. *Mol. Cryst. Liquid Cryst.* 79:319–26
232. Jacobsen, C. S., Pederson, H. J., Mortensen, K., Rindorf, G., Thorup, N., Torrance, J., Bechgaard, K. 1982. *J. Phys. C* 15:2651–63
233. Pouget, J. P., Shirane, G., Bechgaard, K., Fabre, J. M. 1983. *Phys. Rev. B* 27:5203–6
234. Wudl, F. 1981. *J. Am. Chem. Soc.* 103:7064–69
235. Grant, P. M. 1982. *Phys. Rev. B* 26:6888–95
235a. Parkin, S. S. P., Engler, E. M., Schumacher, R. R., Lagier, R., Lee, V. Y., Scott, J. C., Greene, R. L. 1983. *Phys. Rev. Lett.* 50:270–73
236. Parkin, S. S. P., Engler, E. M., Schumacher, R. R., Lagier, R., Lee, V. Y., Voiron, J., Carneiro, K., Scott, J. C., Greene, R. L. 1983. *J. Phys. Colloq.* 44(C3):791–97
237. Rentzepis, P. M. 1982. *Science* 218:1183–90
238. Shank, C. V., Greene, B. I. 1983. *J. Am. Chem. Soc.* 87:732–34
239. Klein, G. 1983. *Chem. Phys. Lett.* 95:305–9; 97:114–18
240. Kalinowski, J. 1981. *Mat. Sci.* 7:44–50
241. Kalinowski, J., Jankowiak, R., Bässler, H. 1981. *J. Lumin.* 22:397–18
242. Kolendritskii, D. D., Kurik, M. V., Piryatinskii, Yu. P. 1979. *Phys. Status Solidi B* 91:741–51
243. Klöpffer, W. 1982. In *Electronic Properties of Polymers*, ed. J. Mort, G. Pfister, pp. 161–213. New York: Wiley
244. Ritsko, J. J. 1982. In *Electronic Properties of Polymers*, ed. J. Mort, G. Pfister, pp. 13–58. New York: Wiley
245. Duke, C. B. 1983. In *Physicochemical Aspects of Polymer Surfaces*, ed. K. L. Mittle, 1:463–75. New York: Plenum
246. Duke, C. B., Fabish, T. J. 1978. *J. Appl. Phys.* 49:315–21
247. Alzetta, G., Chudacek, I., Scarmozzino, R. 1970. *Phys. Status Solidi* 1:775–85
248. Nowak, R., Krajewska, A., Samoc, M. 1983. *Chem. Phys. Lett.* 94:270–71
249. Wada, Y. 1982. In *Electronic Properties of Polymers*, ed. J. Mort, G. Pfister, pp. 109–60. New York: Wiley
250. Kepler, R. G. 1978. *Ann. Rev. Phys. Chem.* 29:497–18
251. Davies, G. R. 1980. In *Physics of Dielectric Solids*, ed. C. H. L. Goodman, pp. 50–63. Conf. Ser. No. 58. Bristol: Inst. Physics Techno House
252. Spannring, W., Bässler, H. 1981. *Chem. Phys. Lett.* 84:54–58

END

FILMED

3-86

DTIC